Elettra Sincrotrone Trieste

X-ray Powder Diffraction and Synchrotron Radiation

Topics

- What is powder diffraction

- How do we measure powder diffraction and what do we have to be aware of

- Instrumentation at synchrotron beamlines for powder diffraction

- Why perform powder diffraction at synchrotrons

- Applications of SR-XRPD

Powder diffraction

Synchrotron Radiation: Basics, Methods and Applications

- ## Chapter 10:
  ## Powder Diffraction and synchrotron radiation

- Chapter 18:
  - Diffraction from nanocrystalline materials
- Chapter 24:
  - Synchrotron radiation and earth sciences
- Chapter 25:
  - Synchrotron radiation and environmental sciences
- Chapter 26:
  - Synchrotron radiation in art, archeology and cultural heritage
- Chapter 29:
  - Studies of matter at extreme conditions
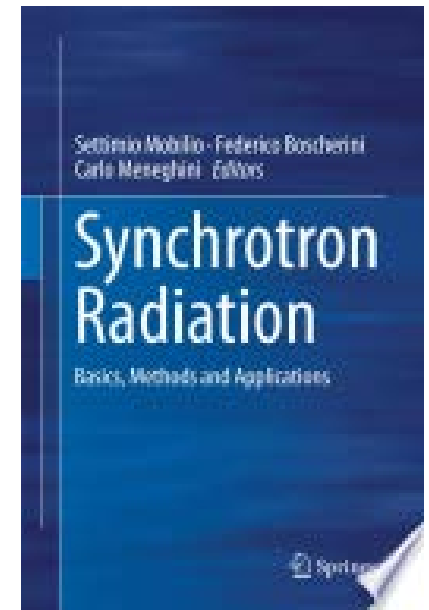
- Oxford Dictionary:

powder
Pronunciation: /ˈpaʊdə/
fine, dry particles produced by the grinding, crushing, or disintegration of a solid

solid
Pronunciation: /ˈsɒlɪd/
1 a substance or object that is solid rather than liquid or fluid.
**2** *Geometry* a body or geometric figure having three dimensions.

Elettra
Sincrotrone
Trieste
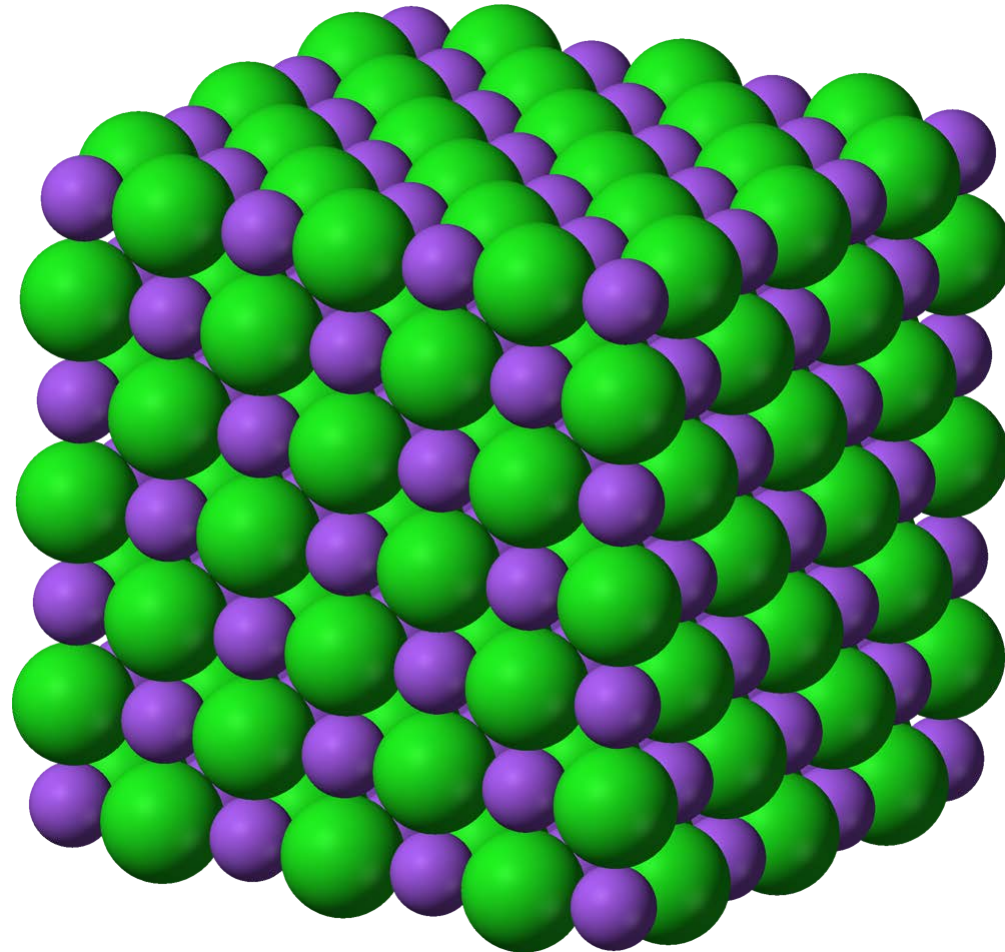
A solid

A solid

Unit cell
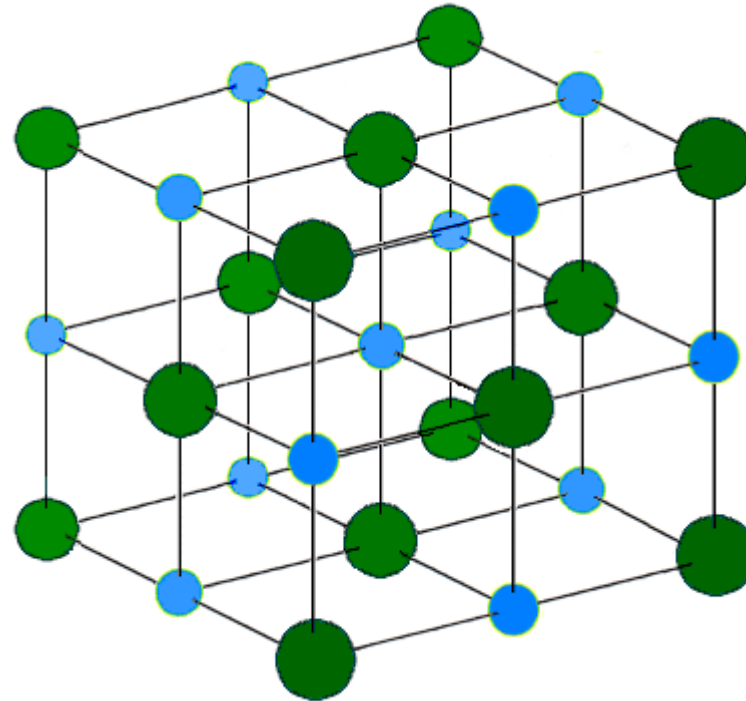
Solids
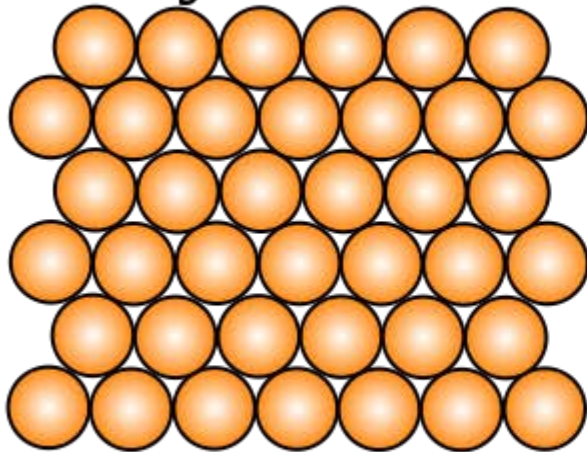
Crystalline · Polycrystalline · Amorphous
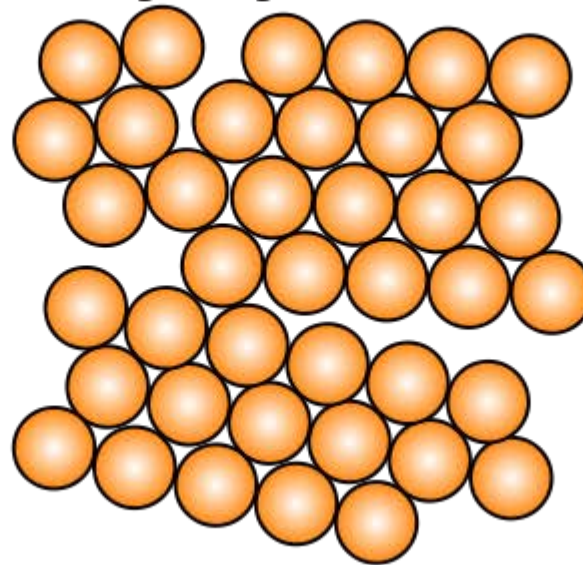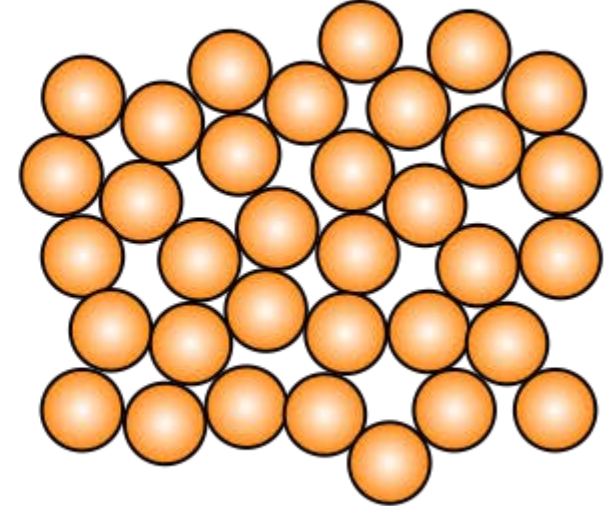
'Powders'
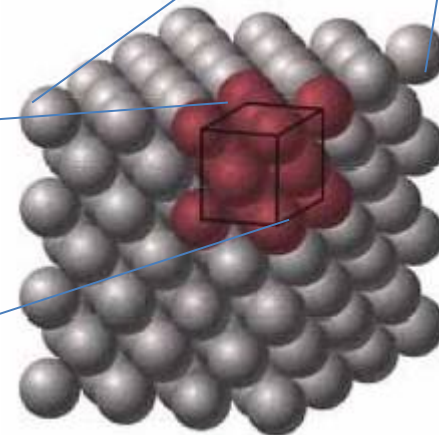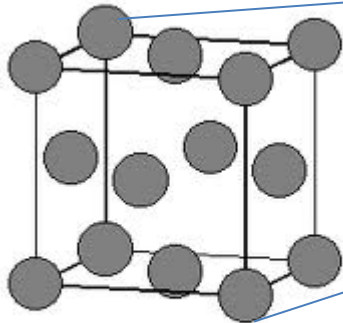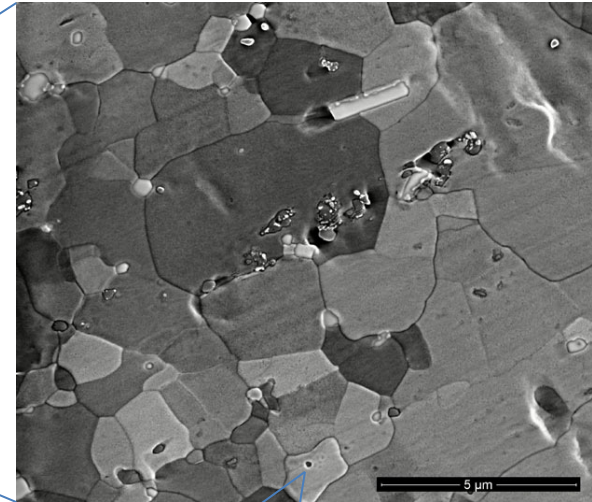
'Powders'
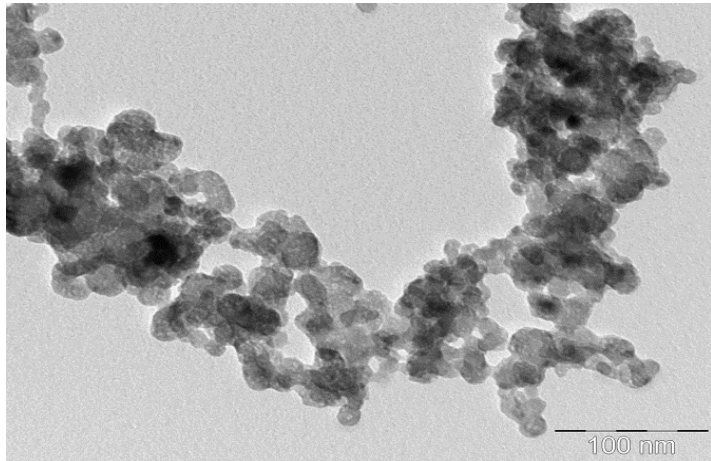
X-ray Diffraction
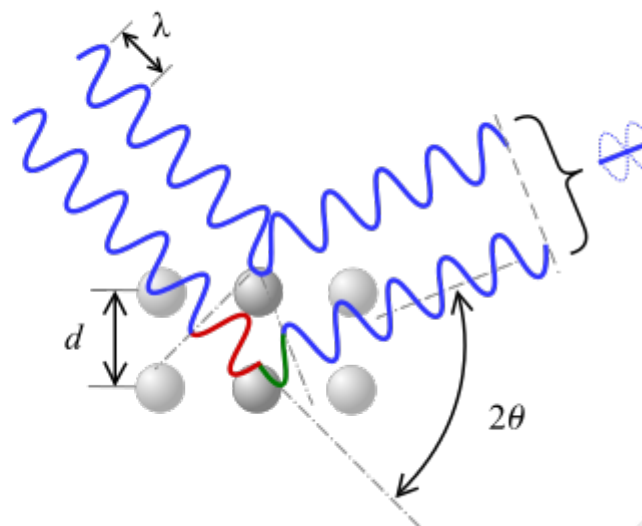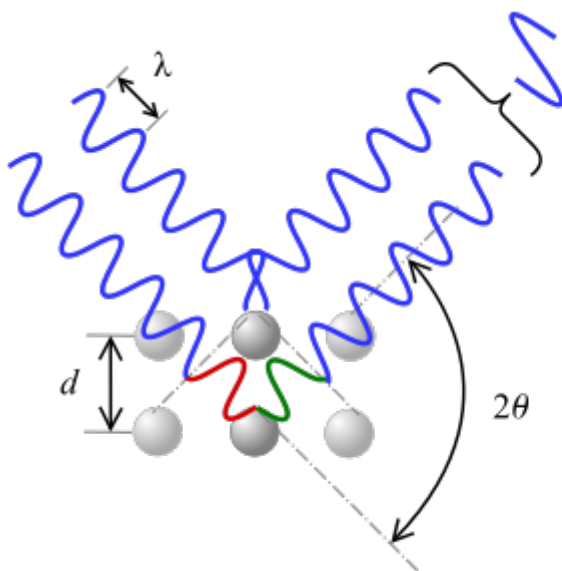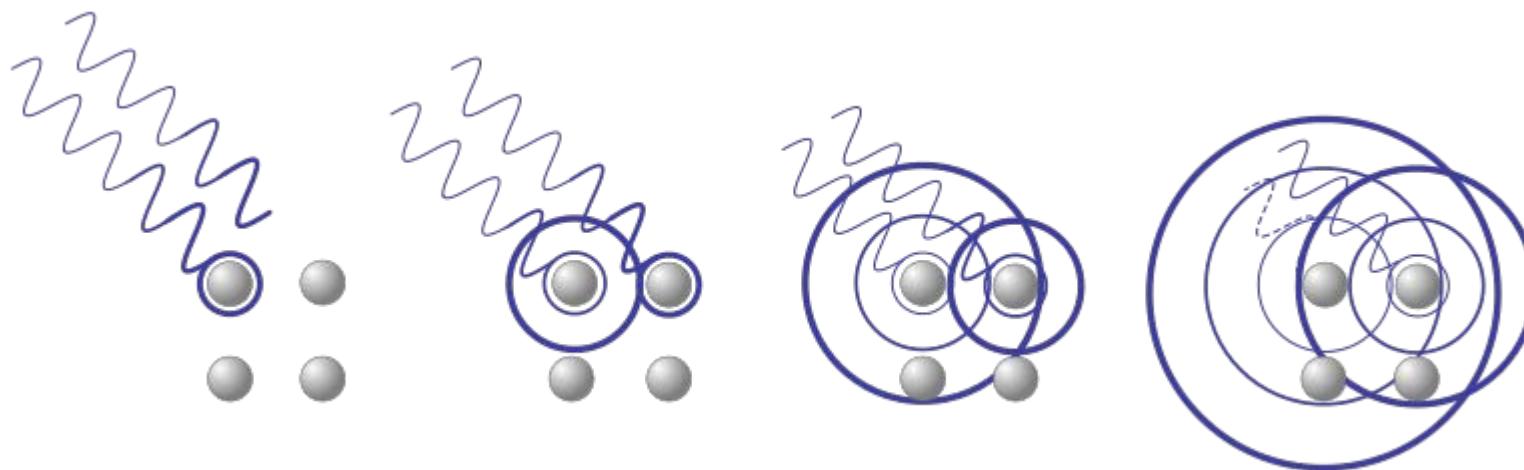
Bragg's law
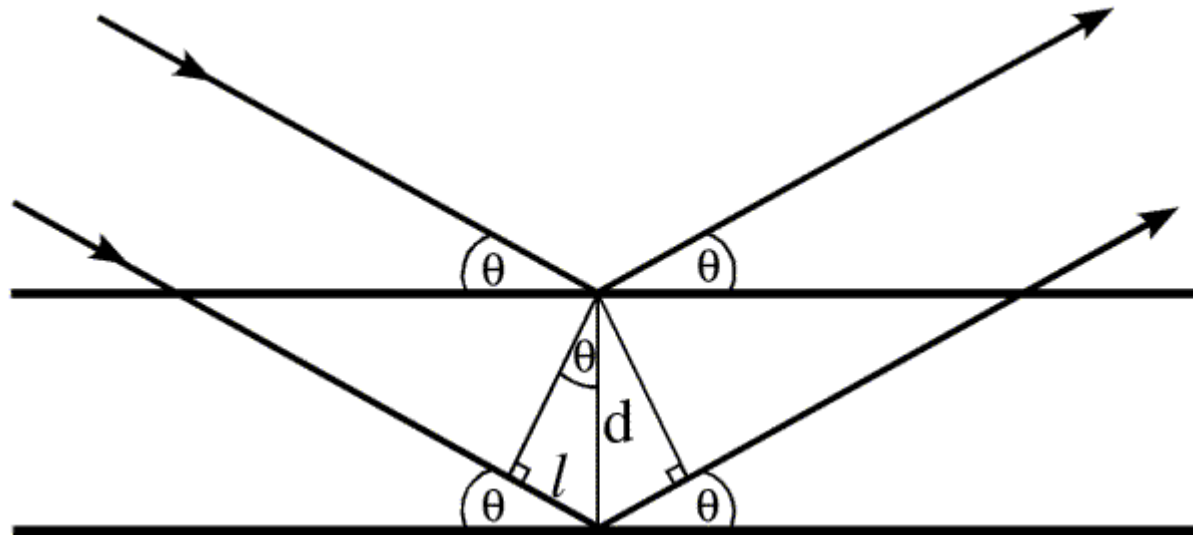
The two X-ray beams travel at different distances. This difference is related to the distance between parallel planes

$$2l = d \, \sin \Theta \qquad n\lambda = 2d \, \sin \Theta$$

Bragg's law

This condition is met when the distance equals an integer multiple of the wavelength, called order of diffraction, n. The final equation is the BRAGG'S LAW

$$n\lambda = 2d \sin \Theta$$

Data are collected by using X-rays of a known wavelength. The sample is rotated so that the angle of diffraction changes

When the angle is correct for diffraction a signal is recorded
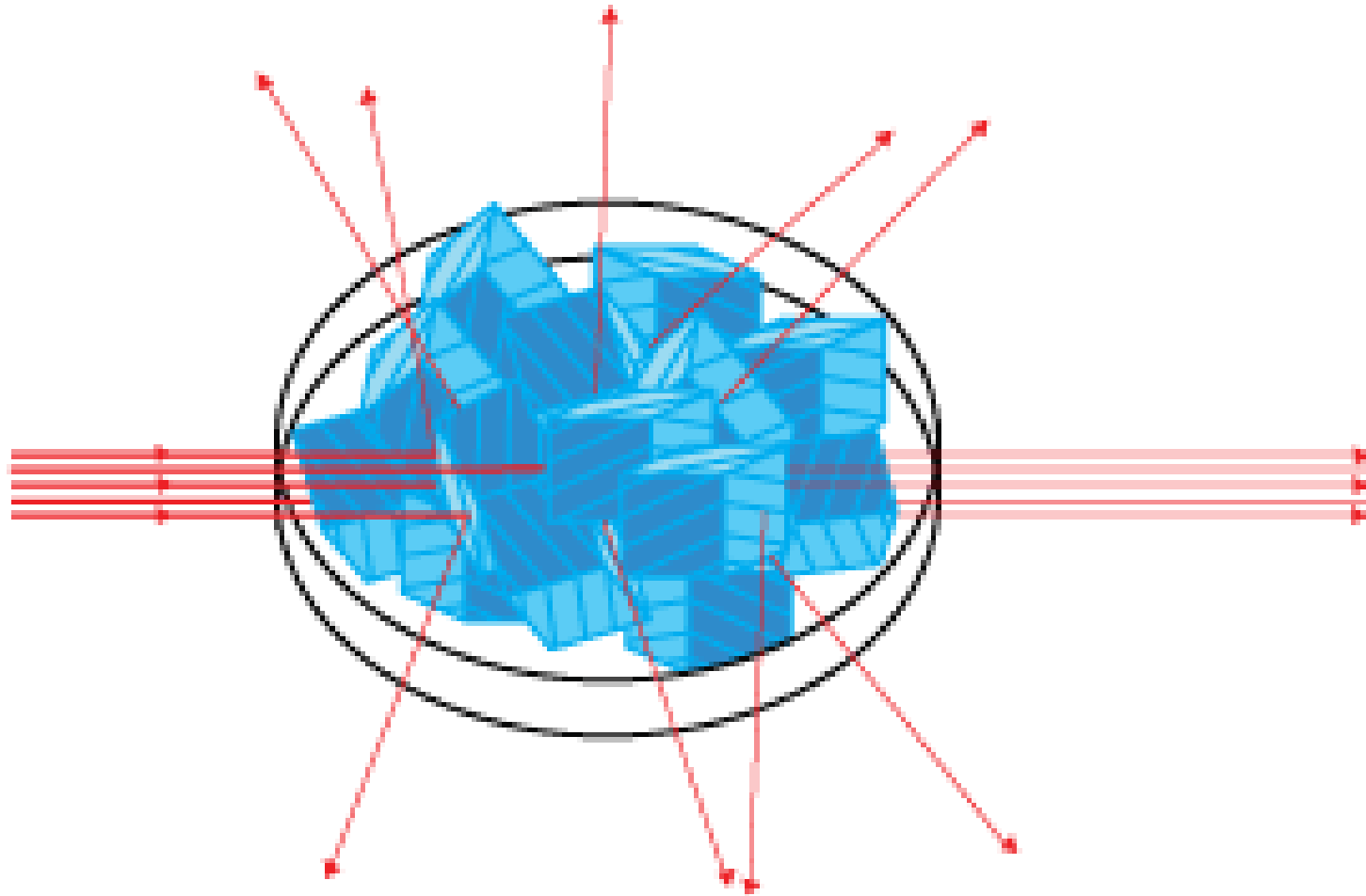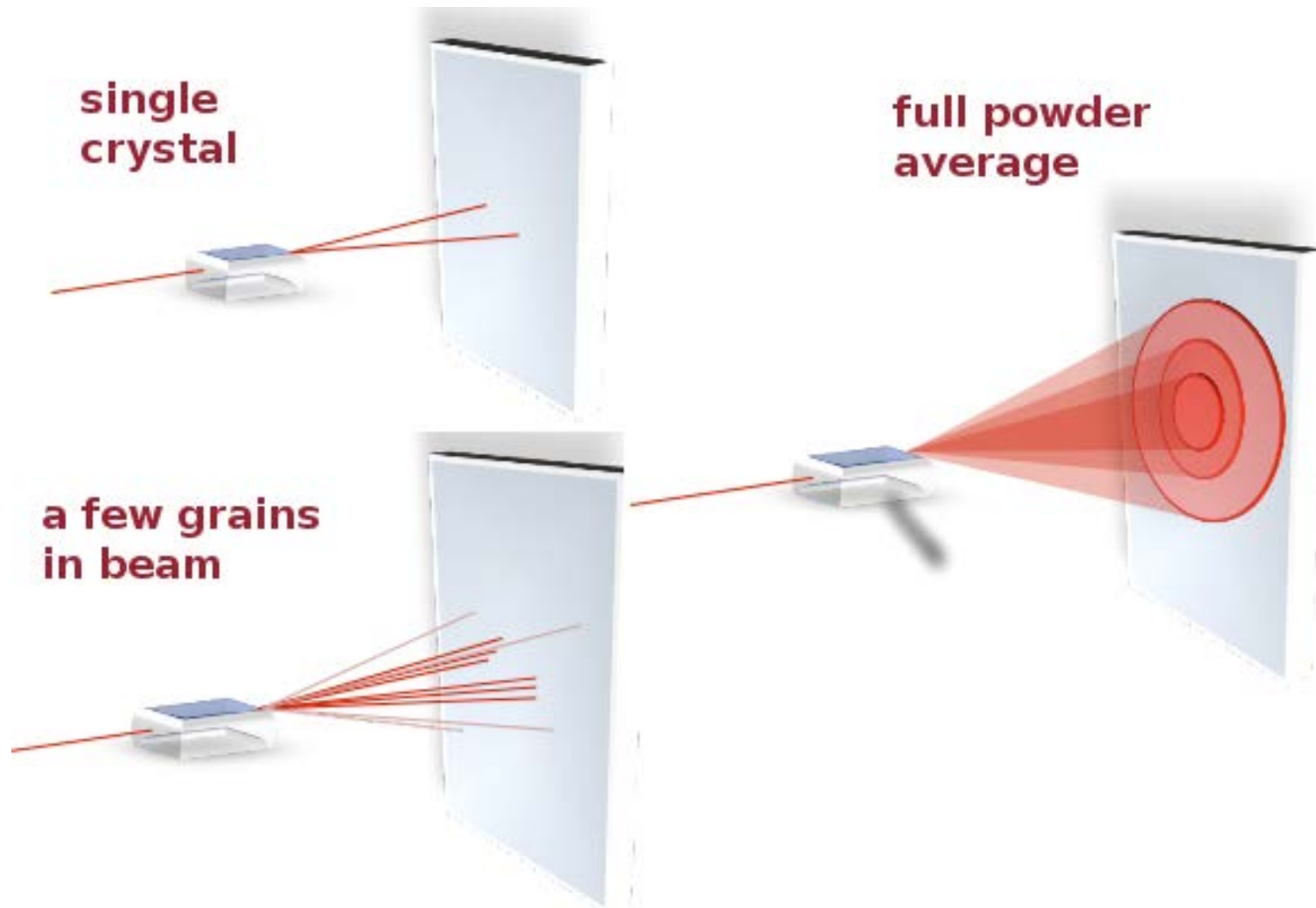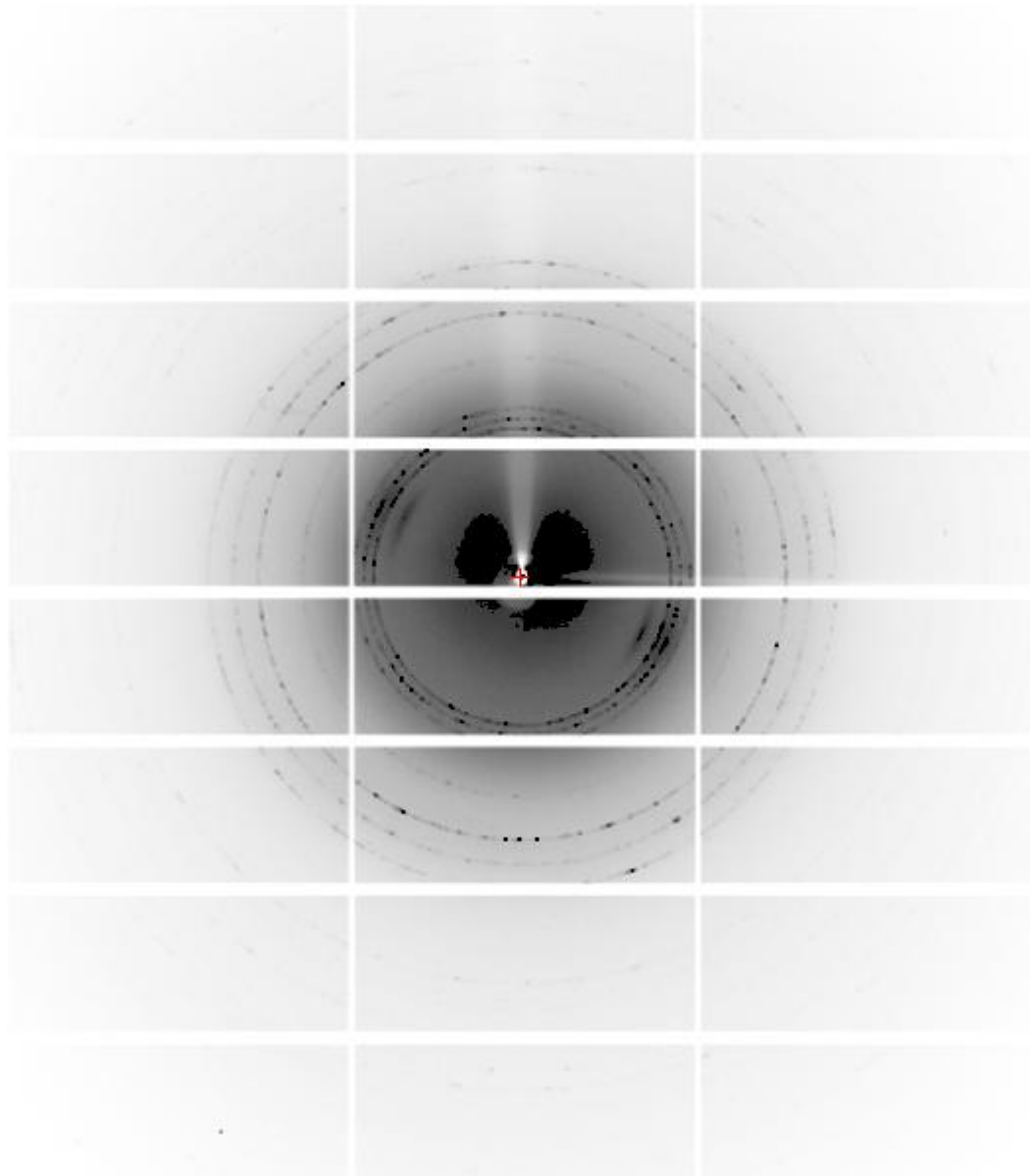
X

single crystal

a few grains in beam

full powder average
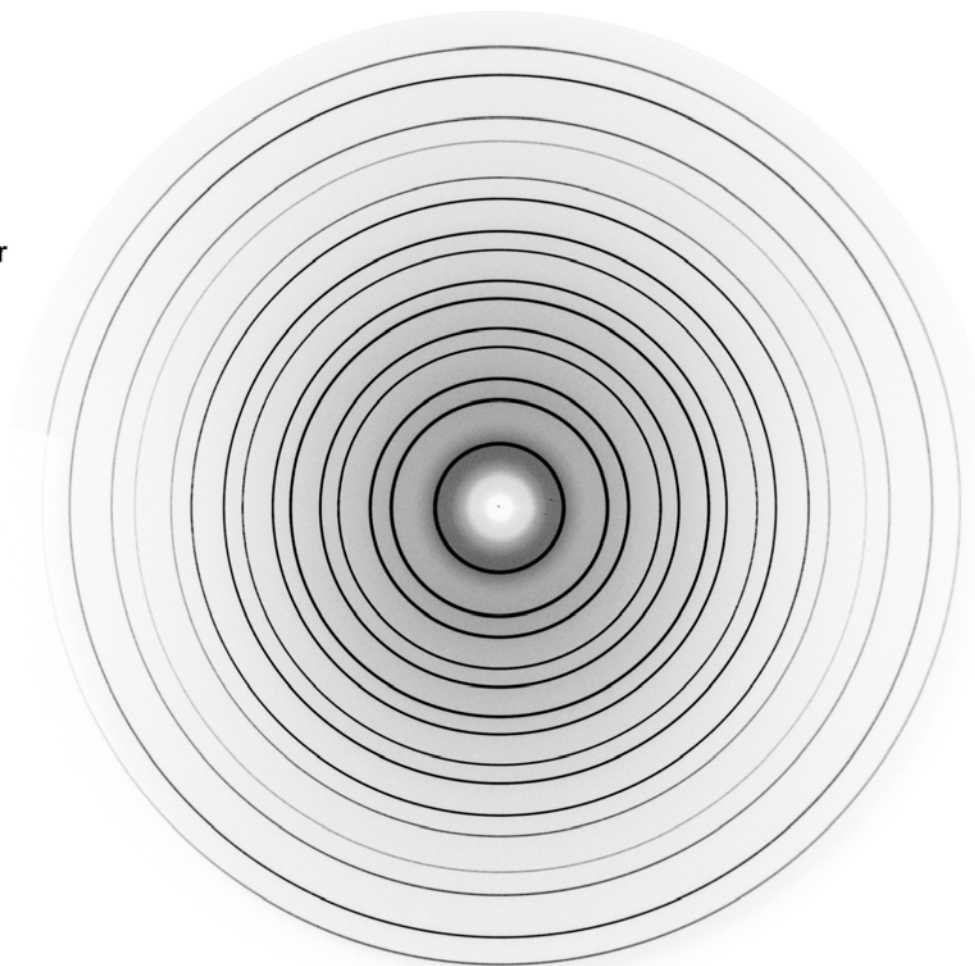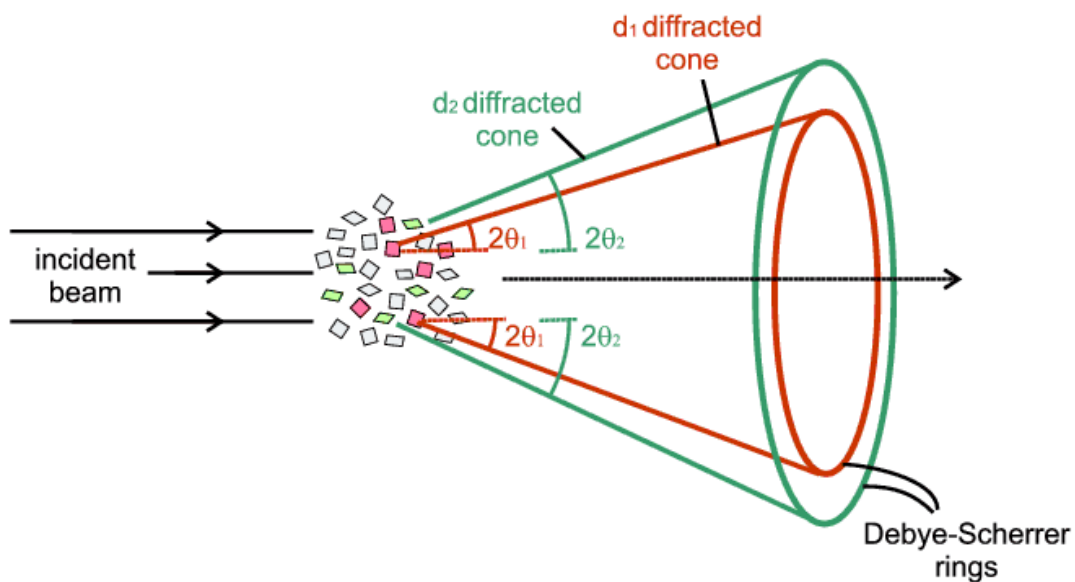
Powder diffraction

Powder diffraction
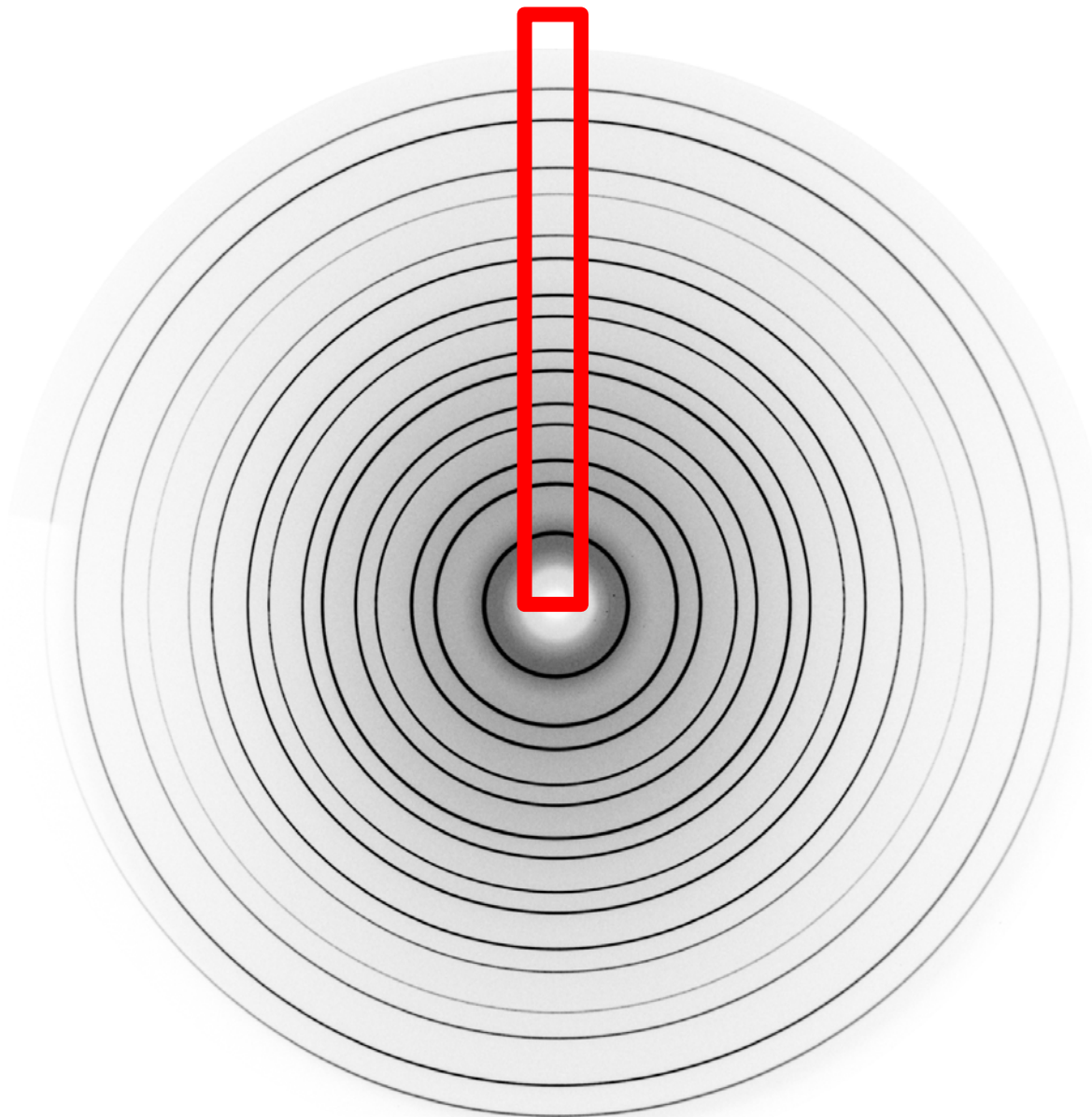
Powder diffraction
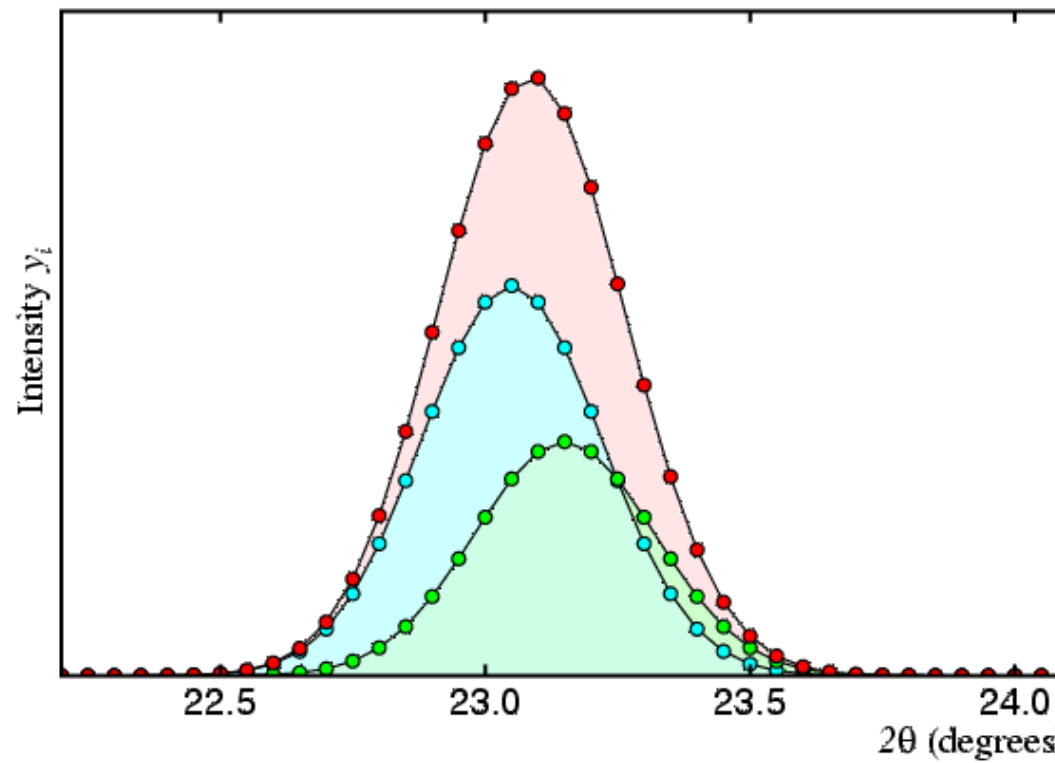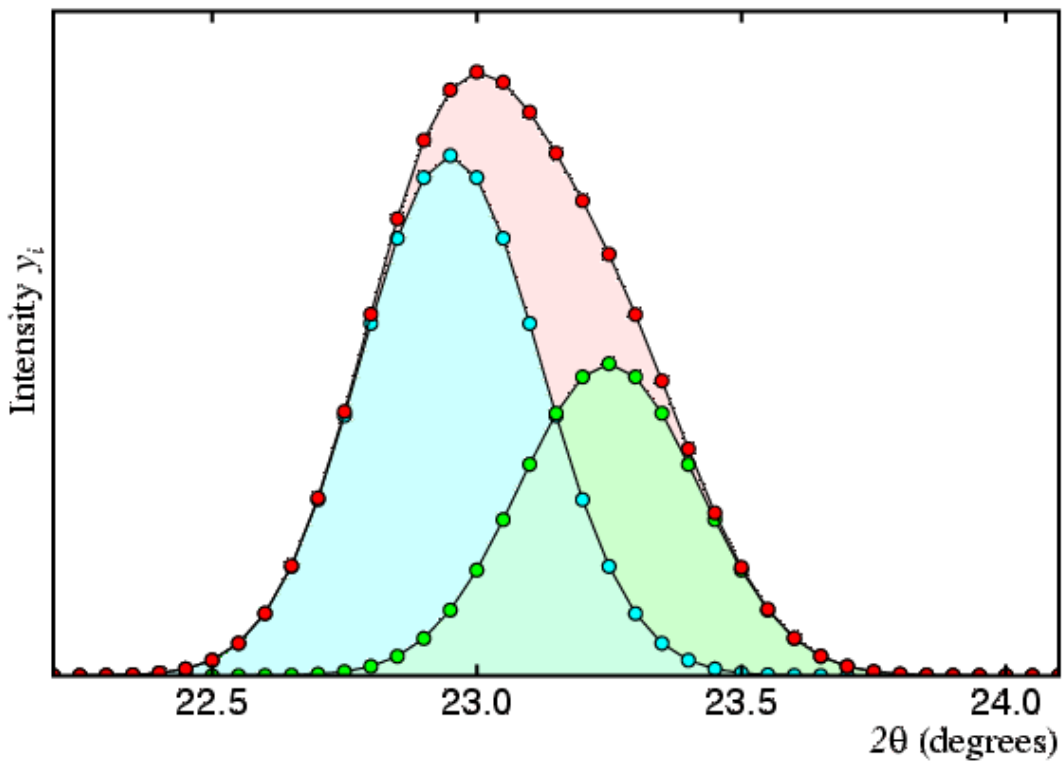
# Diffraction geometries
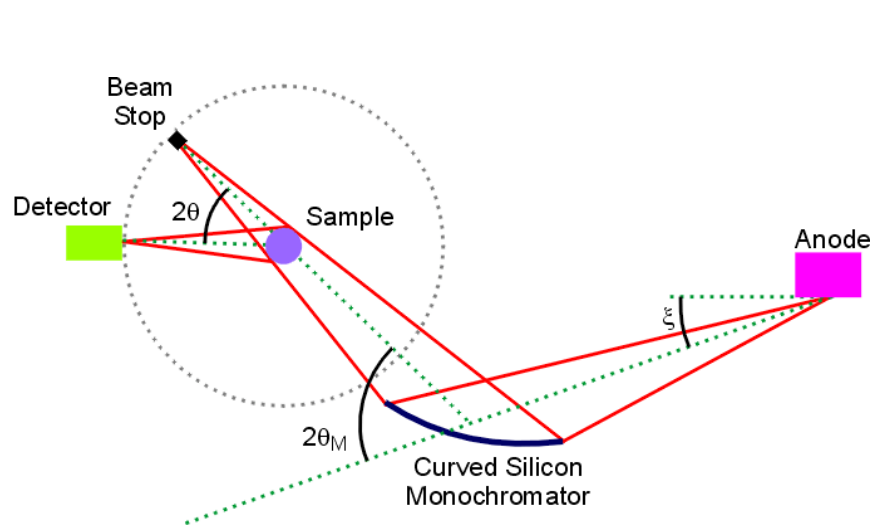
Debije-Scherrer
Transmission
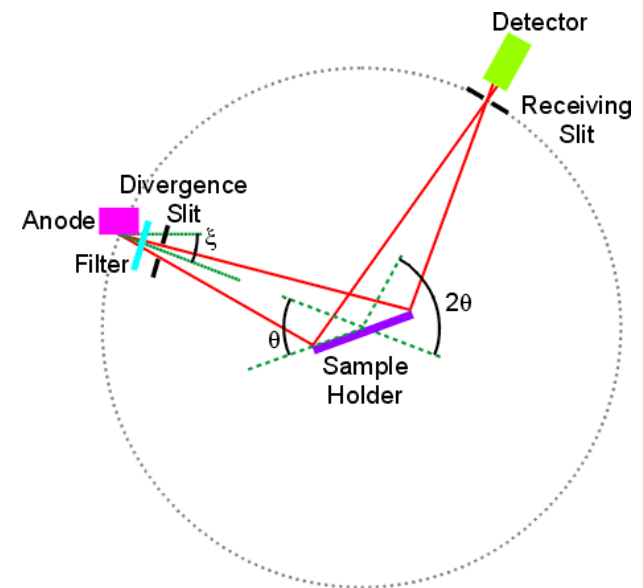
Bragg-Brentano
Reflection

Diffraction geometries
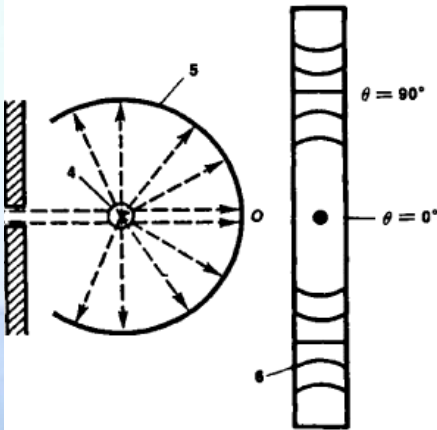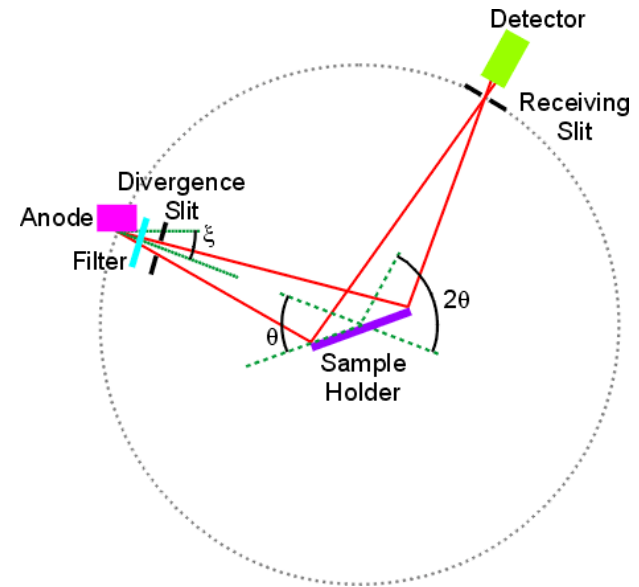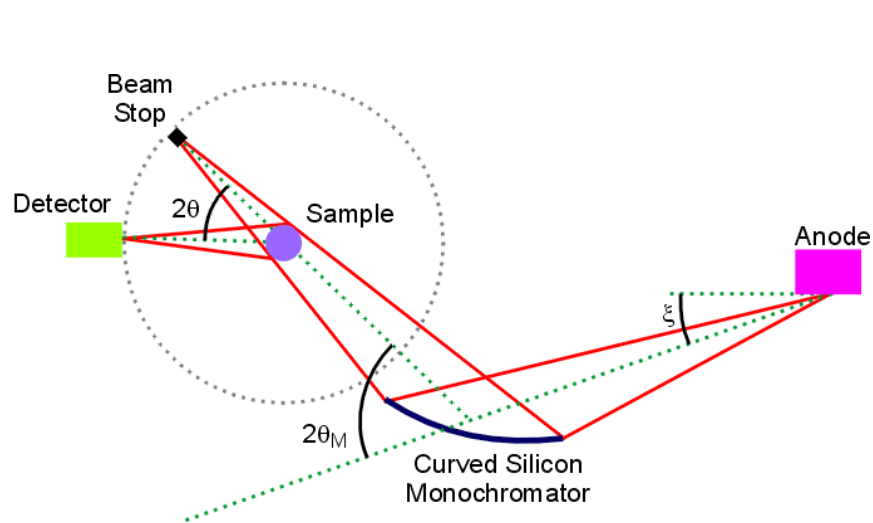
Diffraction geometries in synchrotrons
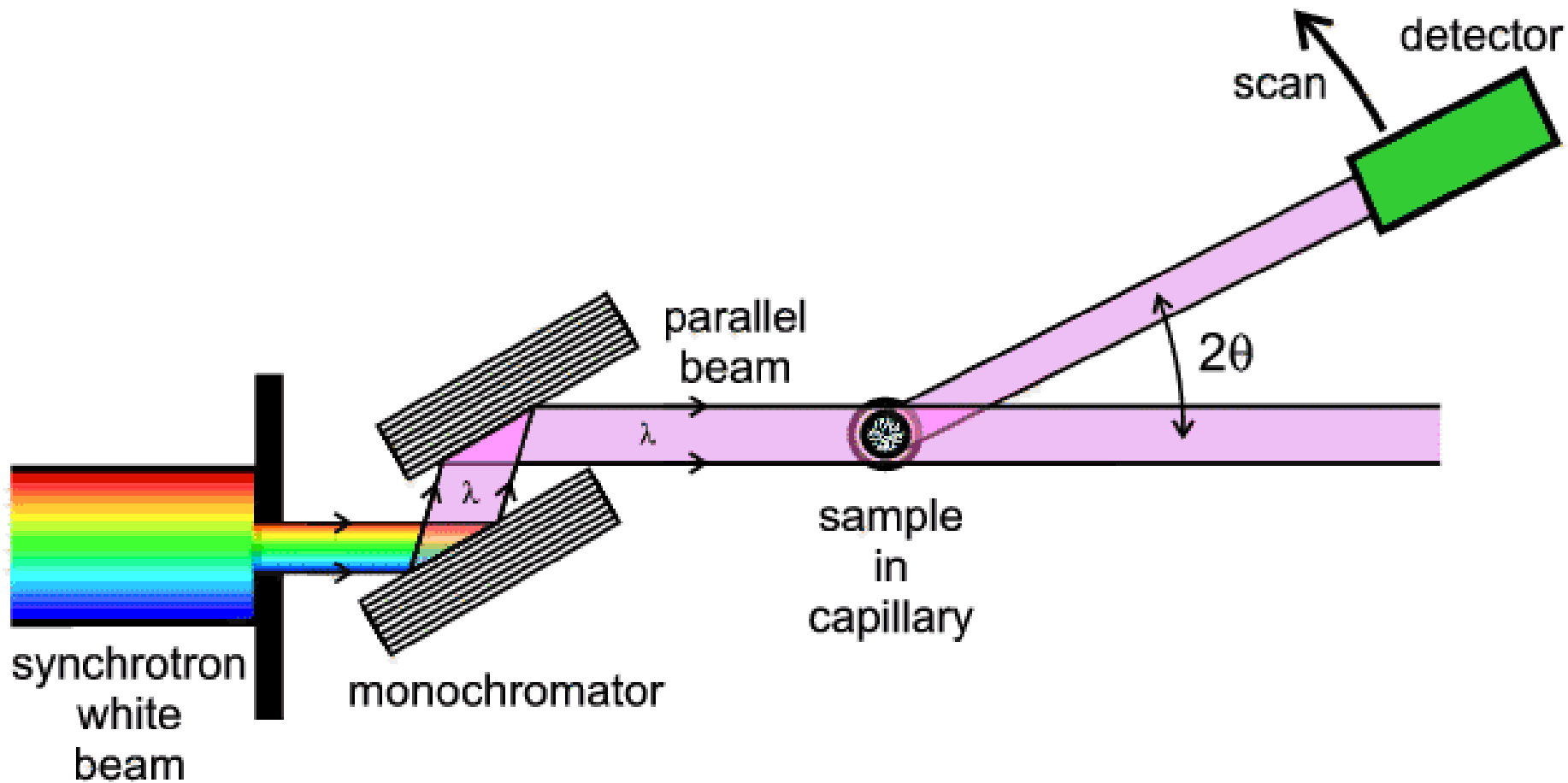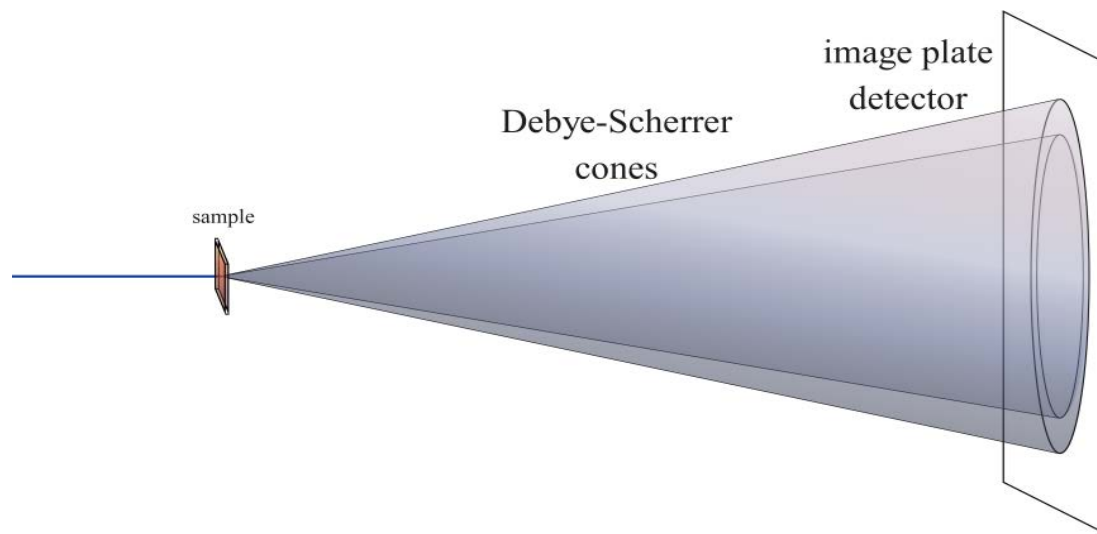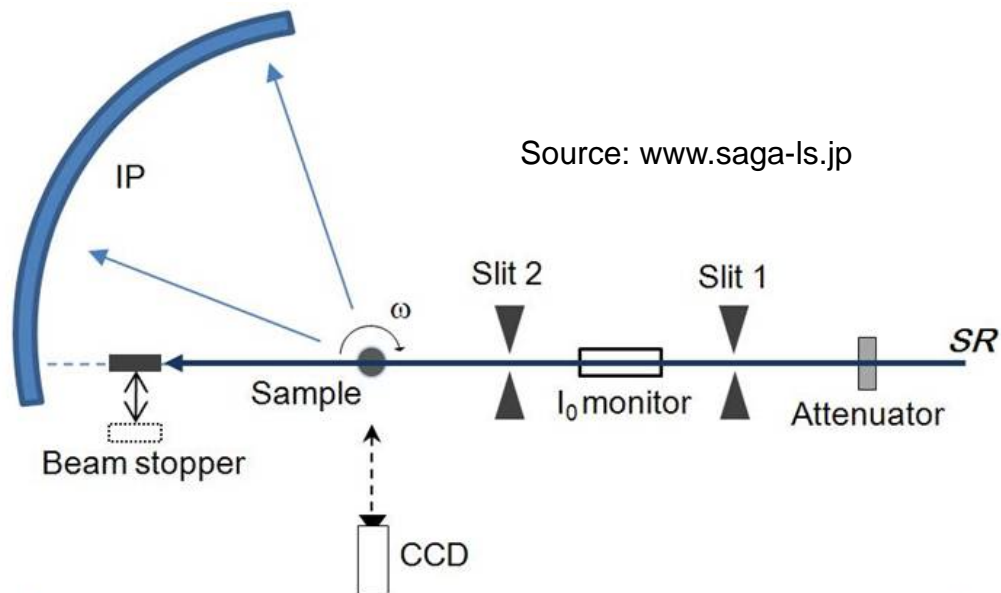
detector

scan

2θ

parallel
beam

λ

sample
in
capillary

λ

synchrotron
white
beam

monochromator

Elettra
Sincrotrone
Trieste

Source: www.saga-ls.jp

IP

Slit 2

Slit 1

ω

SR

Sample

I_0 monitor

Attenuator

Beam stopper

CCD

Debye-Scherrer cones

image plate detector

sample

Diffraction geometries in synchrotrons

detector

flat plate
specimen

SR beam

channel-cut
water-cooled
monochromator

Diffraction geometries in synchrotrons

energy-dispersive detector

collimator

fixed 2θ

synchrotron white beam

$$\lambda = 2d \sin\theta$$

scanned variable (by ED detector)

determined variable

fixed (by collimator)
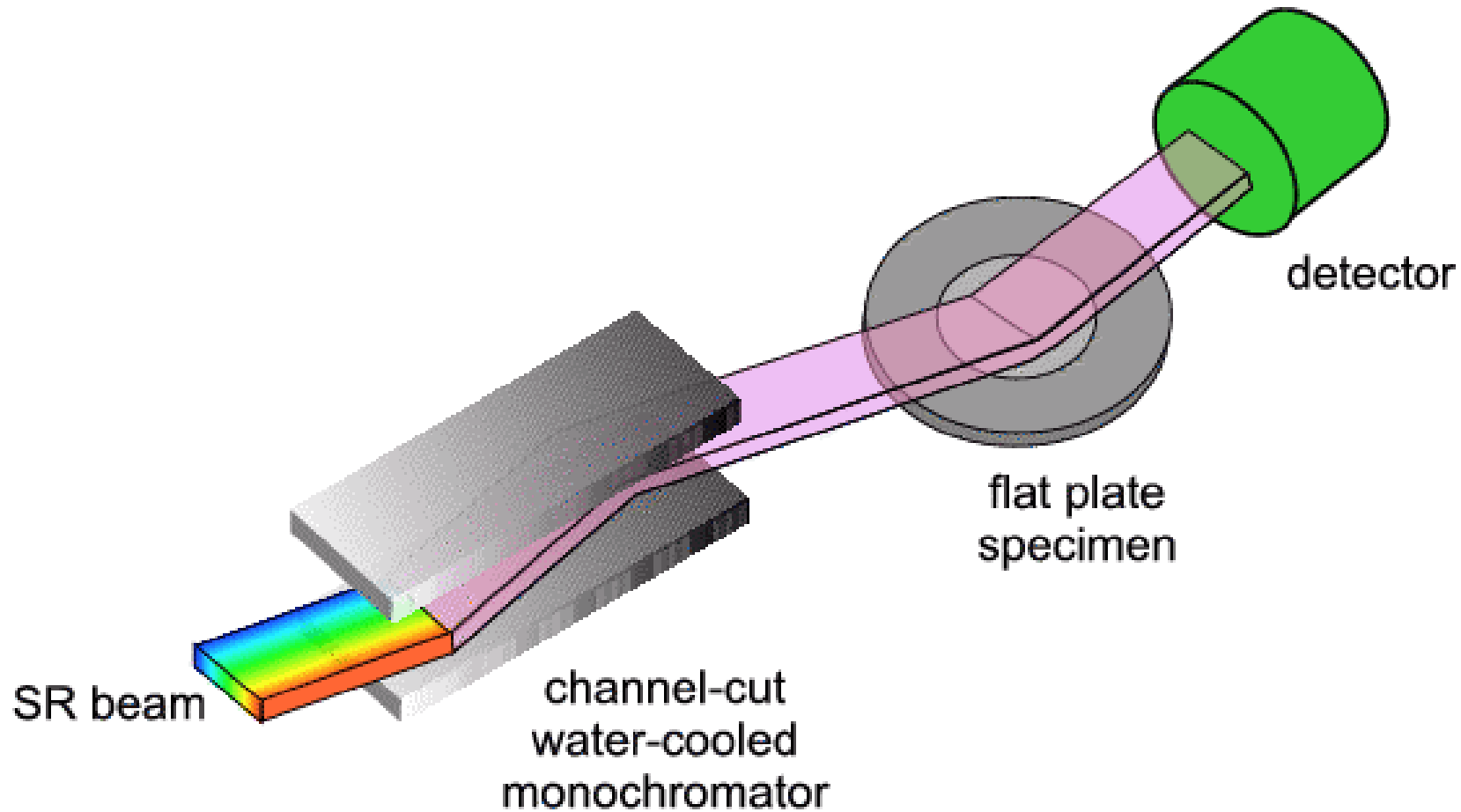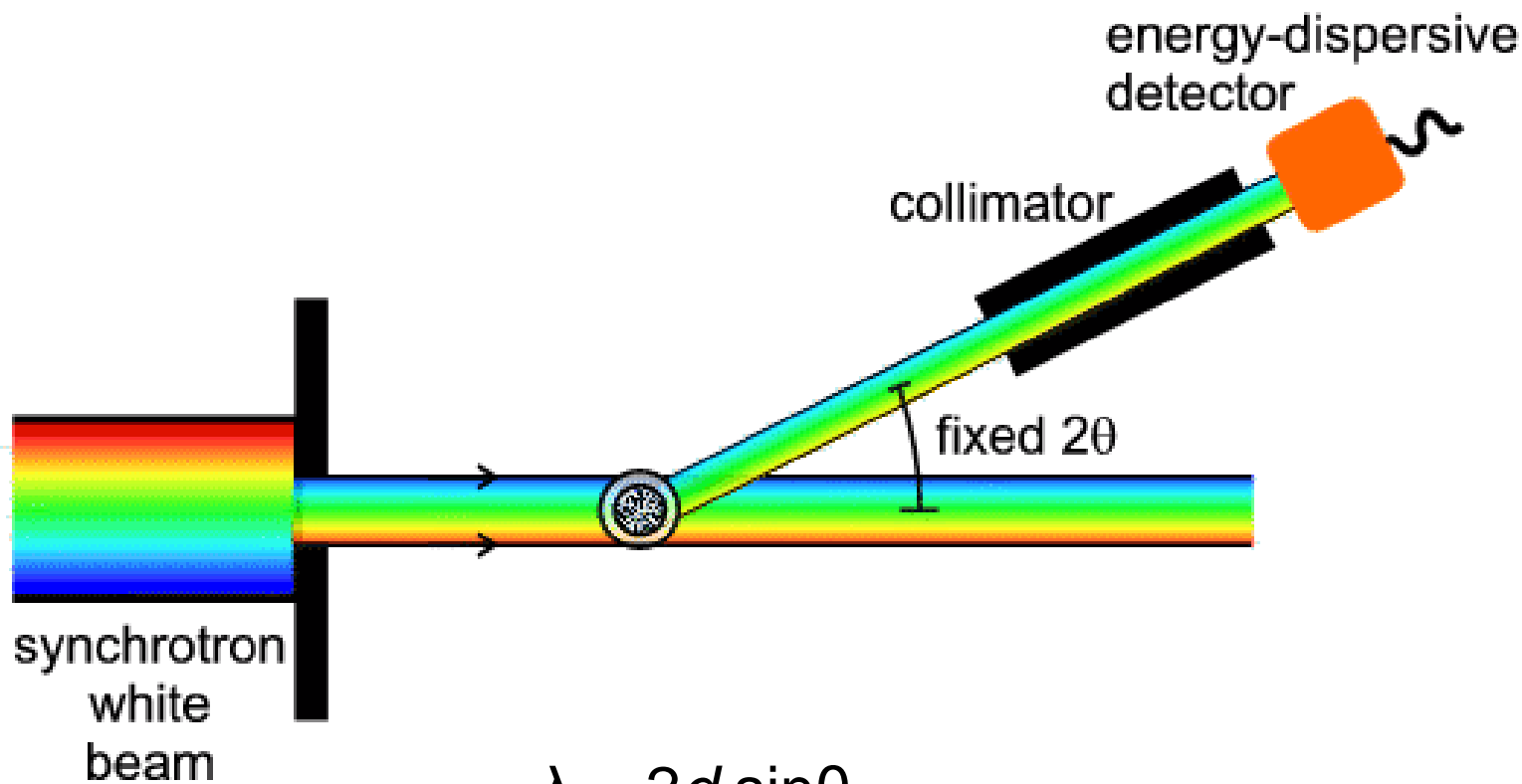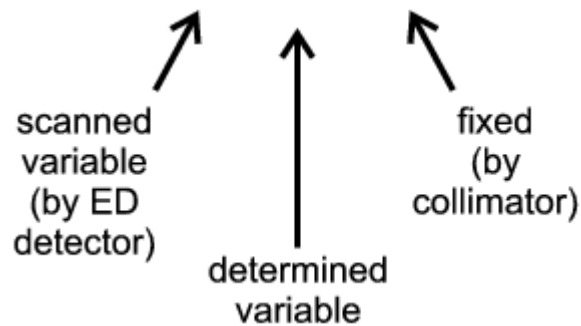
- **High X-ray flux** : Millions count counting statistics in reflection (Bragg-Brentano) as well as in transmission (Debye-Scherrer) modes even with low quantities of powder available

- **Highly collimated photon beam**: angular resolution better due to narrow instrumental profile. FWHM better than 0.01° 2θ obtained with new generation solid state microstrip detectors and down to 0.002° 2θ using multicrystal analyser detectors

- **Tunable photon energy up to high energies:**
  - anomalous scattering experiments
  - collect fluorescence-free XRPD data
  - Extension of d-space that can be probed.
  - depth analysis by varying energy

Instrumentation for X-ray Powder Diffraction at Synchrotrons
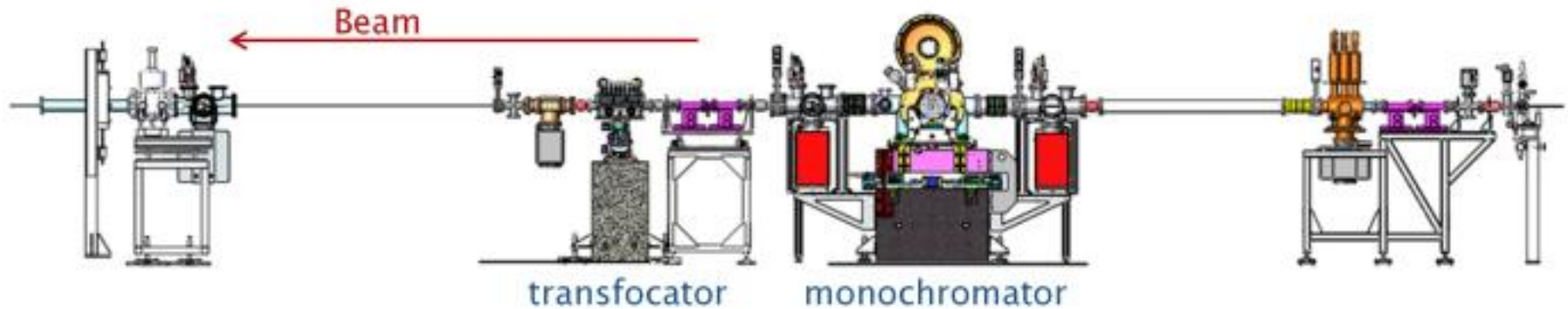
Light source:
 In vacuum undulator

X-rays at **sample:**
 Energy range : 6-80 keV
 Beam size can be focused to 50 um

Elettra - MCX

Light source:
Bending magnet
Critical energy : 3.2keV (2.0) , 5.5keV (2.4)

X-rays at sample:
Energy range : 6-21 keV
Photon flux : 10^{11} photons/sec
Beam size at sample : 10x1 mm^2 - 0.3x0.3 mm^2
Energy resolution : $\Delta E/E$ 2x10^{-4}

EXPERIMENT
line focus (10 mm x 1 mm)
point focus (1 mm x 1 mm)

d=36000

MIRR2
tangential
focusing

cylindrical, dynamically bendable
d=20600

DCM
sagittal
focusing

dynamically bendable 2nd crystal
d=18000

MIRR1
tangential
collimation
cylindrical
d=15400

SOURCE
ELETTRA BM
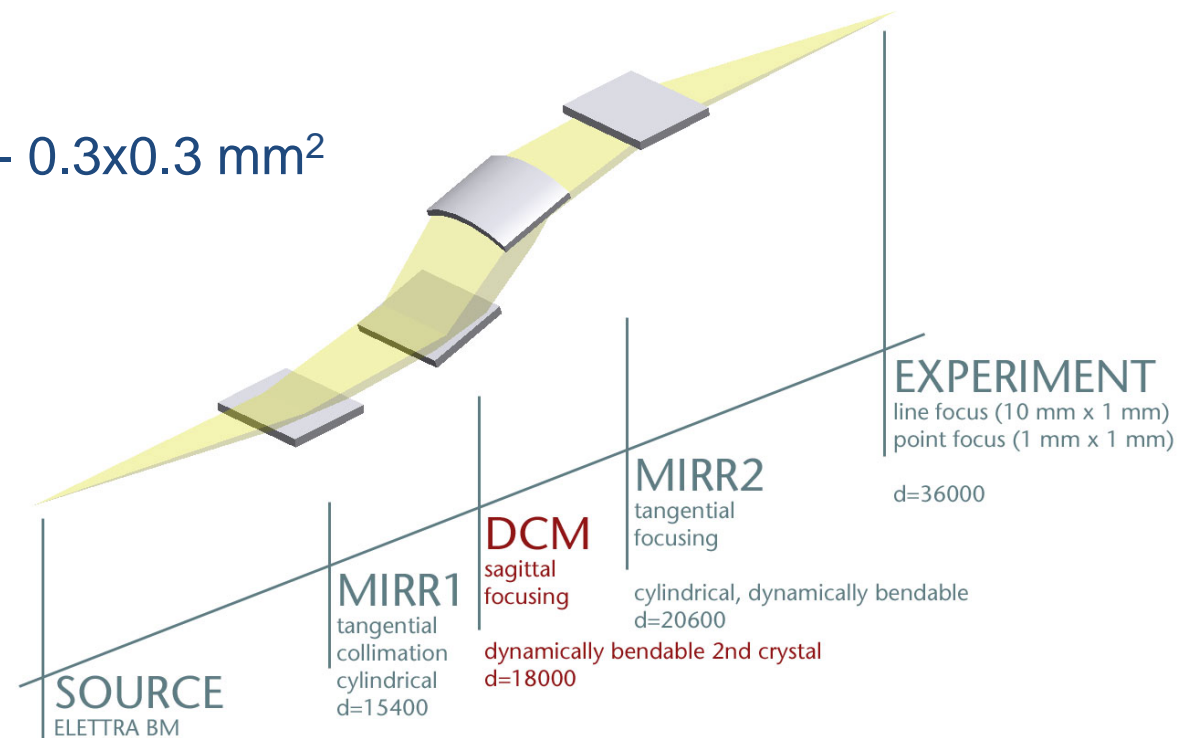
Diffractometer MCX

Elettra
Sincrotrone
Trieste
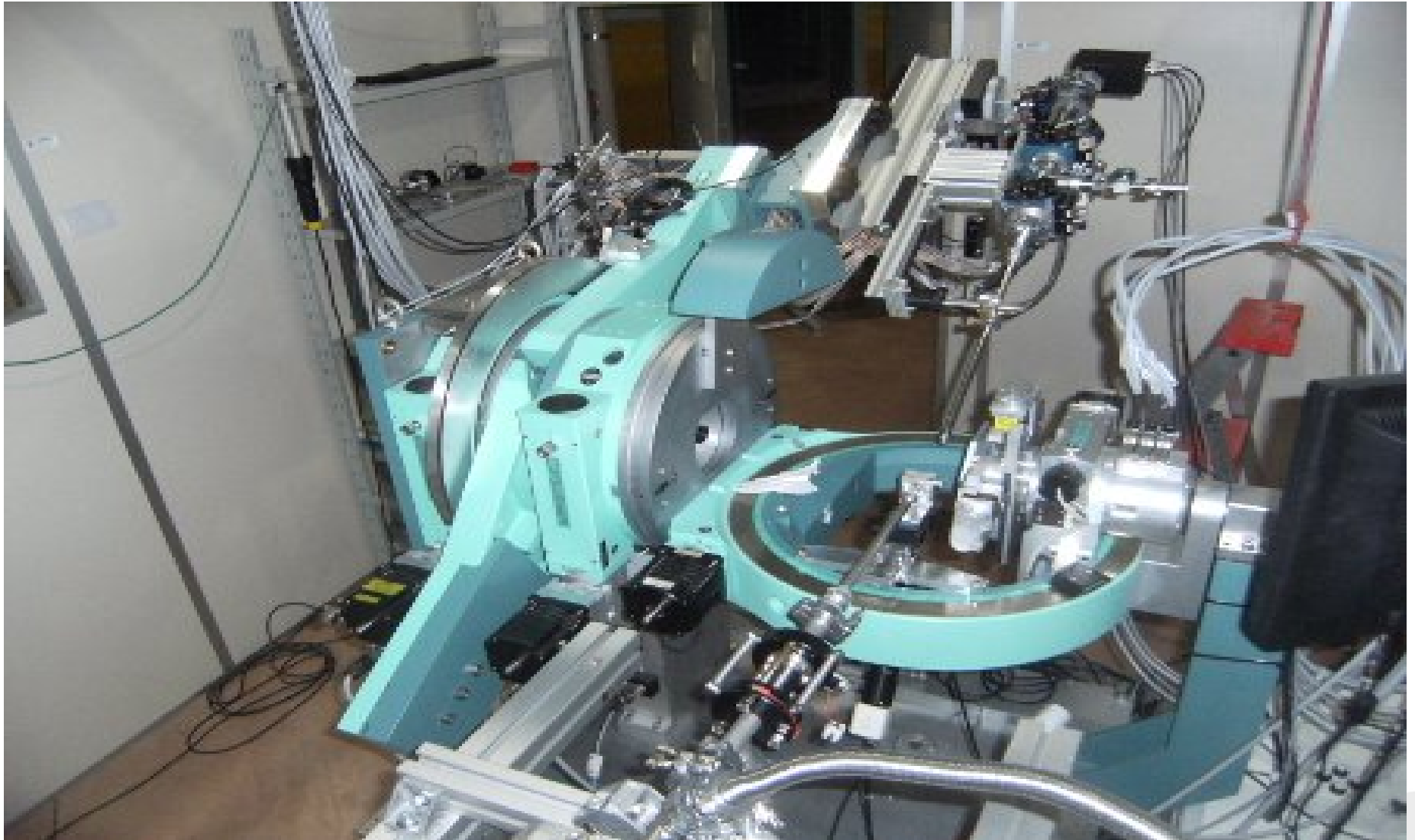
X-ray detectors

0D – (spot) detectors: Scintillators

N

1D – Line detectors: Gas detectors, Strip
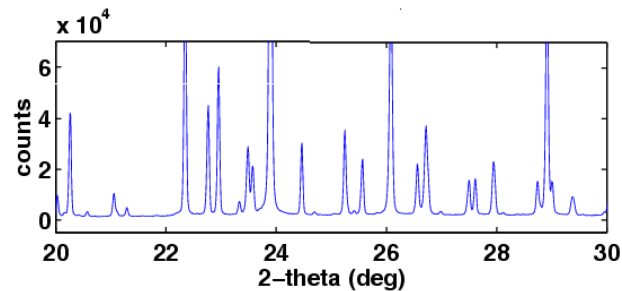
2D -- Area detectors: Image plate, CCD, Pixel
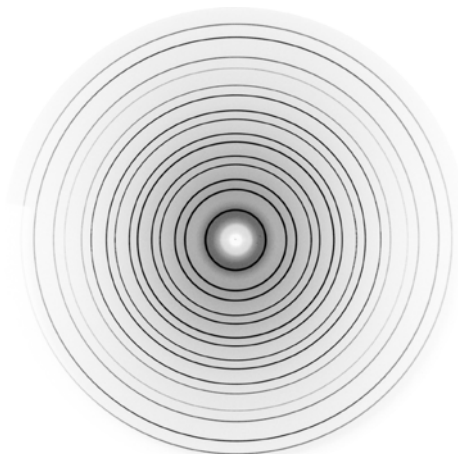
Scintillator detector (0D)
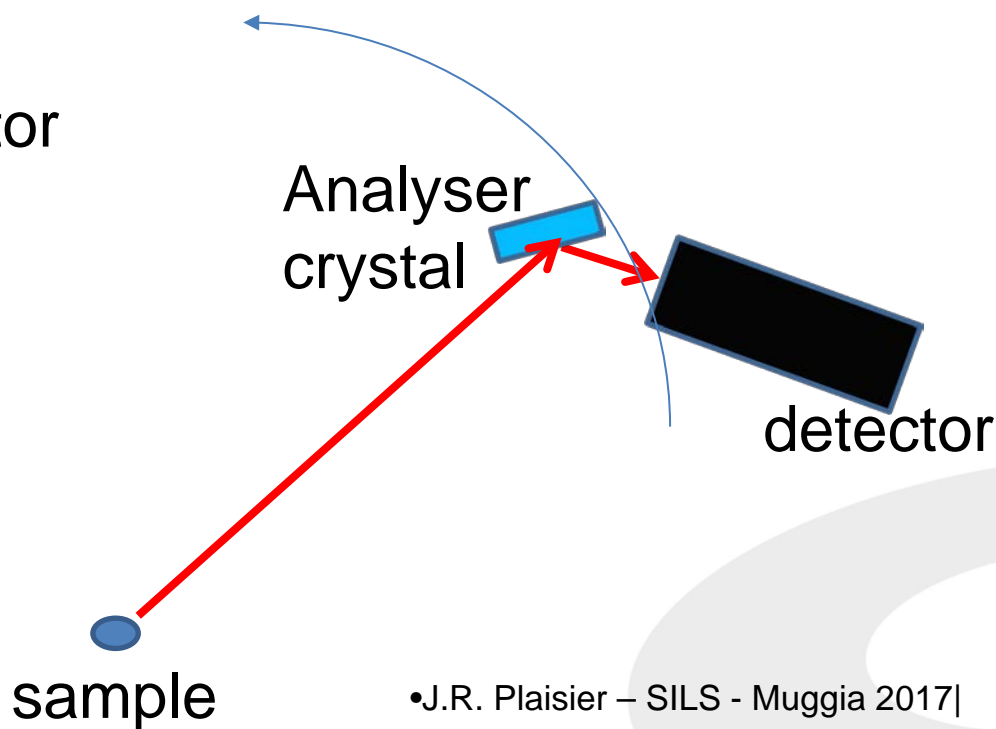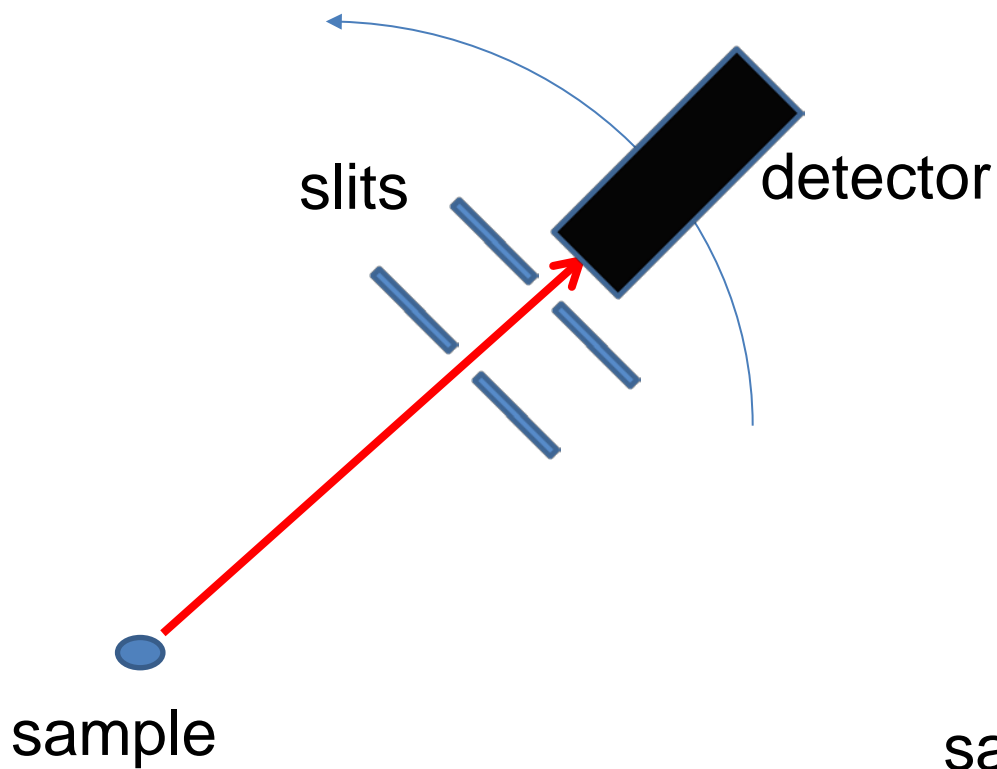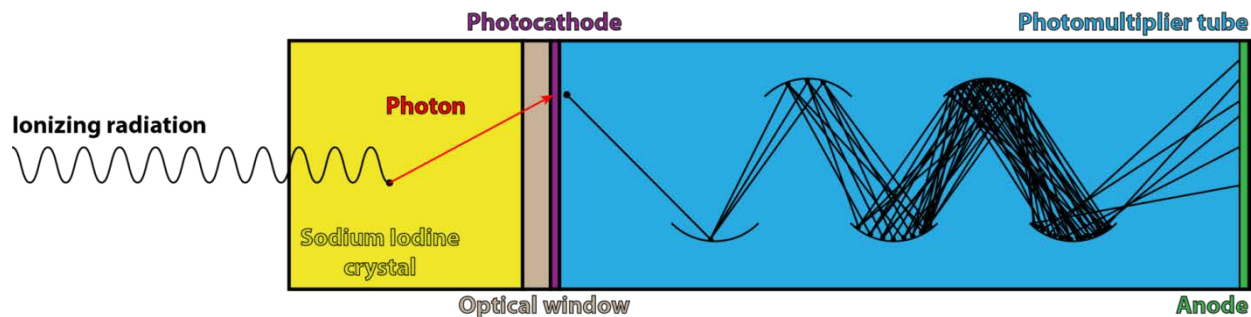
Mythen detector (1D)
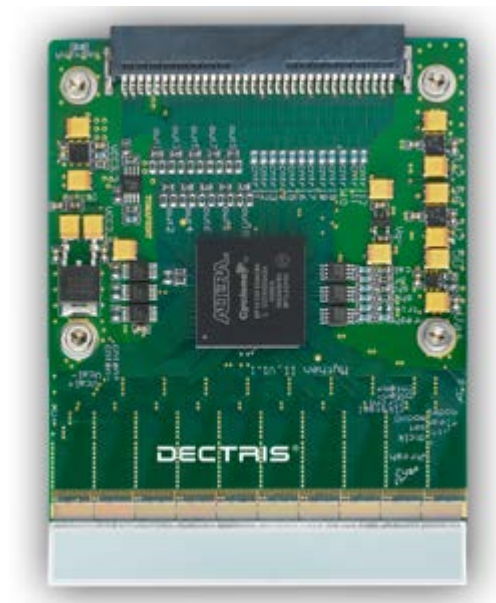
Mythen detector (1D)

|	
Sensor material	Silicon
Sensor	Reverse biased pn-junction array
Detection principle	Single photon counting
Sensor thickness [μm]	320, 450, 1000
Number of channels/module	1280
Sensitive area (width x length) [mm²]	64 x 8
Dimensions of one channel (width x length) [μm²]	50 x 8000
Read out time [ms]	0.3
Maximum count rate per channel [X-rays/s]	$>1\times10^{6}$
Energy range [keV]	5 – 40
Point-spread function	1 channel
Dynamic range [bit]	4, 8, 16, 24 (1 : 16777216)

Image plate (2D)

Unrecorded Imaging Plate

BaFBr : Eu^{2+}

Support

X-ray Photons

Stored Image

Exposure

He-Ne Laser Beam Scanning

Excitation light (633nm)

Luminescence (400nm)

Visible Light

Plate is ready for use again.

Erasing

345

mar
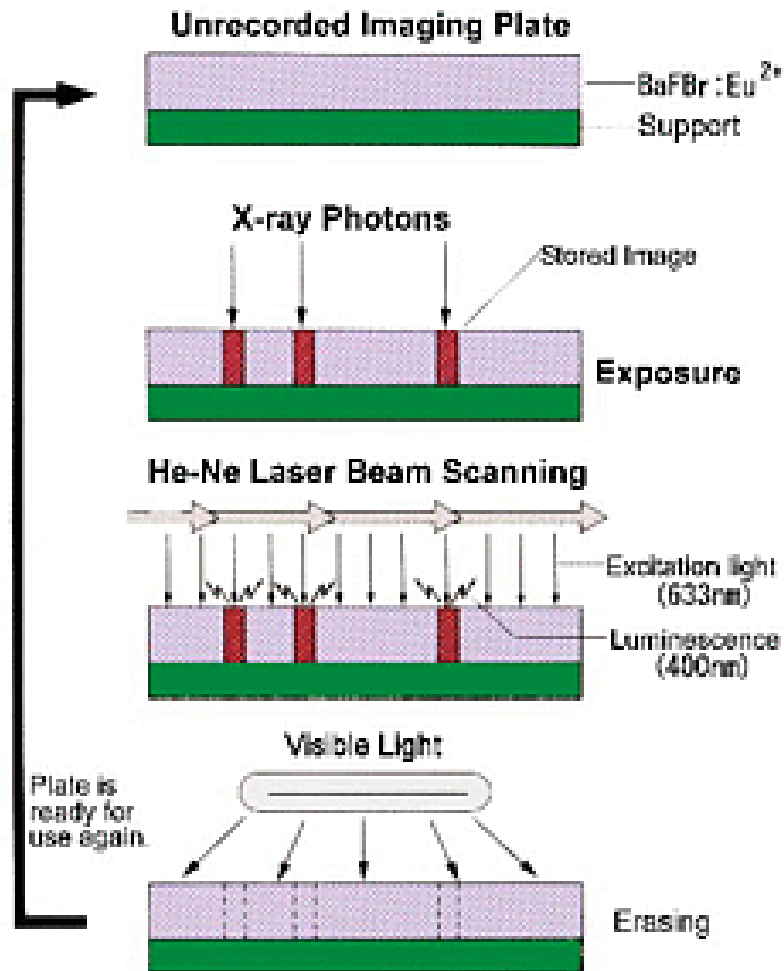
Pilatus detector (2D)

Source: XRD1 - elettra

Source: www.psi.ch
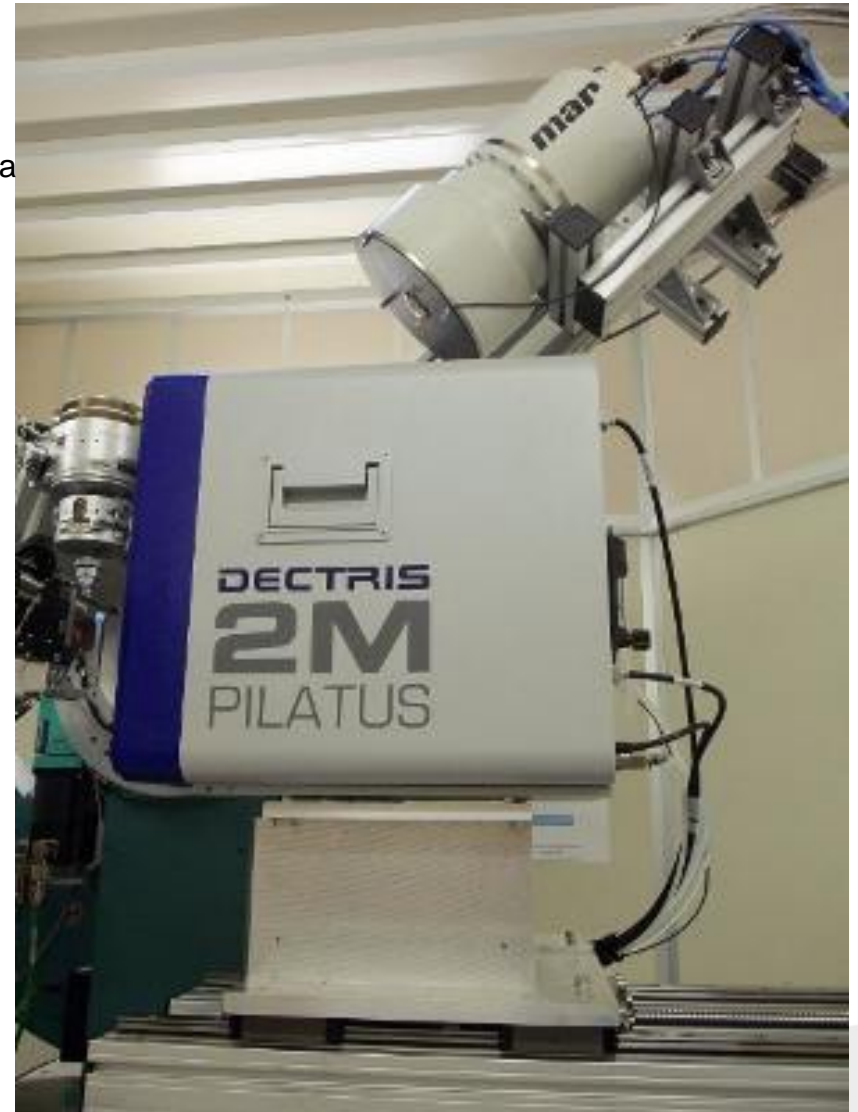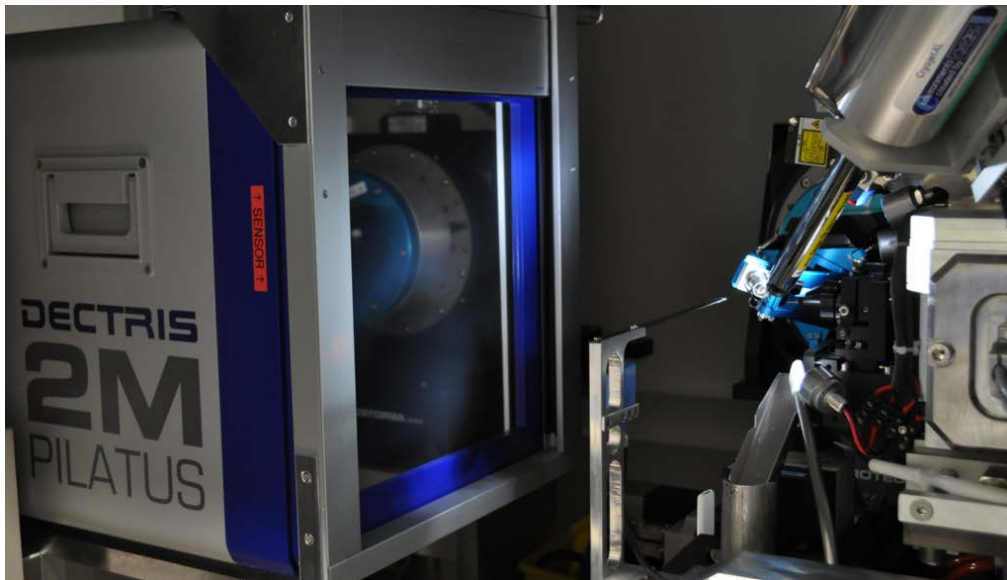
Pilatus detector (2D)

Sensor Pixel
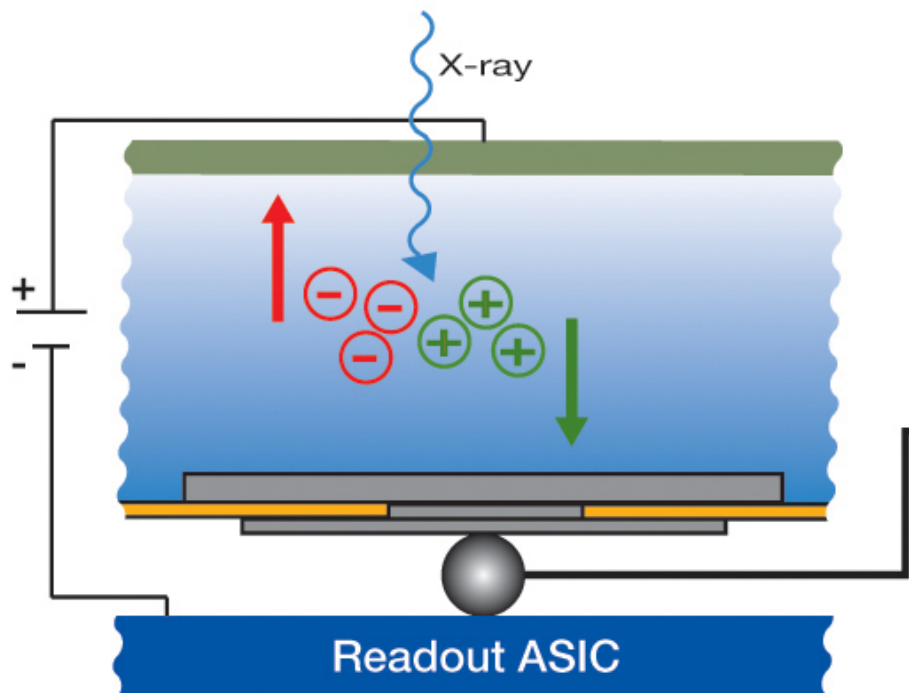
Direct detection of X-rays in semiconductor sensor

→ Point Spread Function 1 pixel

Readout Pixel
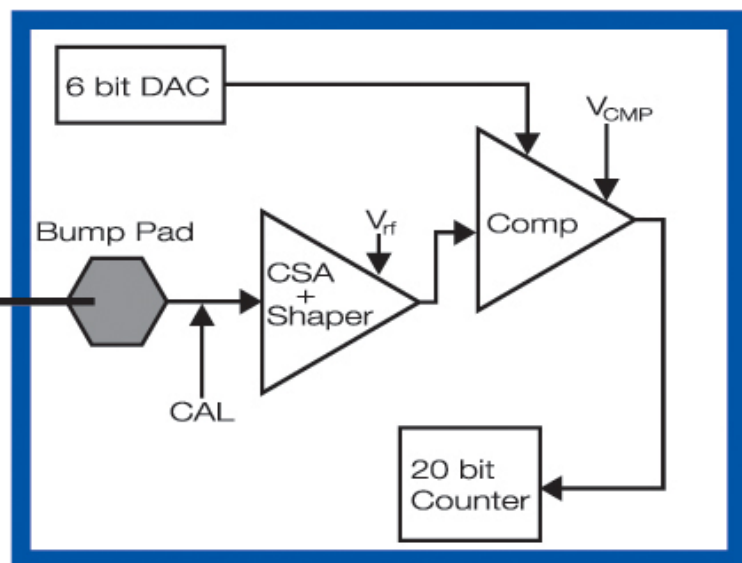
Single Photon Counting ASIC

→ No readout noise or dark current
→ High dynamic range (20 bit)
→ Fast readout

Pilatus detector (2D)

Sensor material	Silicon
Sensor	Reverse biased pn-junction array
Detection principle	CMOS hybrid-pixel technology - single photon counting
Sensor thickness [µm]	320
Number of pixels/module	1475 x 1679 = 2476525 pixels
Sensitive area (width x length) [mm^2]	254 x 289
Dimensions of one pixel (width x length) [µm^2]	172 x 172
Read out time [ms]	3.6 (frame rate 30Hz)
Maximum count rate per channel [X-rays/s]	>1x10^6
Energy range [keV]	3 - 30 keV (quantum efficiency: 3 keV 80%; 8 keV 99%; 15 keV 55%)
Point-spread function	1 pixel
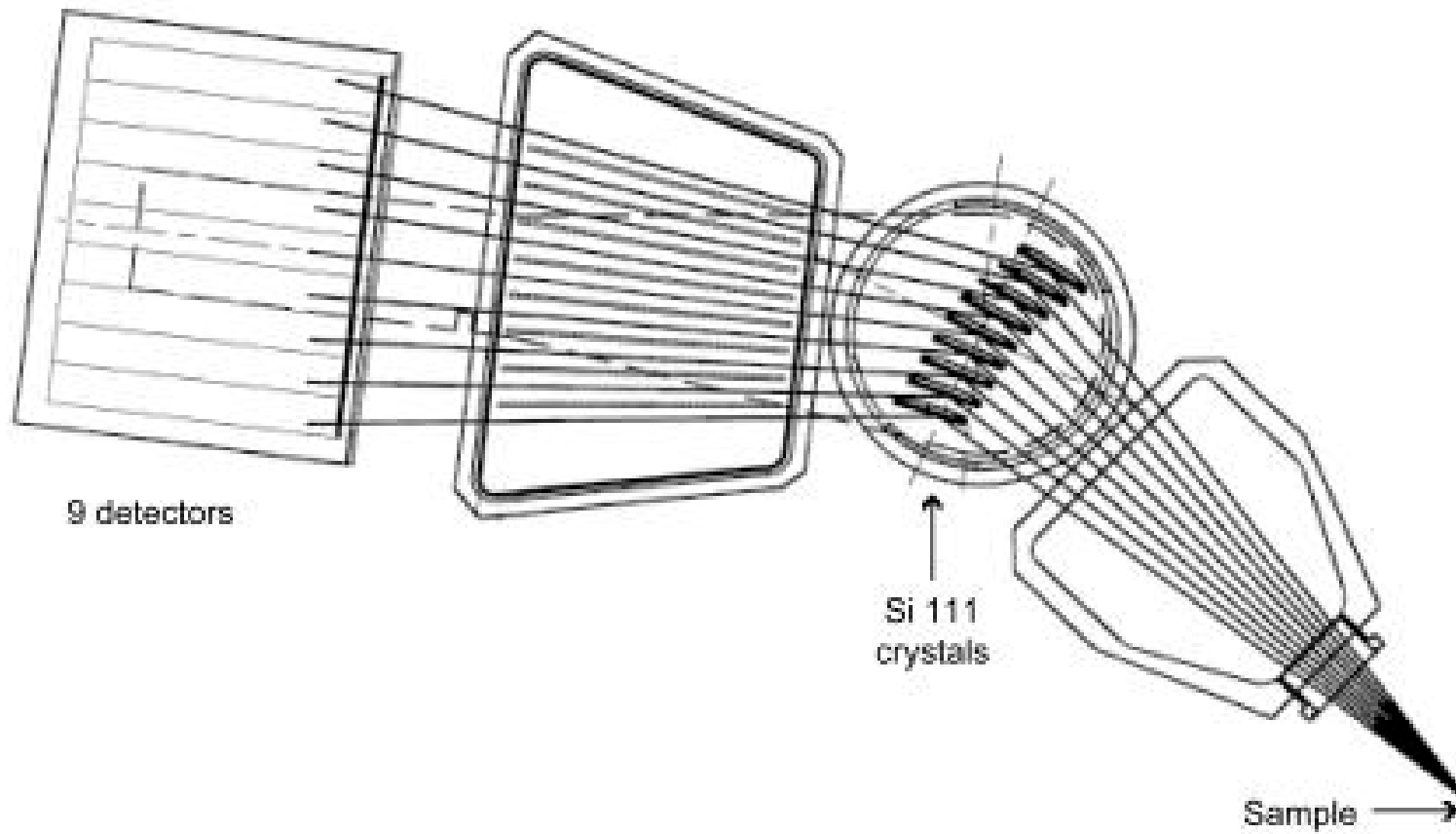
Elettra
Sincrotrone
Trieste

9 detectors

Si 111
crystals

Sample →
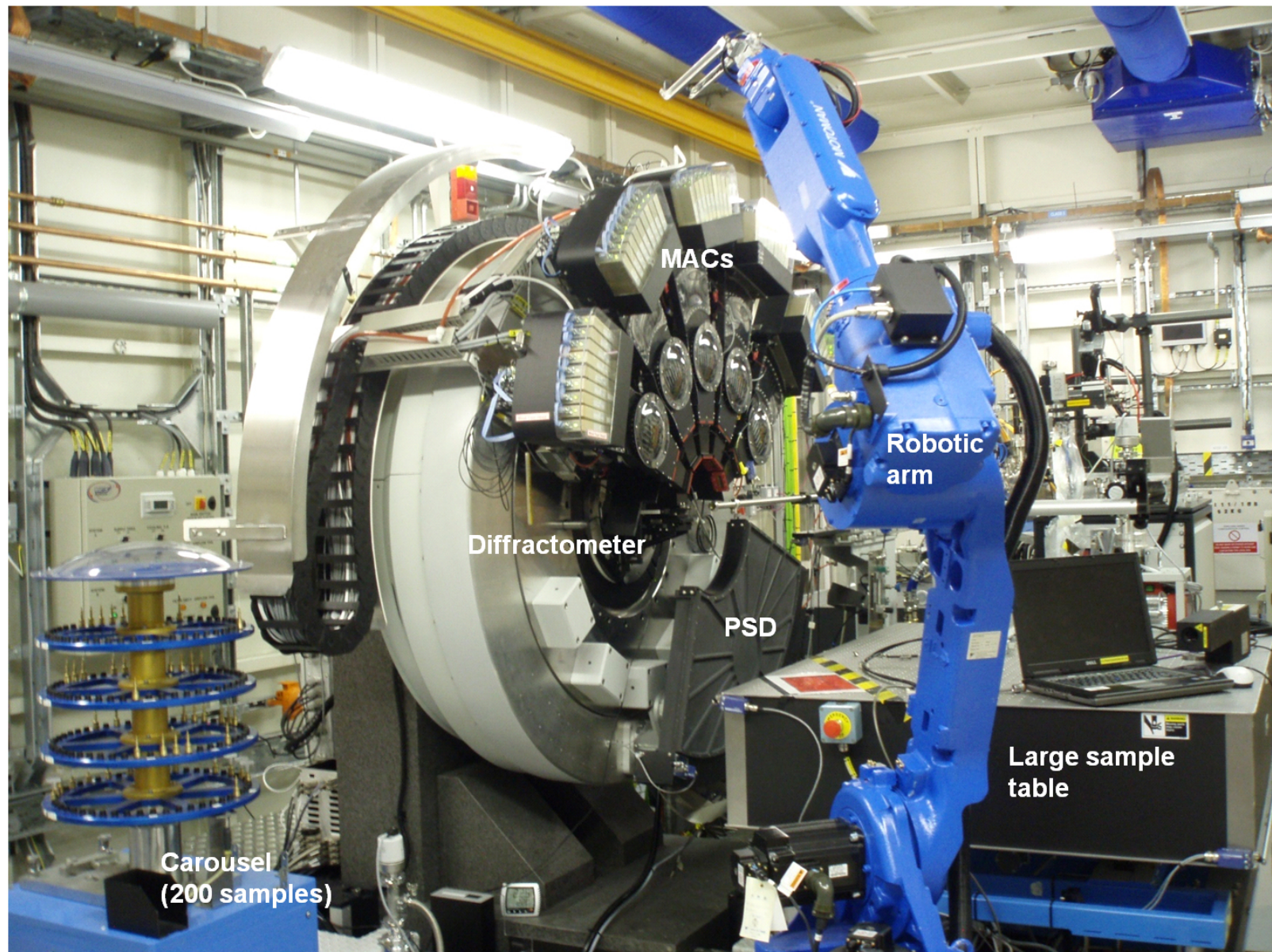
Diffractometer MS

Information from Powder Diffraction

Information from powder diffraction

- The diffraction peak positions give information on the size and shape of the unit cell.

- Shifts in peak positions give information about deformation (eg. Residual stress)

$$\lambda = 2d \sin\theta$$

$$\frac{1}{d^2_{hkl}} = h^2 \frac{b^2 c^2 \sin^2 \alpha}{V^2} + k^2 \frac{a^2 c^2 \sin^2 \beta}{V^2} + l^2 \frac{a^2 b^2 \sin^2 \gamma}{V^2}$$

$$+ 2hk \frac{abc^2 (\cos\alpha \cos\beta - \cos\gamma)}{V^2} + 2kl \frac{a^2 bc (\cos\beta \cos\gamma - \cos\alpha)}{V^2}$$

$$+ 2lh \frac{ab^2 c (\cos\gamma \cos\alpha - \cos\beta)}{V^2}$$

$$d_{hkl} = \frac{a_0}{\sqrt{h^2 + k^2 + l^2}}$$

Simple   Face-centered   Body-centered

CUBIC

Simple   End face-centered

MONOCLINIC

Simple   End face-centered   Body-centered   Face-centered

ORTHORHOMBIC

RHOMBOHEDRAL

Simple   Body-centered

TETRAGONAL

120°

HEXAGONAL

TRICLINIC

Information from powder diffraction

- The Intensity of a diffracted beam, I_{hkl} is related to an imaginary number called the structure factor, F_{hkl} : $I_{hkl} \propto |F_{hkl}|^2$

$$F(hkl) = \sum_n f_n N_n e^{2\pi i(hx_n + ky_n + lz_n)} e^{-B\sin^2\theta/\lambda}$$

- The Intensity of a diffracted beam gives information on the positions of the atoms in the unit cell and hence the 'atomic structure' of the material

- In case of mixtures the intensities give information on the quantity of various materials in the mixture

Structure determination

- **Steps in structure determination from SR-XRPD:**

  - Indexing (DICVOL ecc.)

  - Space group determination

  - Finding a model structure
    - Direct methods
    - Simulated annealing etc. (eg. DASH)
    - Model from similar compounds

  - Refining the structure (Rietveld)
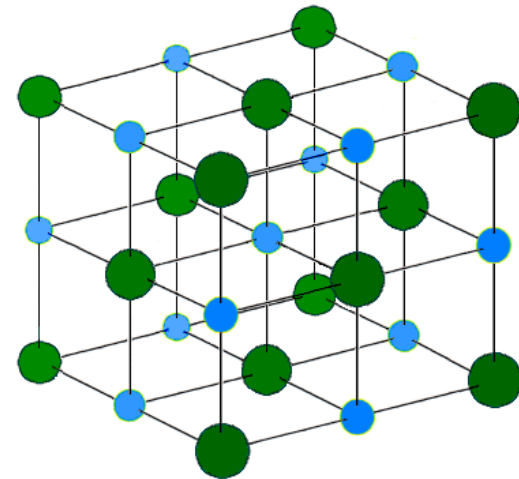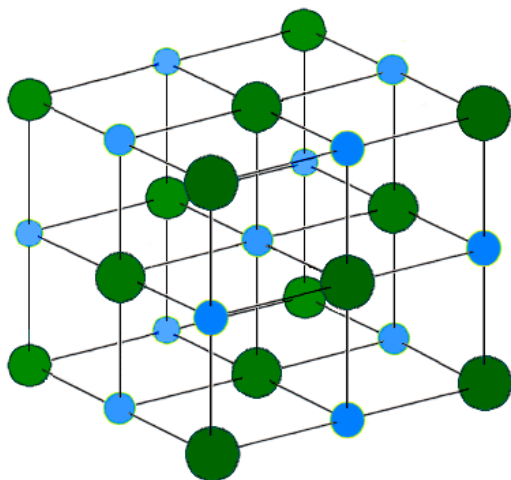
Structure determination Indexing
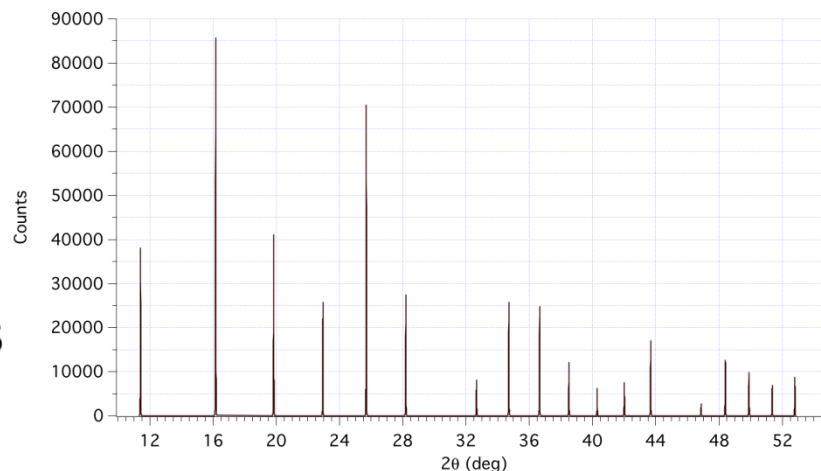
- Known parameters: peak positions
- Unknowns:
  - Unit cell a,b,c, α, β, γ
  - Miller indices: h, k ,lfor each reflection
  - Zero shift ($2\Theta_0$)

$$\frac{1}{d_{hkl}^2} = h^2 \frac{b^2 c^2 \sin^2 \alpha}{V^2} + k^2 \frac{a^2 c^2 \sin^2 \beta}{V^2} + l^2 \frac{a^2 b^2 \sin^2 \gamma}{V^2}$$

$$+ 2hk \frac{abc^2(\cos\alpha\cos\beta - \cos\gamma)}{V^2} + 2kl \frac{a^2 bc(\cos\beta\cos\gamma - \cos\alpha)}{V^2}$$

$$+ 2lh \frac{ab^2 c(\cos\gamma\cos\alpha - \cos\beta)}{V^2}$$

$$d = \lambda / 2\sin(\Theta - 2\Theta_0/2)$$
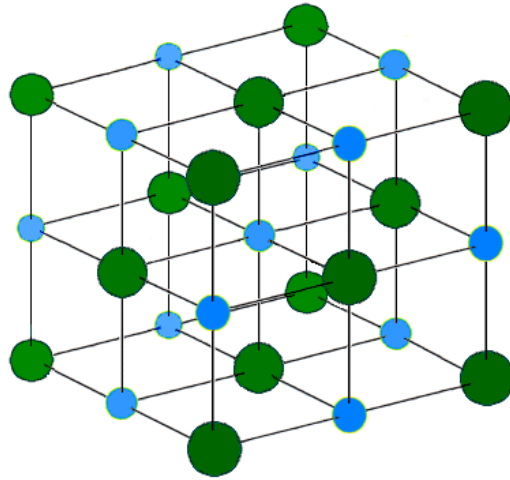
Structure determination
Fining the space group
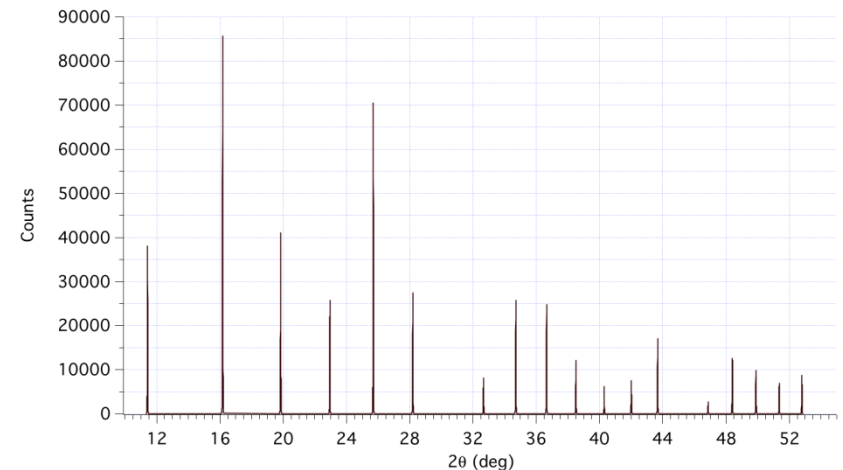
- The space group describe the symmetry in the unit cell (e.g. Centering, mirror planes, rotation axes)

- Some symmetry elements may cause certain reflections to have zero intensity.

- Indentifying these reflection conditions allows to identify the proper space group candidates.

Unit-Cell Geometry	Inferred Crystal System(s)	No. of Space Groups
$a \neq b \neq c$ and $\alpha \neq \beta \neq$ & gamma; & ne; 90°	Triclinic	2
$a \neq b \neq c$ and $\alpha = \gamma = 90°$ and $\beta \neq 90°$	Monoclinic	13
$a \neq b \neq c$ and $\alpha = \beta = \gamma = 90°$	Orthorhombic	59
$a = b \neq c$ and $\alpha = \beta = \gamma = 90°$	Tetragonal	68
$a = b = c$ and $\alpha = \beta = \gamma \neq 90°$	Trigonal (Rhombohedral)	7
$a = b \neq c$ and $\alpha = \beta = 90°$ and $\gamma = 120°$	Trigonal or Hexagonal	45
$a = b = c$ and $\alpha = \beta = \gamma = 90°$	Cubic	36
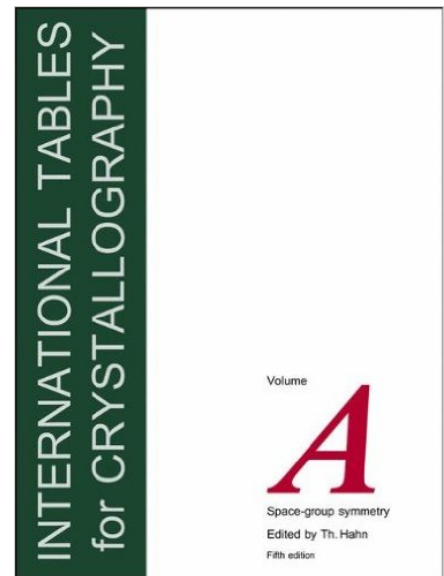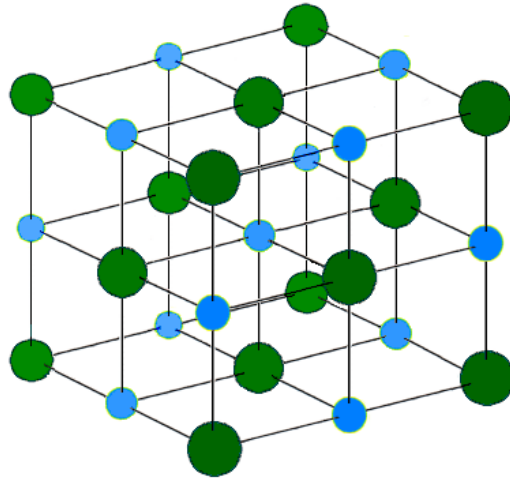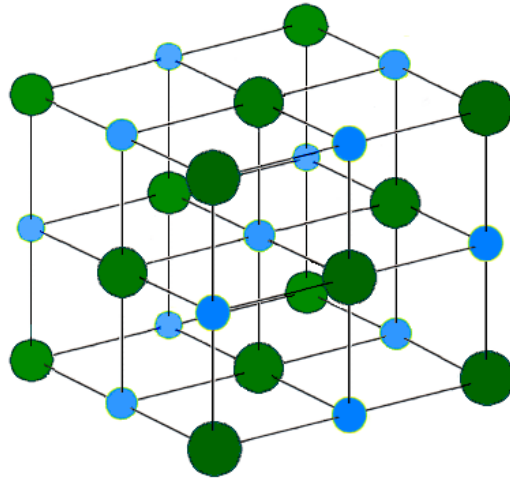
Structure determination
Finding the space group

Reflection Condition(s)		Possible Space Group(s)	
None	$\rightarrow$	$P2$ Pm $P2/m$	(3) (6) (10)
$0k0: k = 2n$	$\rightarrow$	$P2_1$ $P2_1/m$	(4) (11)
$h0l: l = 2n$	$\rightarrow$	Pc $P2/c$	(7) (13)
$h0l: l = 2n$ and $0k0: k = 2n$	$\rightarrow$	$P2_1/c$	(14)
$hkl: h + k = 2n$	$\rightarrow$	$C2$ Cm $C2/m$	(5) (8) (12)
$hkl: h + k = 2n$ and $h0l: l = 2n$	$\rightarrow$	Cc $C2/c$	(9) (15)

Structure determination
Finding a starting model

a)

b)

O

N

C
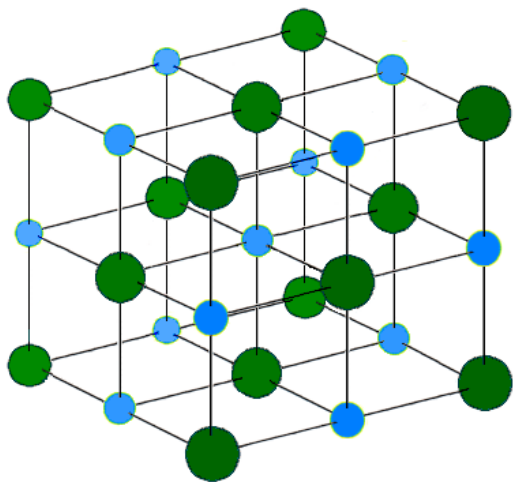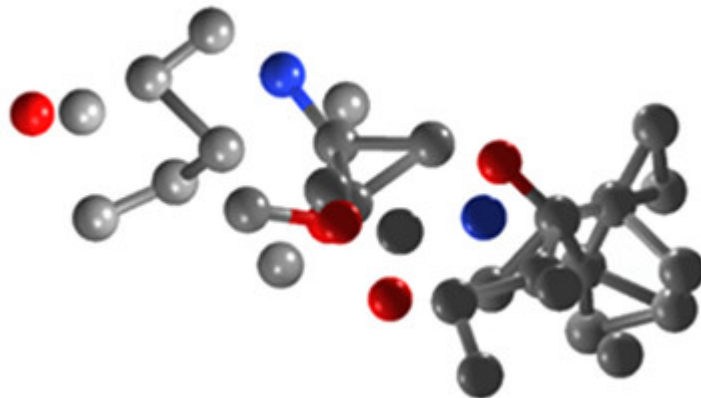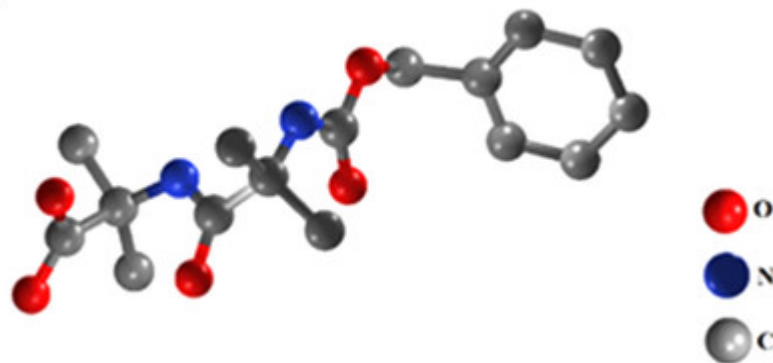
Parameters refined in Rietveld refinement:

- Background (fixed, functions)
- Peak shape (microstructural parameters, functions)
- Lattice constants – Zero pont correction – Sample displacement
- Scaling – phase fractions
- Structural parameters (Atoms positions, occupancies, B)
- Preferred orientation
- Absorption

Parameters are adjusted, and a diffraction pattern is calculated until the best fit wih the measured pattern is obtained

$$F(hkl) = \sum_{n} f_n N_n e^{2\pi i(hx_n + ky_n + lz_n)} e^{-B\sin^2\theta/\lambda}$$

$$I(hkl) \sim |F(hkl)|^2$$

$$y_i = I_k \exp\left[\frac{-4\ln(2)}{H_k^2}(2\theta_i - 2\theta_k)^2\right]$$

$$H_k^2 = U\tan^2\theta_k + V\tan\theta_k + W$$

$$M = \sum_{i} W_i \left\{ y_i^{obs} - \frac{1}{c} y_i^{calc} \right\}^2$$
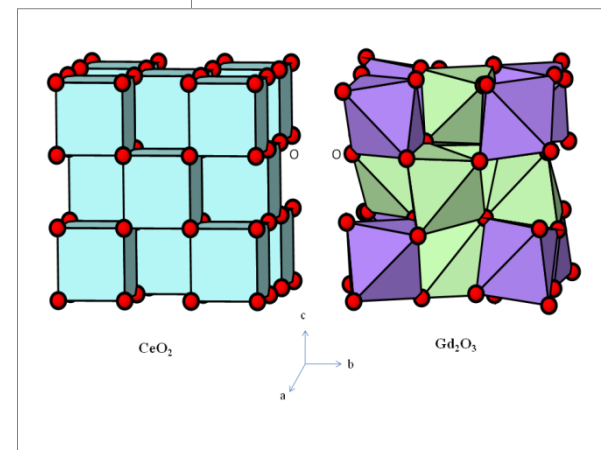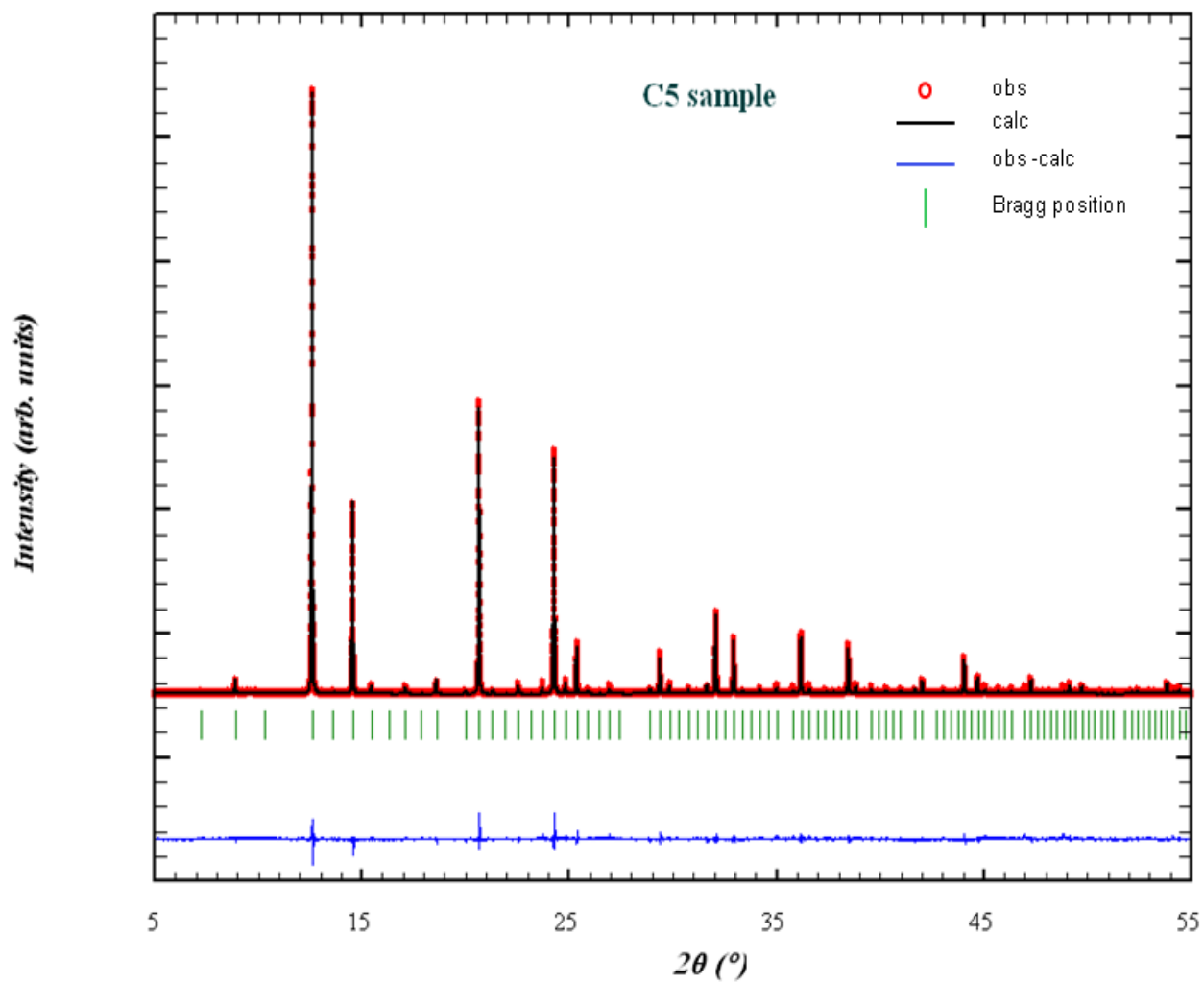
Information from powder diffraction

- **1895** Rontgen discovered X-rays

- **1912** Laue measured the first diffraction pattern of crystal

- **1913** Braggs published first crystal structures

- **1918** Paul Scherrer published the Scherrer formula to determine the size of nanocrystals

$$B(2\theta) = \frac{K\lambda}{L\cos\theta}$$

- Peak width (*B*) is inversely proportional to the nanocrystal size *(L).*

P. Scherrer, "Bestimmung der Grösse und der inneren Struktur von Kolloidteilchen mittels Röntgenstrahlen," *Nachr. Ges. Wiss. Göttingen* **26** (1918) pp 98-100.

- The shape of the peak give information about the microstructure of the materials

A diffraction peak is a **convolution** ( ) of *profile components* produced by different sources.
These are instrumental factors (IP) and effects due to domain size (S), microstrain (D), faulting (F), anti-phase domain boundaries (APB), stoichiometry fluctuations (C), grain surfacerelaxation (GSR), etc.

$$I(s) = I_{IP}(s) \otimes I_S(s) \otimes I_D(s) \otimes I_F(s) \otimes I_{APB}(s) \otimes I_C(s) \otimes I_{GRS}(s)...$$

Information from powder diffraction

Instrumental profile

LaB$_6$ Diffraction Profile, E = 15 keV

GoF = 0.647

FWHM ≈ 0.016 deg

FWHM ≈ 0.017 deg
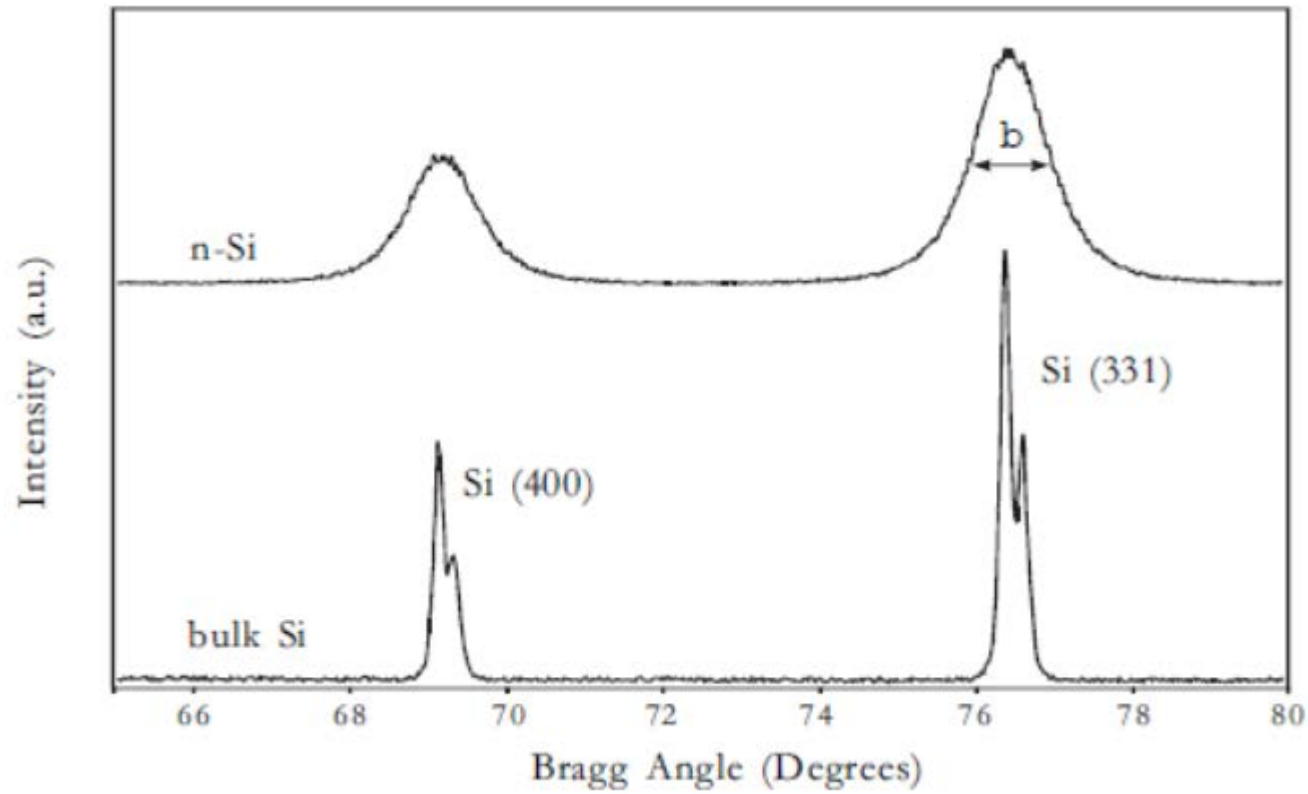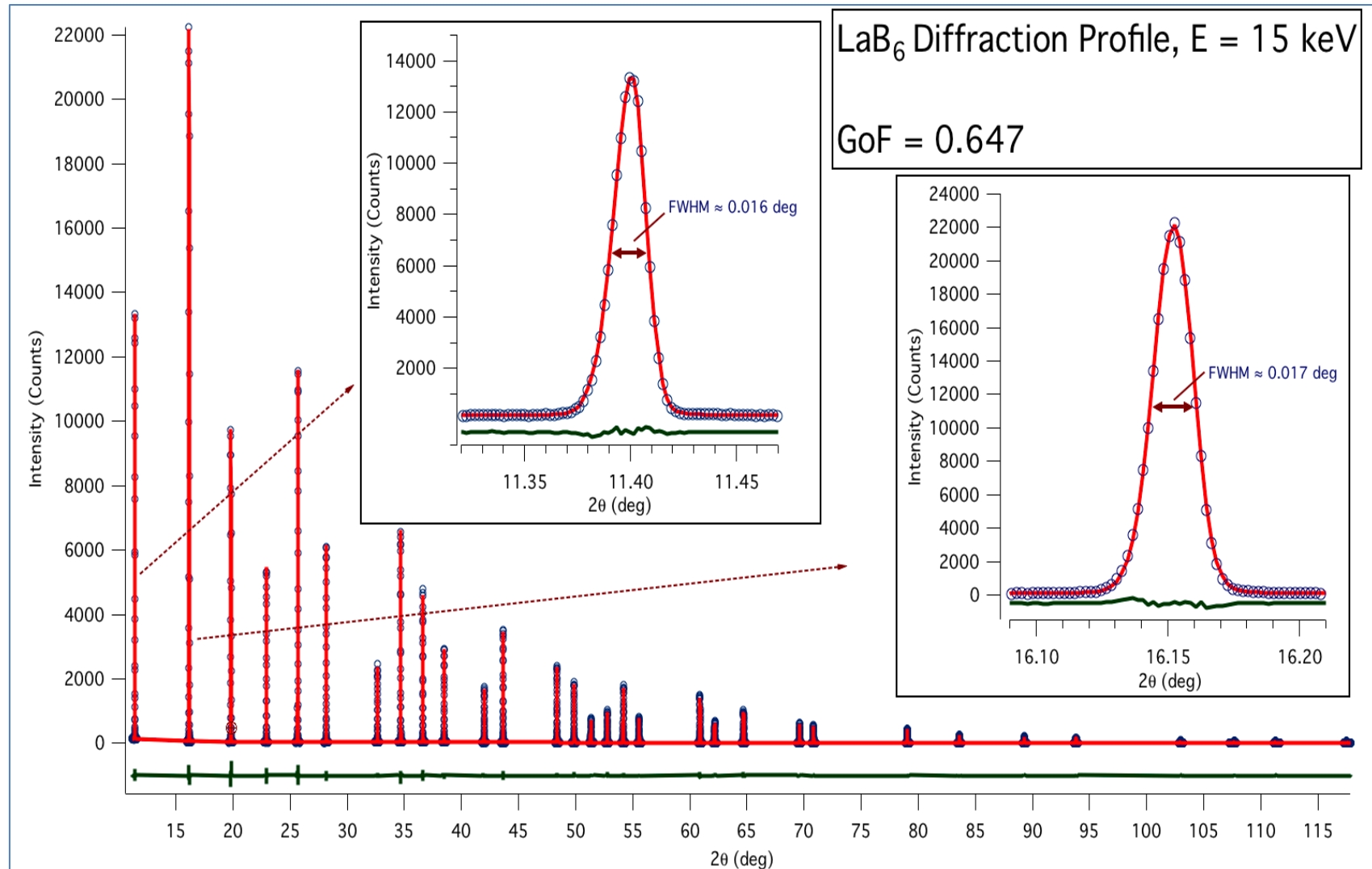
- We want to measure the intensity profile in reciprocal space
  - position of diffraction peaks (d_{hkl})
  - intensity (I_{hkl})
  - peak profile

- **IMPORTANT**: a correct measurement assumes:
  - the homogeneous spatial distribution of the crystallites in the sample
  - the homogeneous probing of the material by the beam
  - the statistically correct measurement of intensity
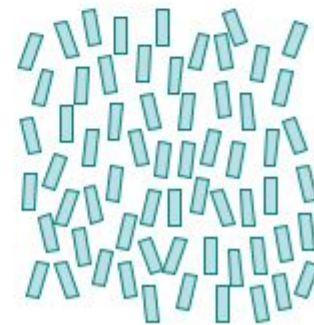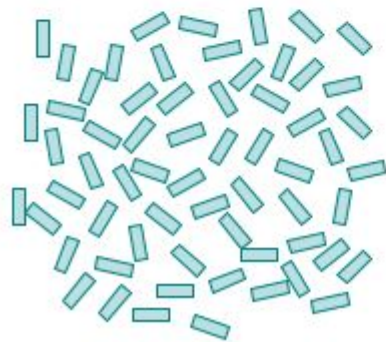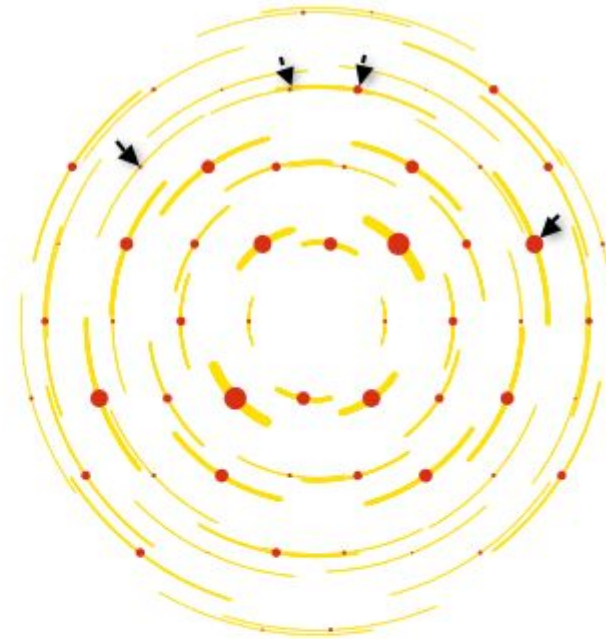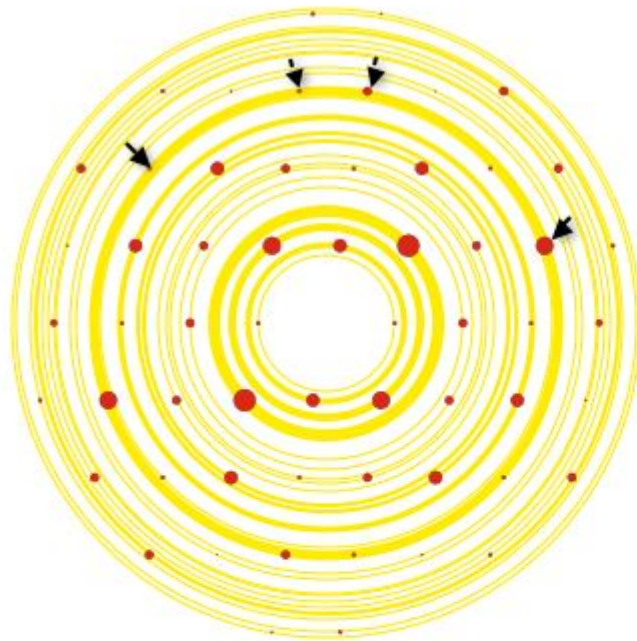
Texture

Texture
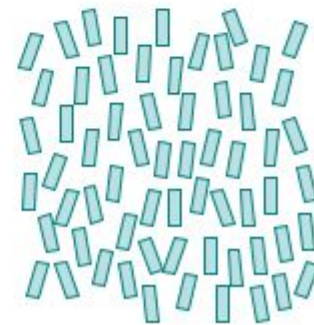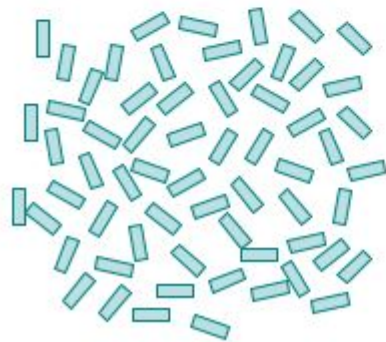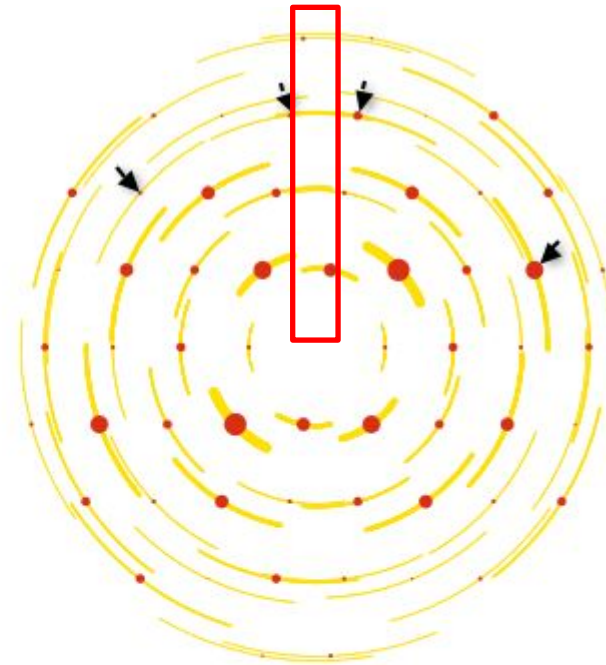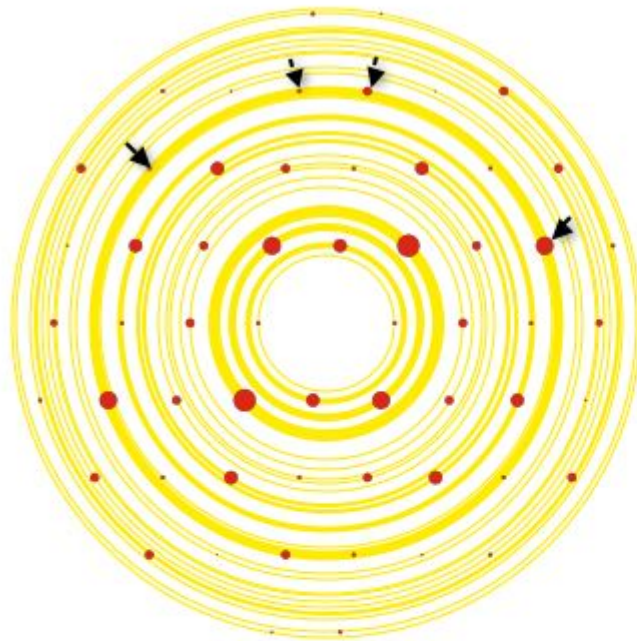
Few cristallites
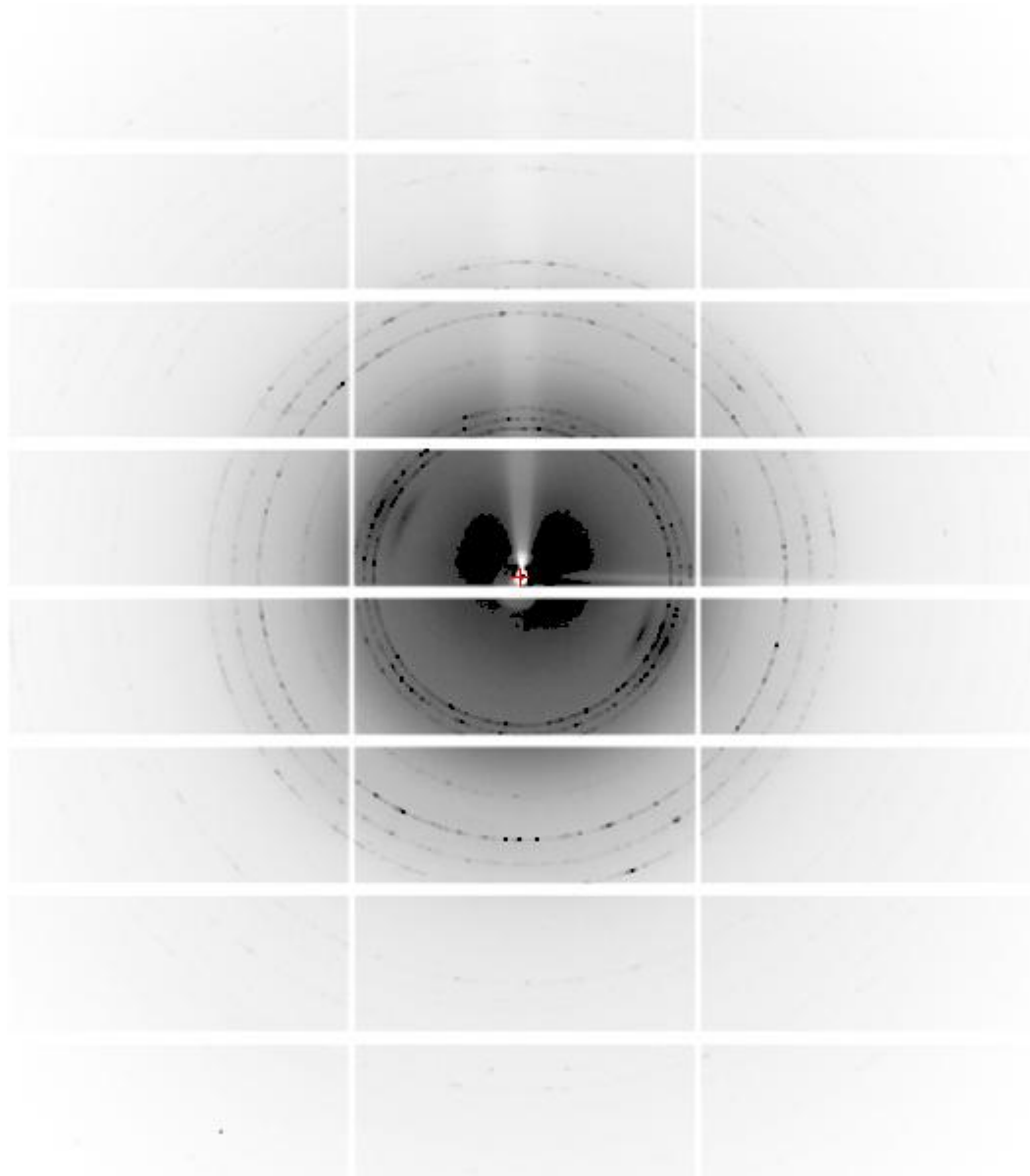
Polarisation
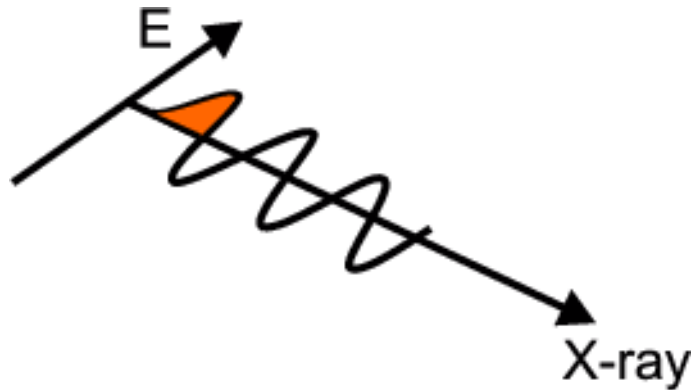
Synchrotron
Radiation is horizontally polarised in the plane of the electron orbit
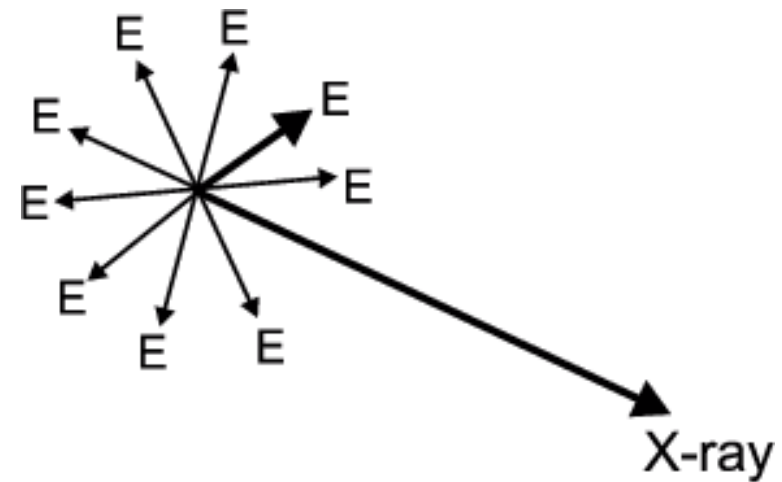
Laboratory source
Unpolarised radiation
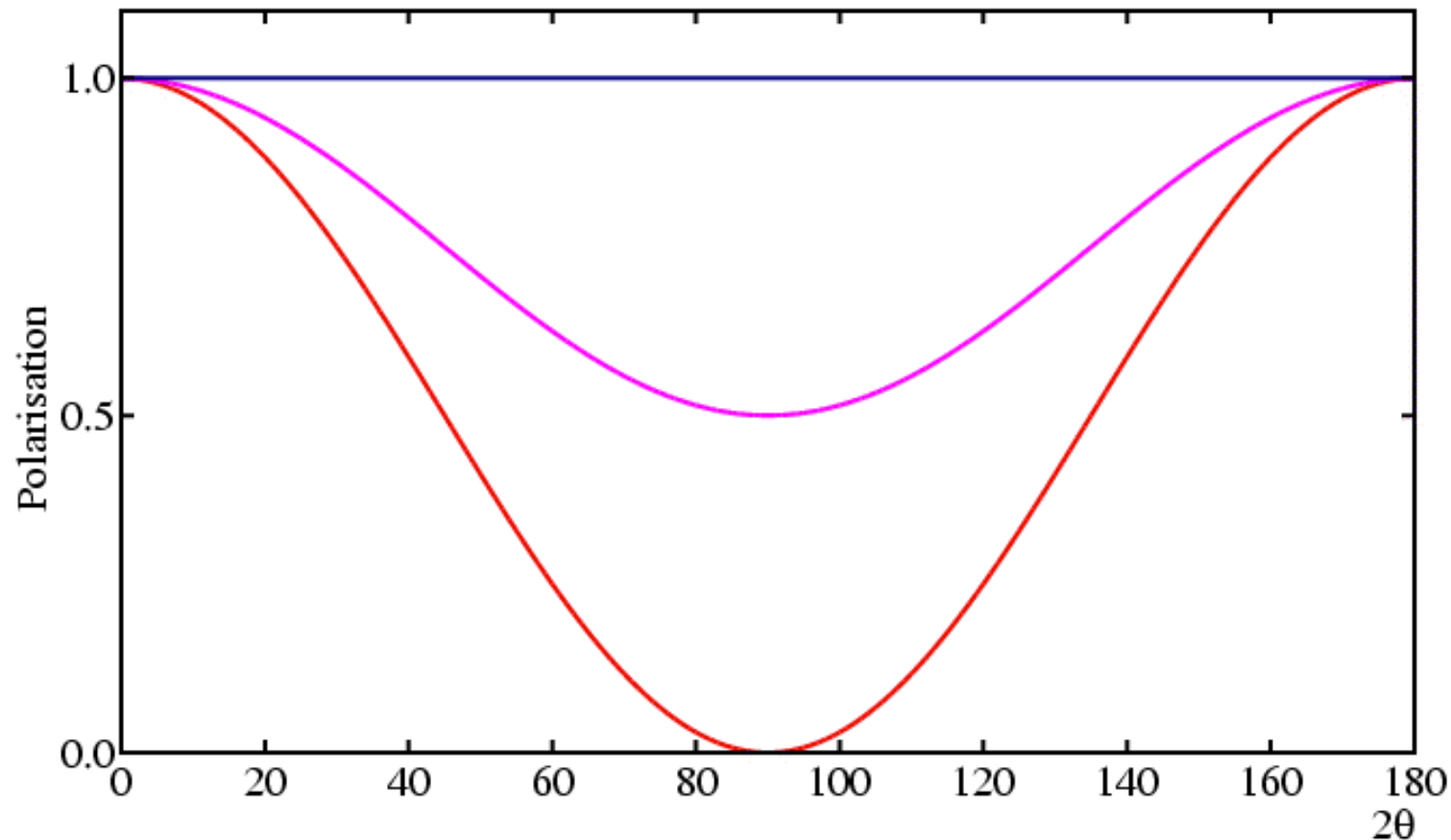
Red: Polarisation in plane of scattering $\quad P = \cos^2 2\theta$

Blue: Polarisation perpendicular to plane of scattering $\quad P = 1$

Pink: Unpolarised X-rays $\quad P = (1 + \cos^2 2\theta)/2$

Polarisation
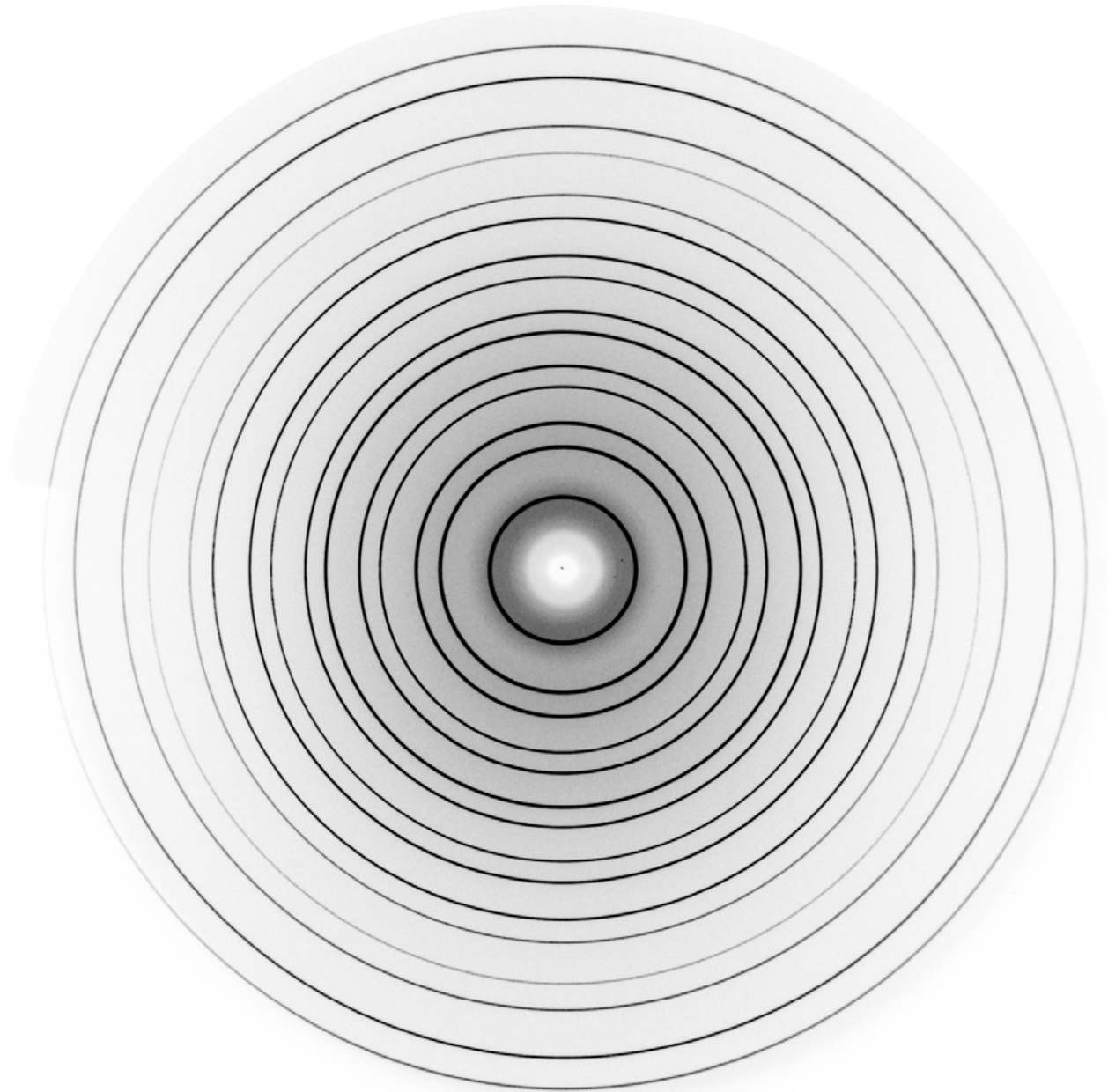
Absorption
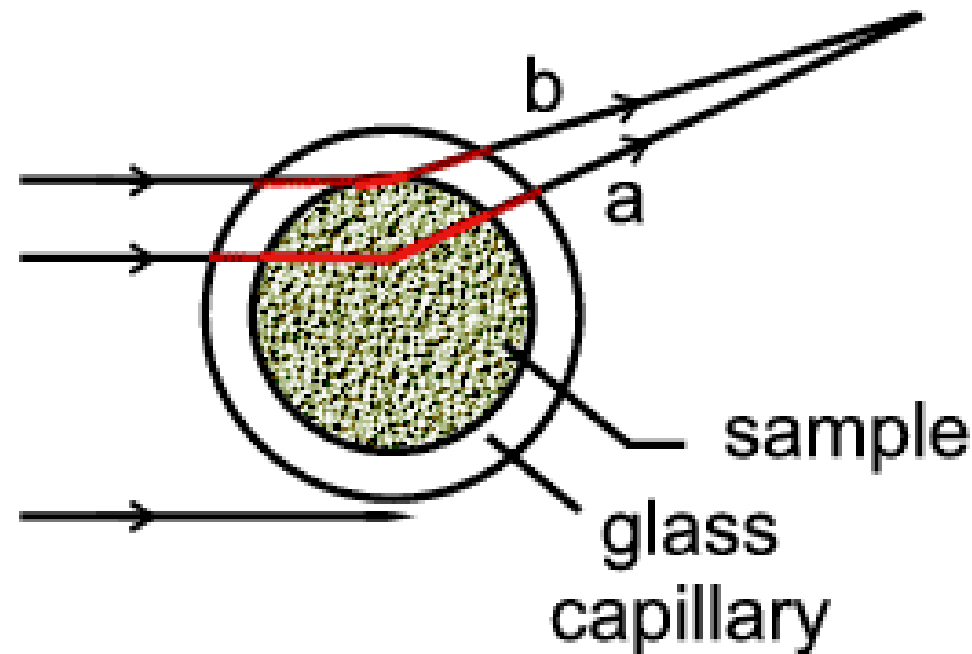
Capillary: The effect is not easy to calculate but the result is satisfying. As the example above illustrates, some paths appear to be like transmission (a) and others like reflection (b). Correction for this effect can be made if the absorption of the sample is not too large.

Absorption

BaTiO3 Density=3.5 Thickness=200. microns
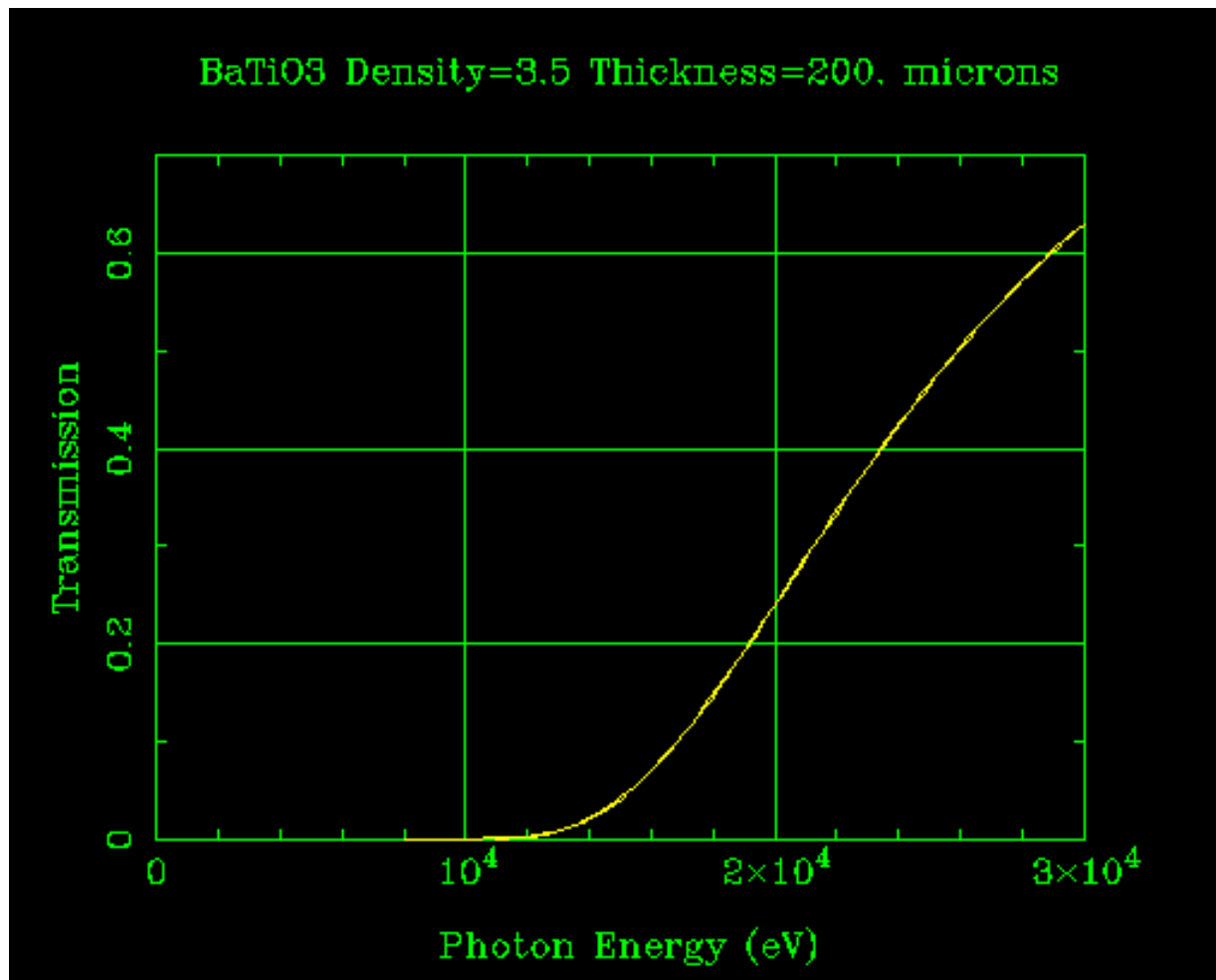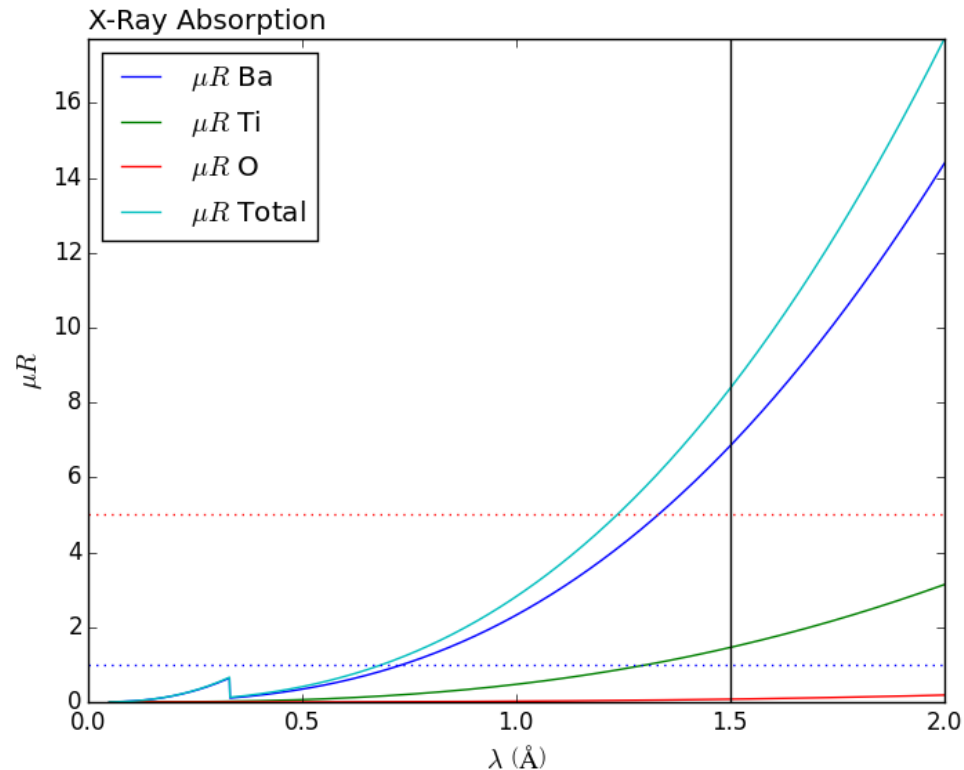
Absorption

The plot above shows the absorption for each input element and for the specified composition as a function of X-ray wavelength/energy. The blue dotted line indicates a muR value of 1. In a capillary (Debye-Scherrer) geometry, it is ideal when muR is 1 or below, as sample absorption is minimal and no correction is usually needed. The red dotted line indicates a muR value of 5. For muR >= 5, measurements are generally not possible in a capillary geometry, as there will be very severe levels of absorption and corrections are inaccurate. (source: http://11bm.xray.aps.anl.gov/absorb/absorb.php)

Absorption

high angle

glancing

θ   θ

θ
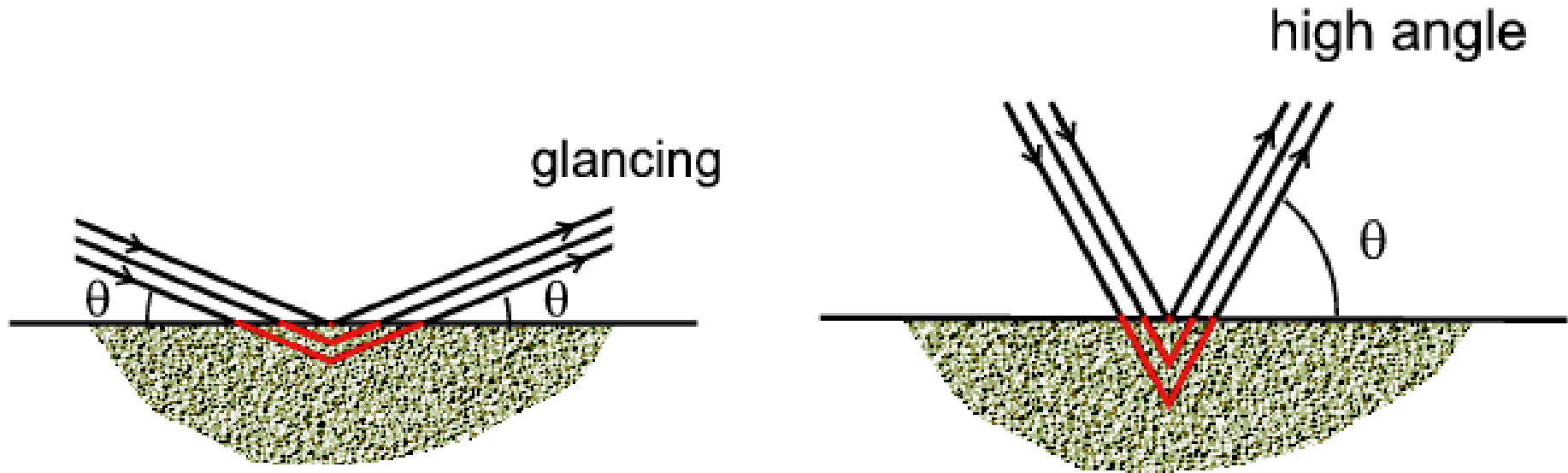
Bragg-Brentano: The effect might not be so obvious how to calculate but result is that when all the possible path lengths are taken in to account, the net absorption remains constant with θ. This means that the effect of absorption can effectively be ignored in this case since it affects all reflections equally. Therefore this geometry may be an alternative when dealing with strongly absorbing samples

Applications of XRPD

- Phase identification (search match procedures)

- Crystal structure determination (ab initio solution and refinement)

- Quantitative Phase Analysis (QPA)

- Amorphous phase analysis and total Scattering – PDF analysis

- Crystalline domain size/shape and lattice defect analysis (LPA)

- Determination of preferred orientations (Texture Analysis)

- Residual Stress Analysis

- … and more

Phase identification - example

Basilica dei santi Giovanni e Paolo

XIII-XVI century
End XV large stained glass windows

Glass samples: Grisaille

- Low melting glass (SiO_2, PbO,)
- Pigment (metal oxides)
- Paint medium (water, vinegar, oil)
- Firing to fuse the grisaille on the glass

Phase identification - example

SSGP3

SSGP1/2

SSGP2

SSGP1

SSGP2

SSGP3
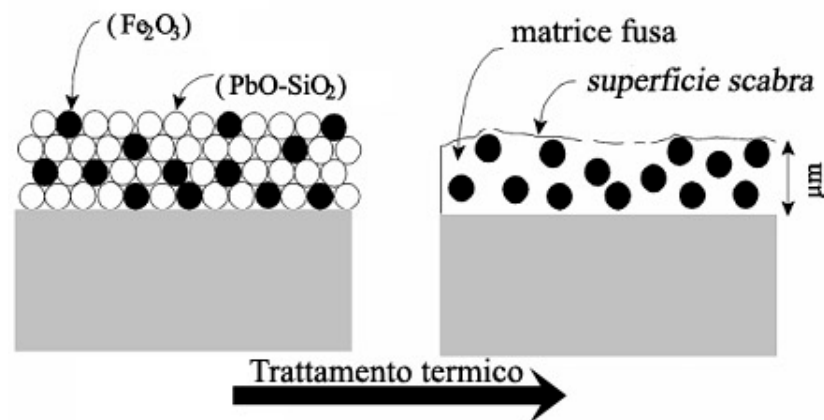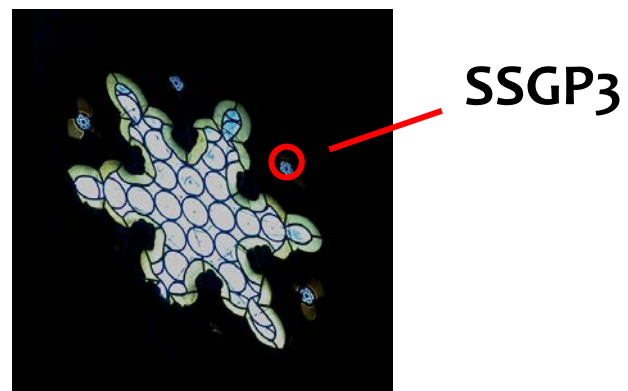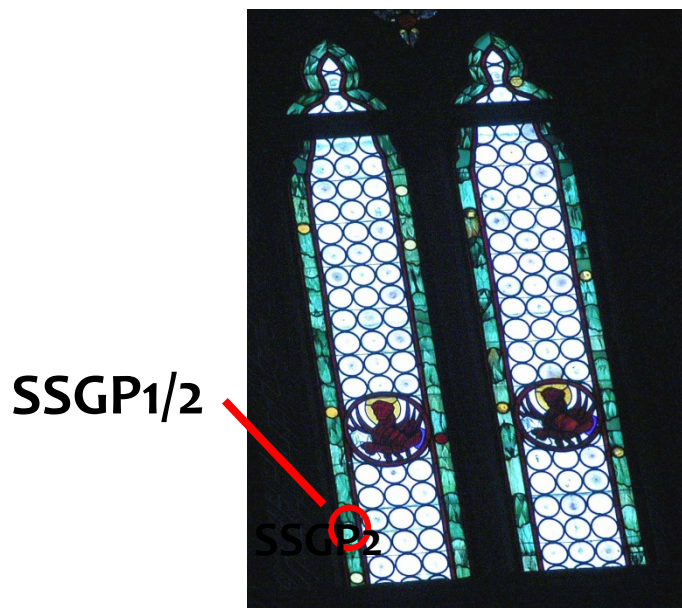
Phase identification - example

E = 9.4 keV
λ = 1.319Å
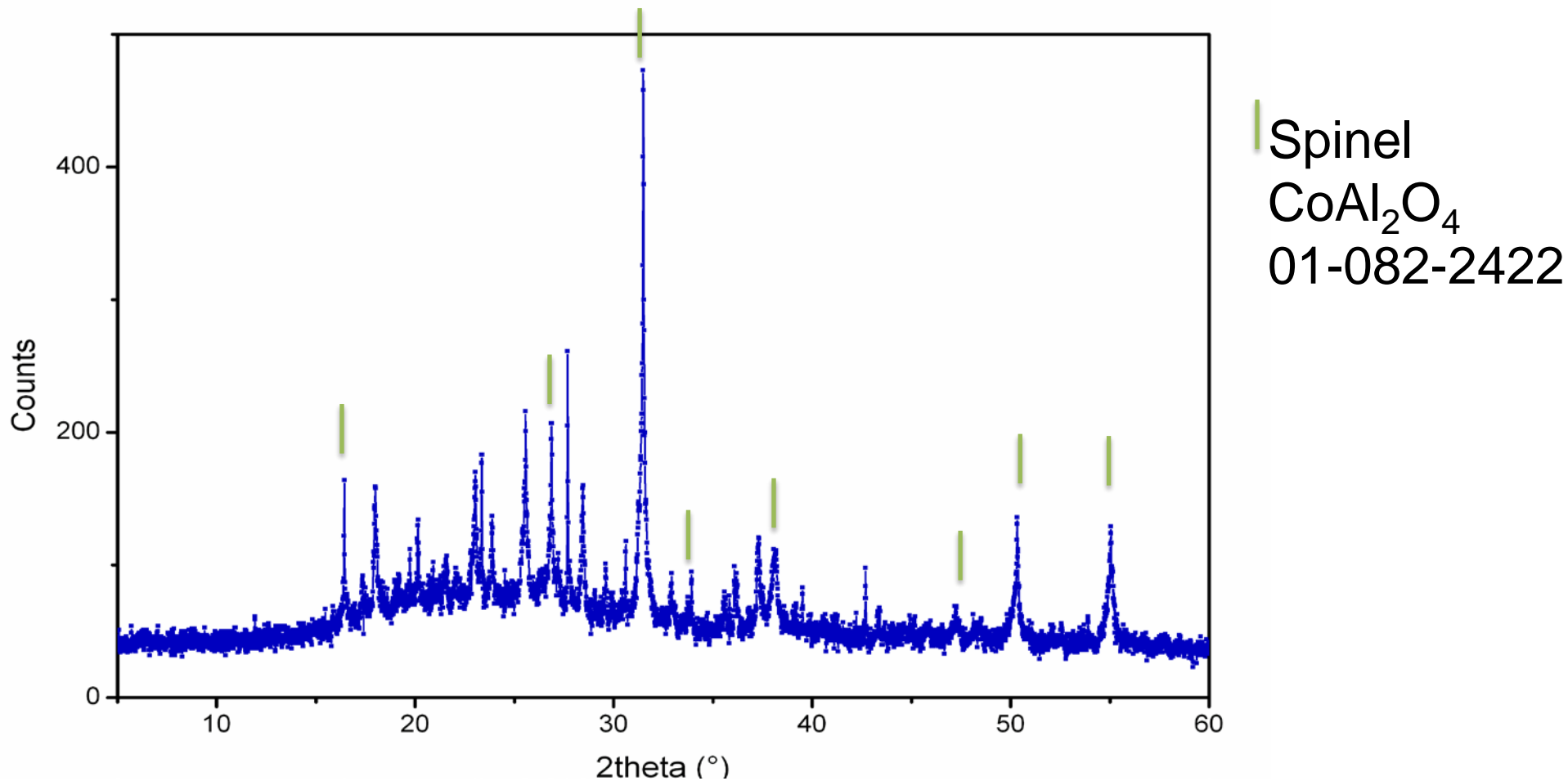
Phase identification - example

Spinel
$CoAl_2O_4$
01-082-2422

Phase identification - example

Spinel
$CoAl_2O_4$
01-082-2422

Laurionite
$PbCl(OH)$
04-012-3672

Phase identification - example

Spinel
$CoAl_2O_4$
01-082-2422

Laurionite
$PbCl(OH)$
04-012-3672

Anglesite
$PbSO_4$
04-008-8386
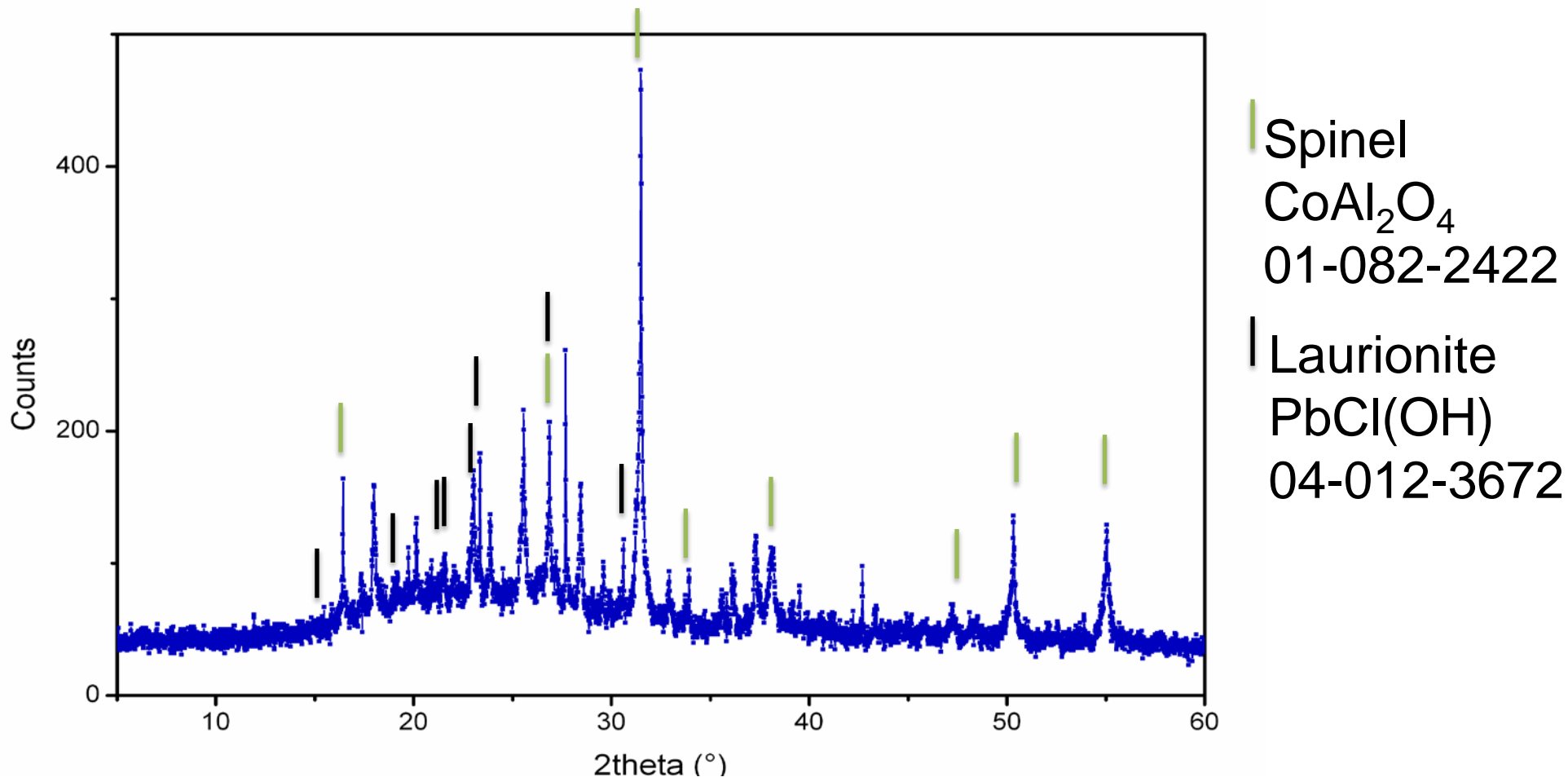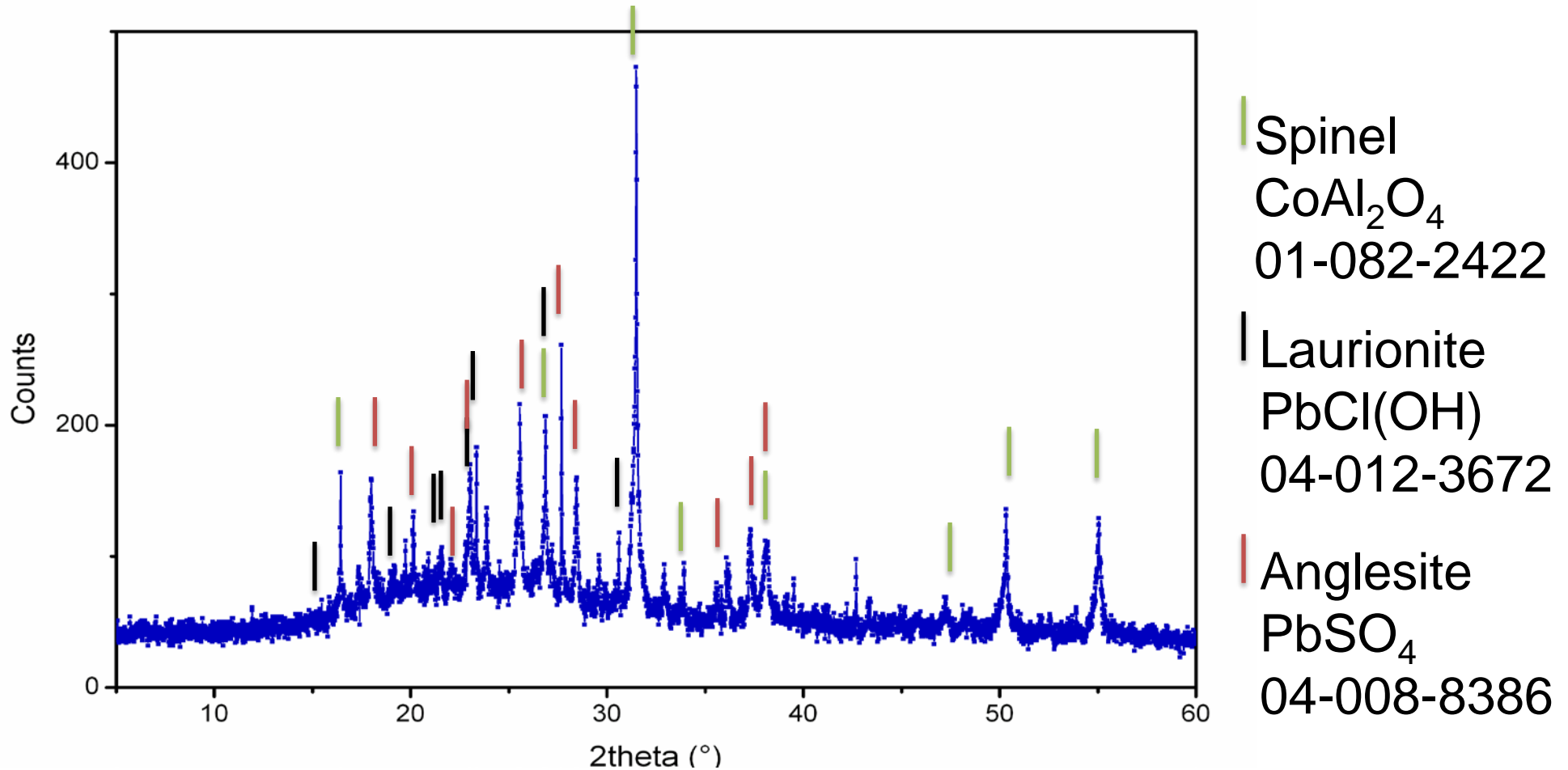
Phase identification - example

GRISAGLIA

PATINA

$CoAl_2O_4$; $PbSO_4$; $Pb(OH)Cl$ Amorphous

$Pb_2Sb_2O_7$; $PbSO_4$;
$CaSO_4(H_2O)_2$; $CaAl_2Si_2O_8$

$FeO(OH)$; $FeSO_4(OH)(H_2O)_2$
$PbSO_4$; $CaSO_4(H_2O)_2$;
$Al_2Si_2O_5(OH)_4$

$CoAl_2O_4$; $PbSO_4$;
$CaPO_3(OH)_2H_2O$

SiO_2; PbS; $PbSO_4$;
$CaCO_3$ (vat)$_2$
$CaPO_3(OH)_2H_2O$

Phase identification - example

- **$Pb_2Sb_2O_7$** : original pigment

- **SO_4^{2-}, S^{2-}, CO_3^{2-}** : alteration product seawater-aerosol , acid rain

- **$FeO(OH)$; $FeSO_4(OH)(H_2O)_2$** : alteration product of original pigments

- **CO_3^{2-}, PO_3^{3-}**: biological origin

- **$CoAl_2O_4$** : intervention at later date?

Elettra
Sincrotrone
Trieste
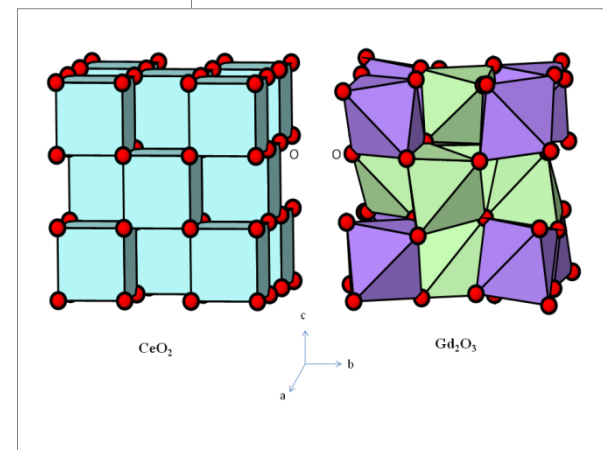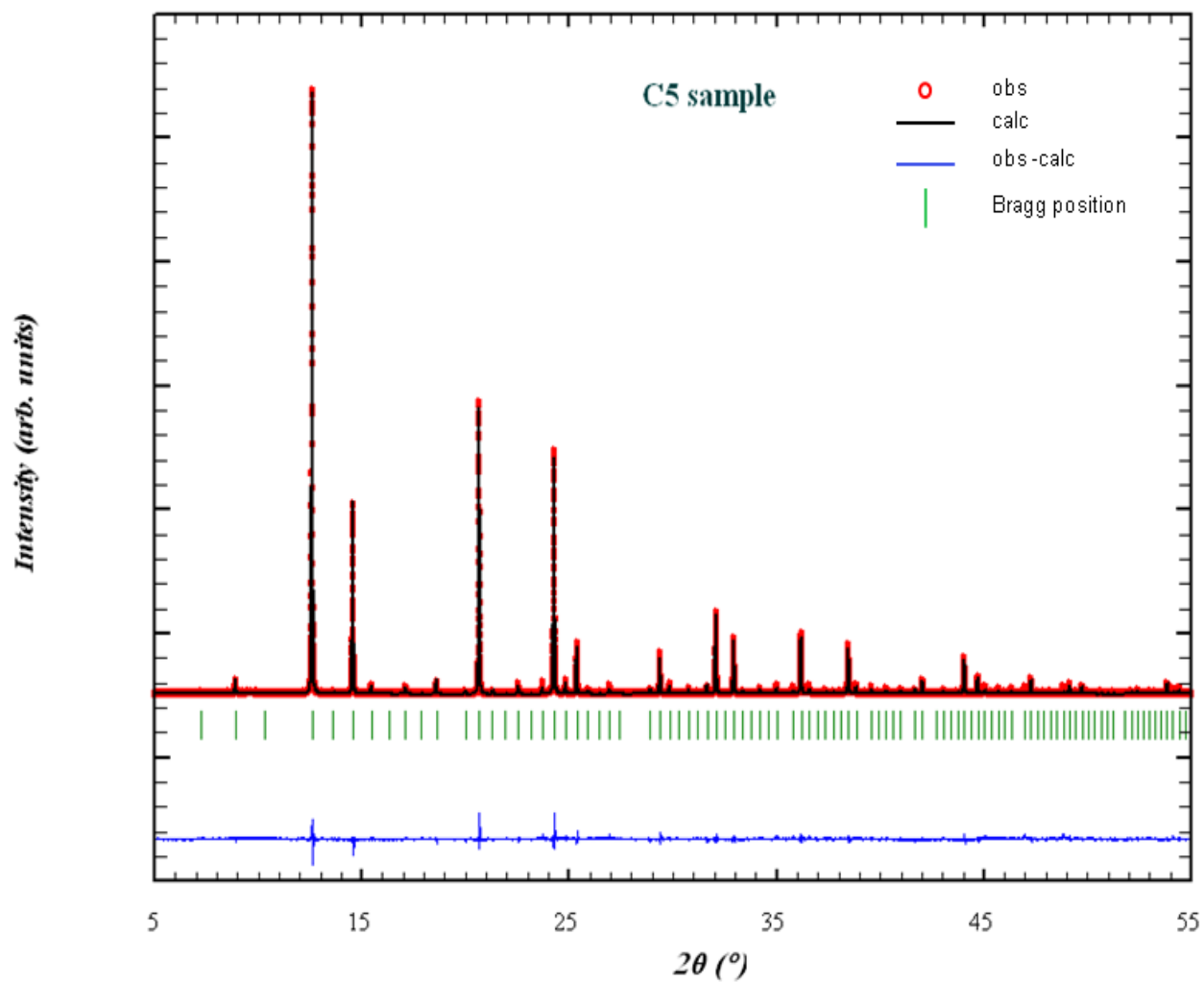
- Direct localzation of atoms in mixed-occupancy powders by resonant contrast diffraction, M.K. Panda *et al.*, H. Palancher *et al.*, *Angew. Chem. Int. Ed.*, **44**, 1725-1729 (2005)
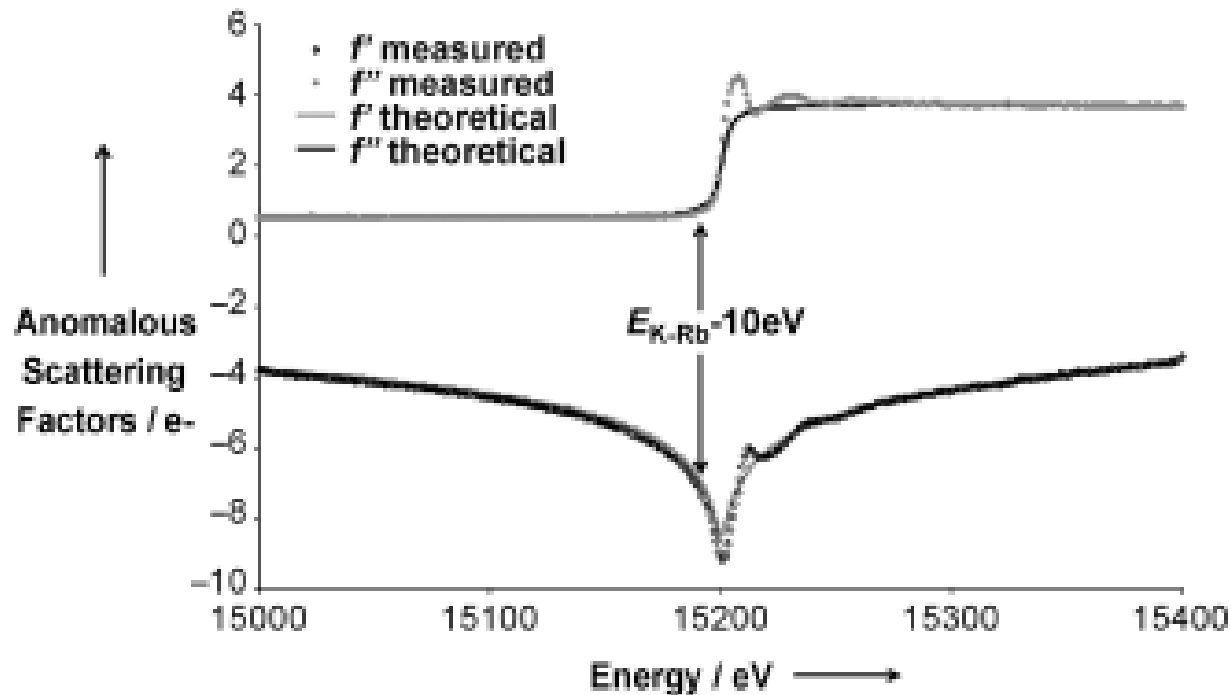
$$f = f_o + \Delta f' + i.\Delta f''$$

Structure determination - example

- Resonant scattering variations near an absorption edge provide chemical sensitivity and are used to extract the contribution of a single element to each crystallographic site.

- The method was demonstrated for highly-crystalline solids of industrial interest: bicationic X zeolites to determine Sr^{2+} and Rb^+ cation distributions in SrRbX

- Since Sr^{2+} and Rb^+ have the same number of electrons and similar neutron scattering lengths (b_{Sr} = 0.702 x 10^{-12} cm; b_{Rb} = 0.709 x 10^{-12} cm) this is a particularly difficult case for conventional X-ray or neutron diffraction
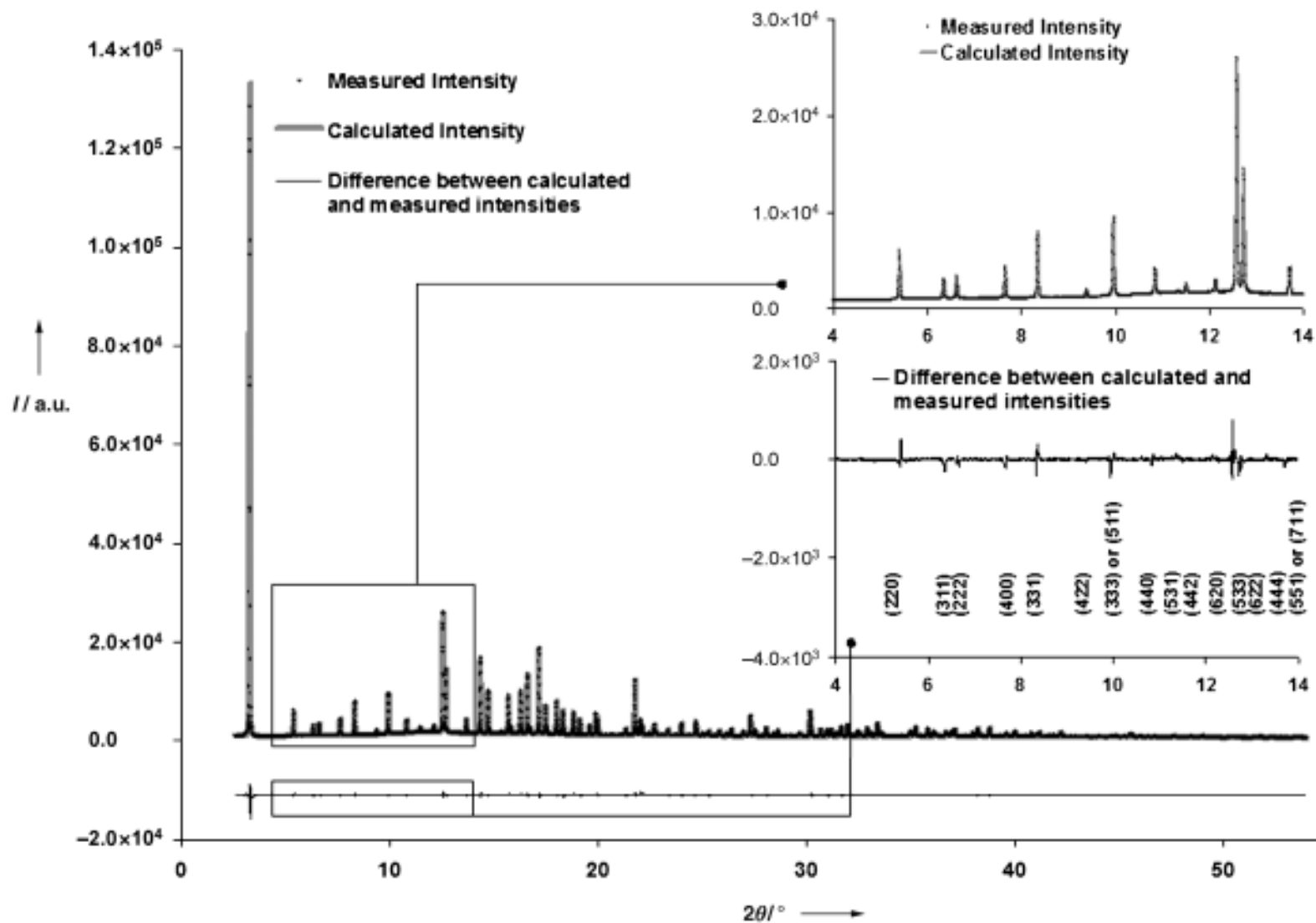
Structure determination - example
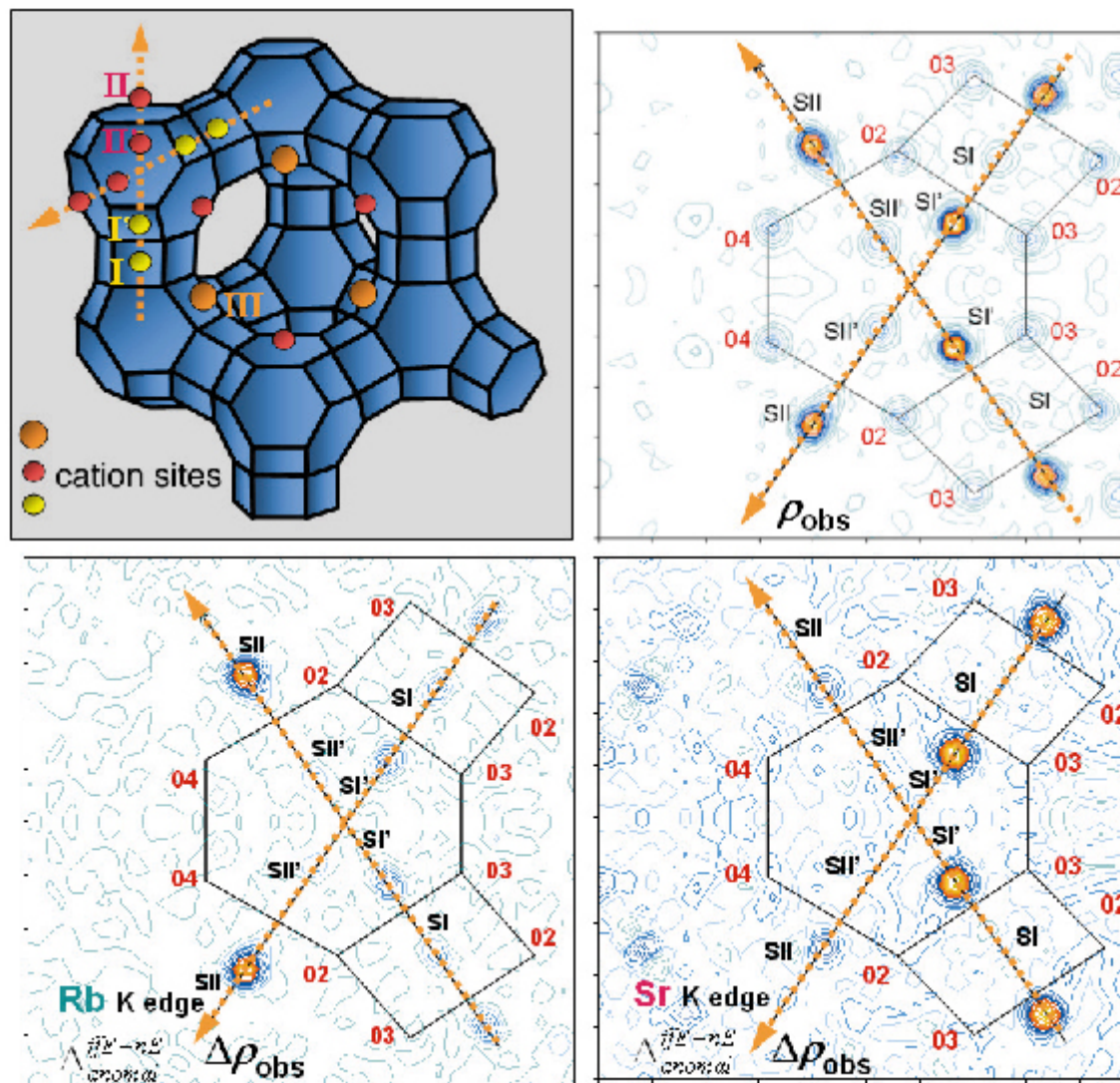
Structure determination - example

XRPD in non ambient conditions

Gas out

Gas in

Goniometer head
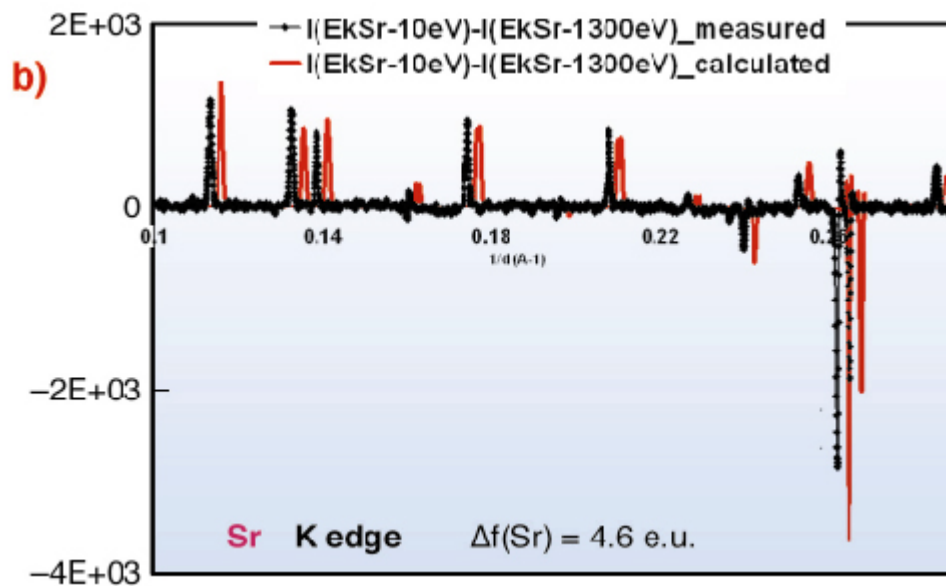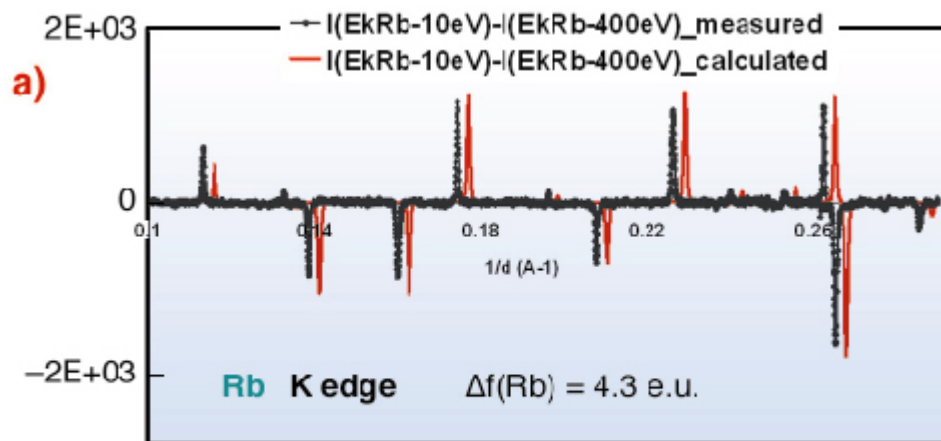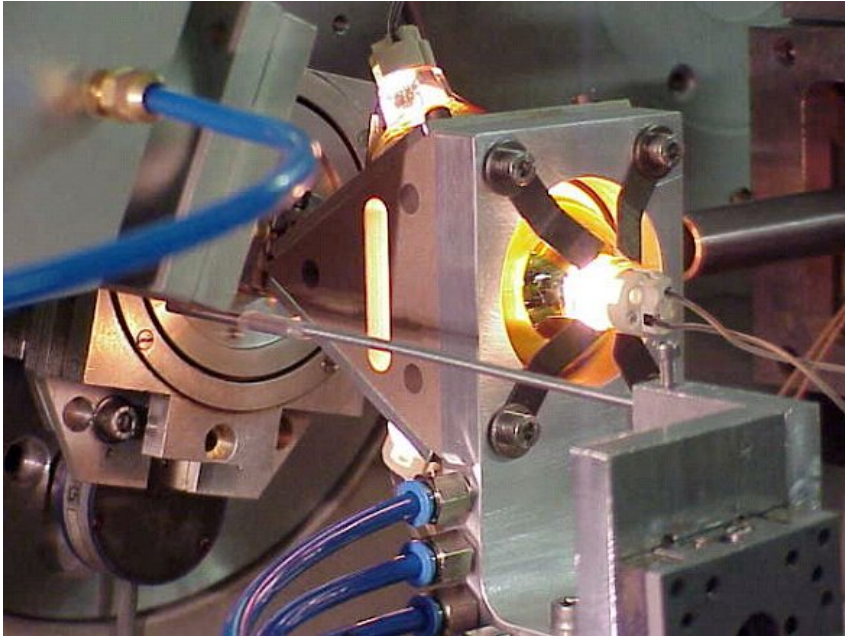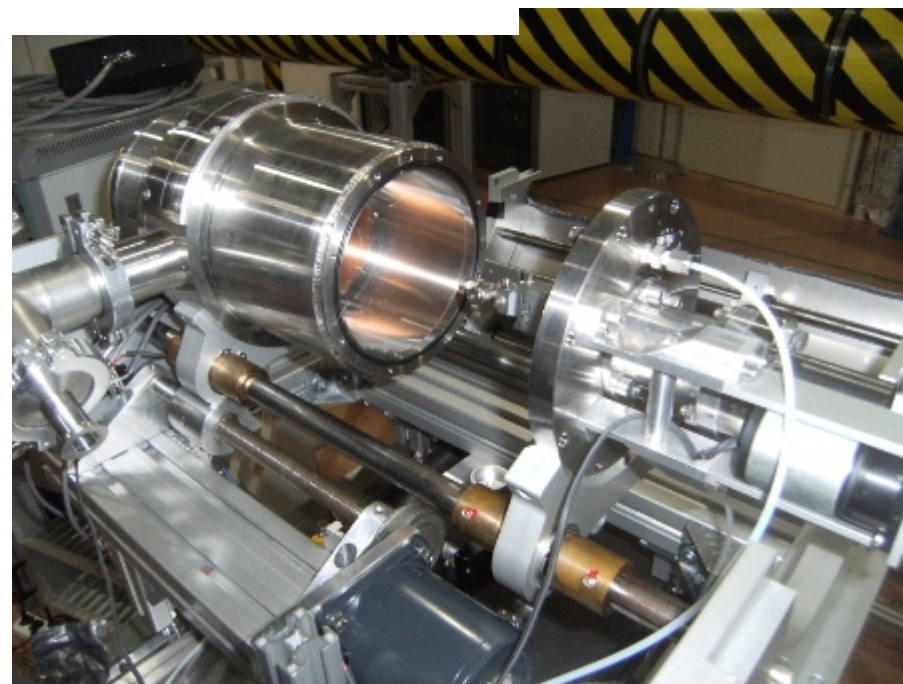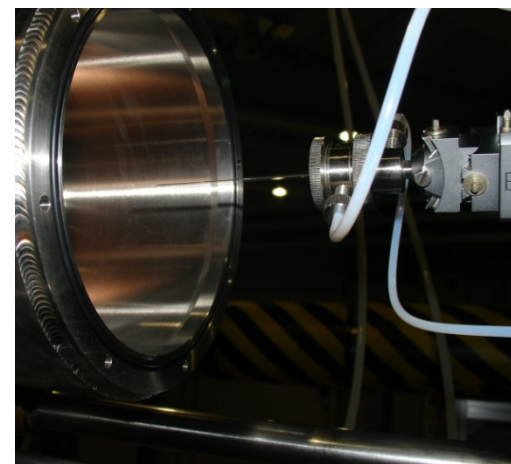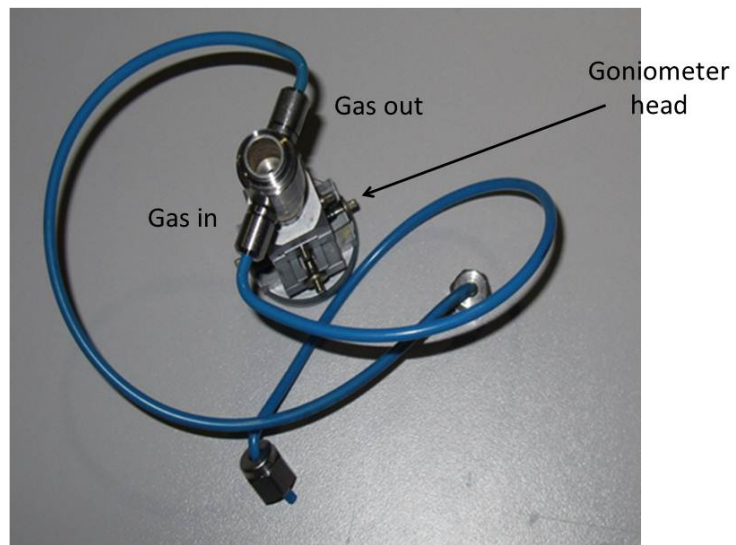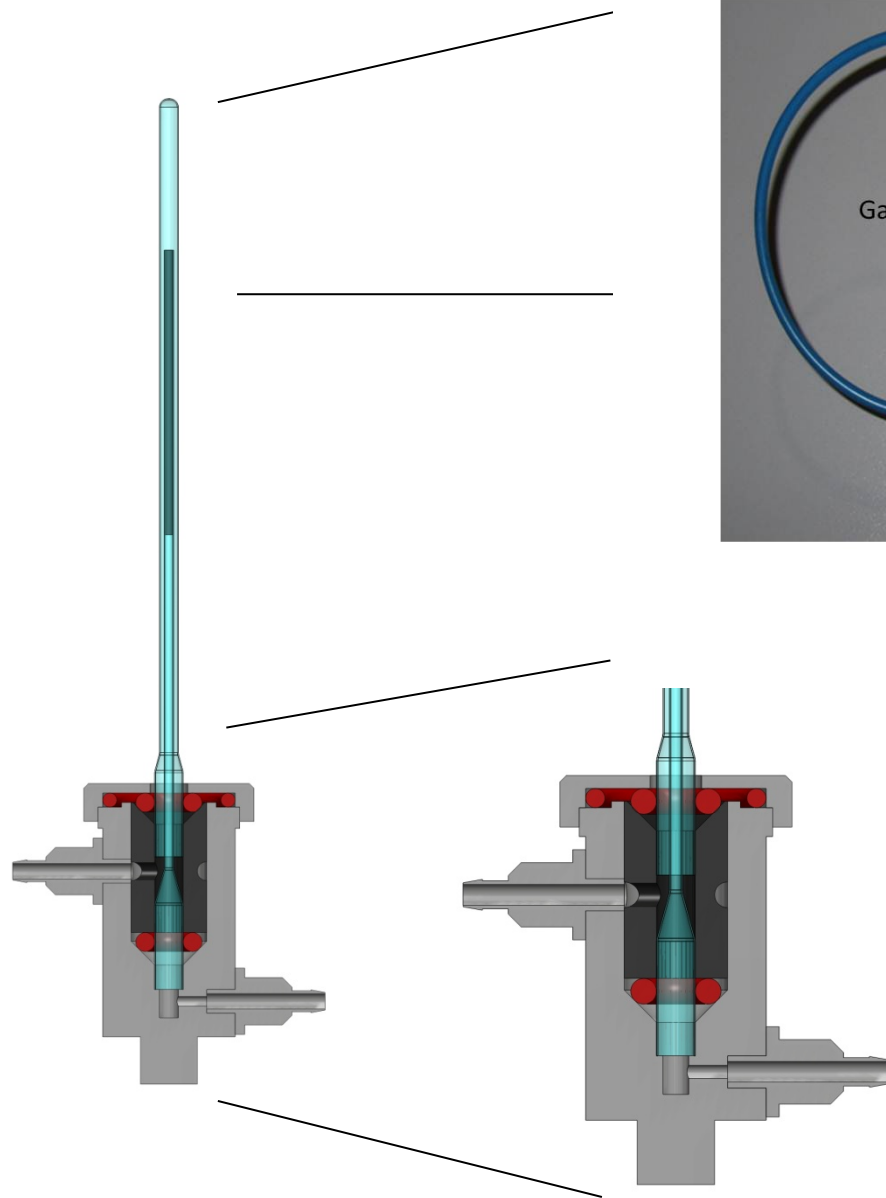
Furnace Design
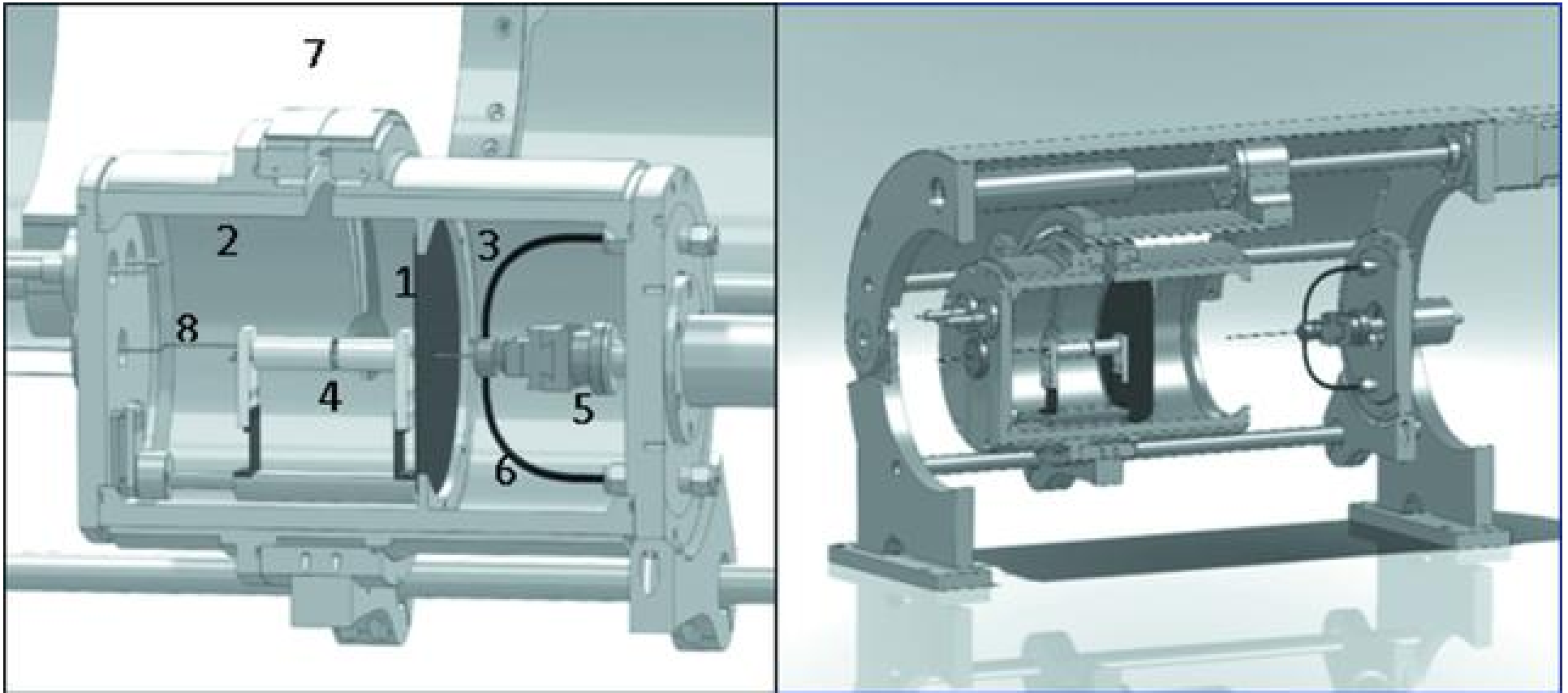
In situ reaction furnace for real-time XRD studies
Riello P., Lausi A., MacLeod J., Plaisier J.R., Zerauschek G., Fornasiero P.
Journal of Synchrotron Radiation, Vol. 20 - 1, pp. 194-196 (2013)

XRPD in non ambient conditions

600 °C

800°C

1000 °C

XRPD in non ambient conditions

600 °C
Fe-dolomite

800 °C
Fe-dolomite + $CaCO_3$ + $(Mg,Fe)O$

1000 °C
$Ca_2Fe_2O_5$ + $CaCO_3$ + MgO
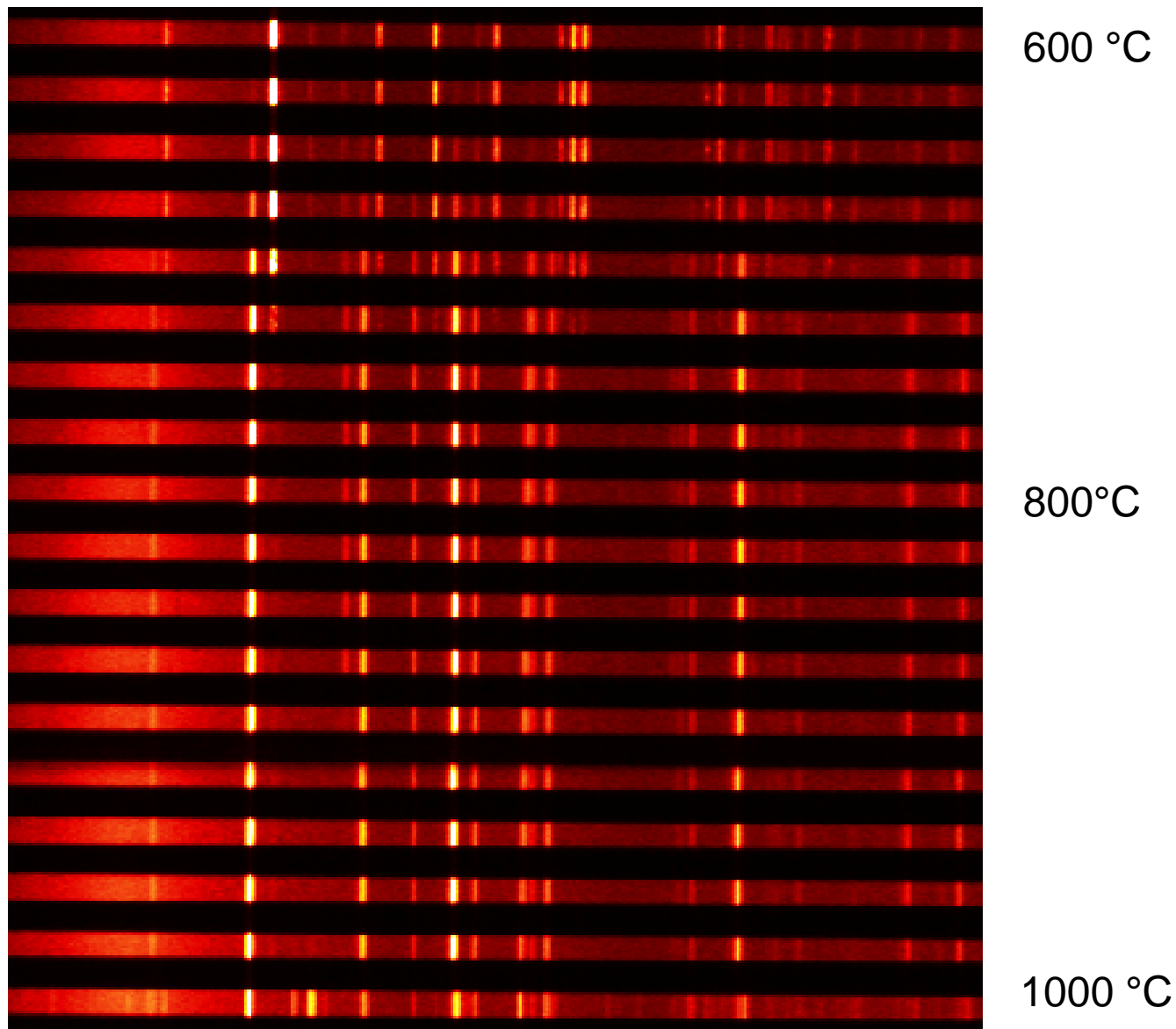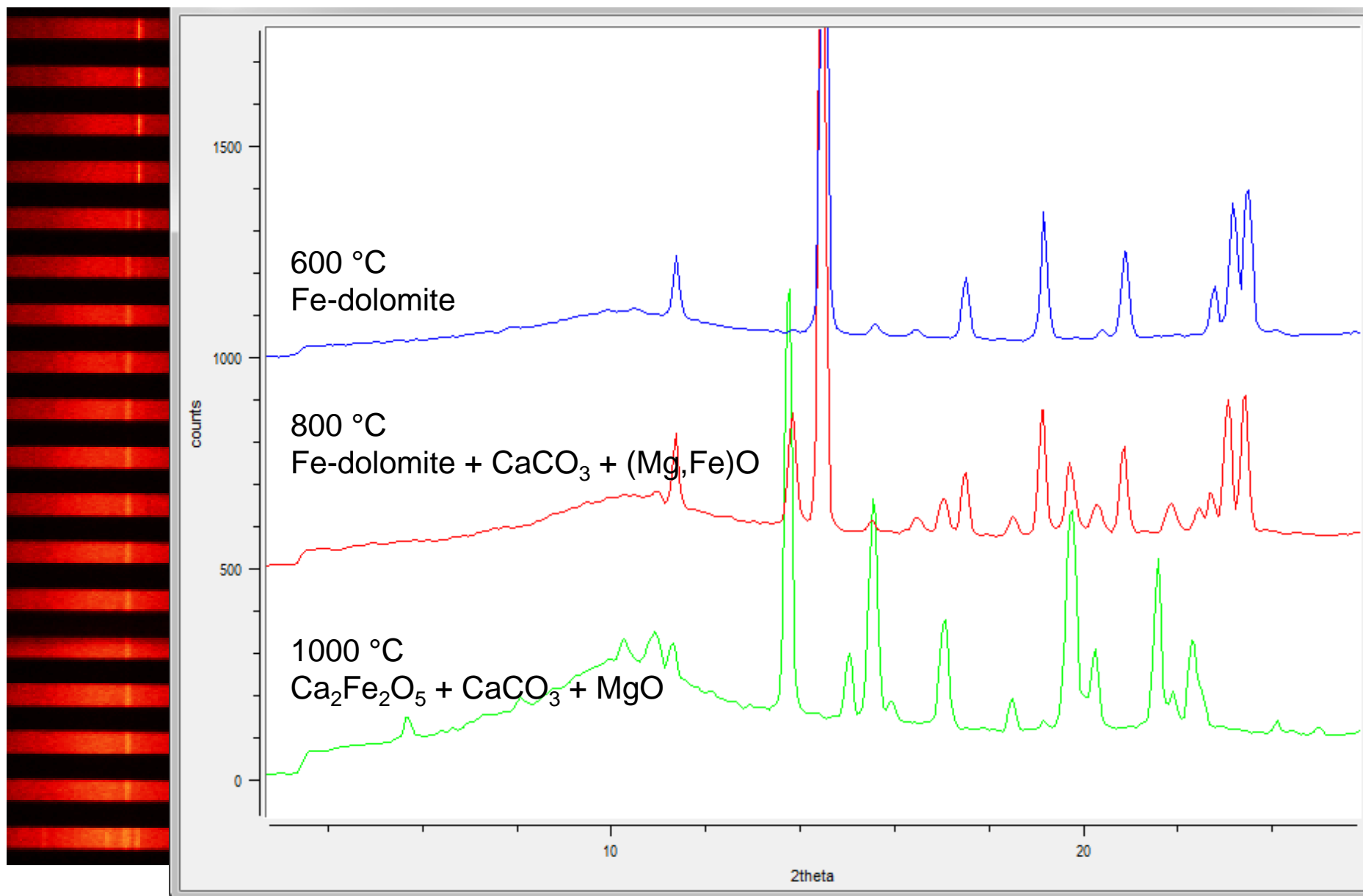
2D-3D transition
In Cu–TiS$_2$ system

- Phase transitions between 2D (layered) and 3D (cubic) phases in Cu$_x$TiS$_2$ (x = 0-0.5) intercalation compounds have been studied *in situ* by the X-ray diffraction technique in the temperature range 20–1000 °C.

- The discovery of CDW (charge density wave) quantum states and superconductivity in the Cu–TiSe$_2$ system arouses interest to isostructural materials, but known phase transformations to the spinel structure make comparison difficult.

- Samples were prepared by intercalation of Cu at room temperature. All samples had the layered hexagonal structure.

2D-3D transition
In Cu–TiS$_2$ system

2D-3D transition
In Cu–TiS$_2$ system
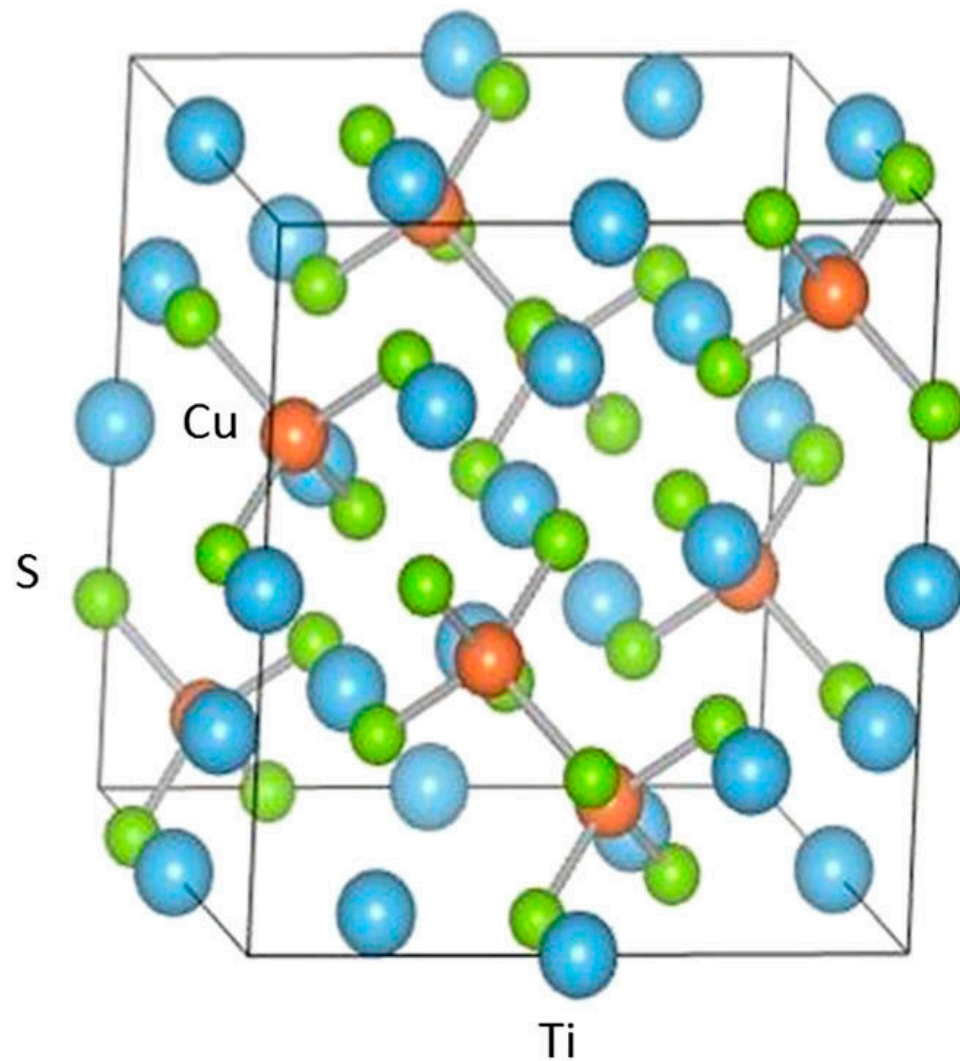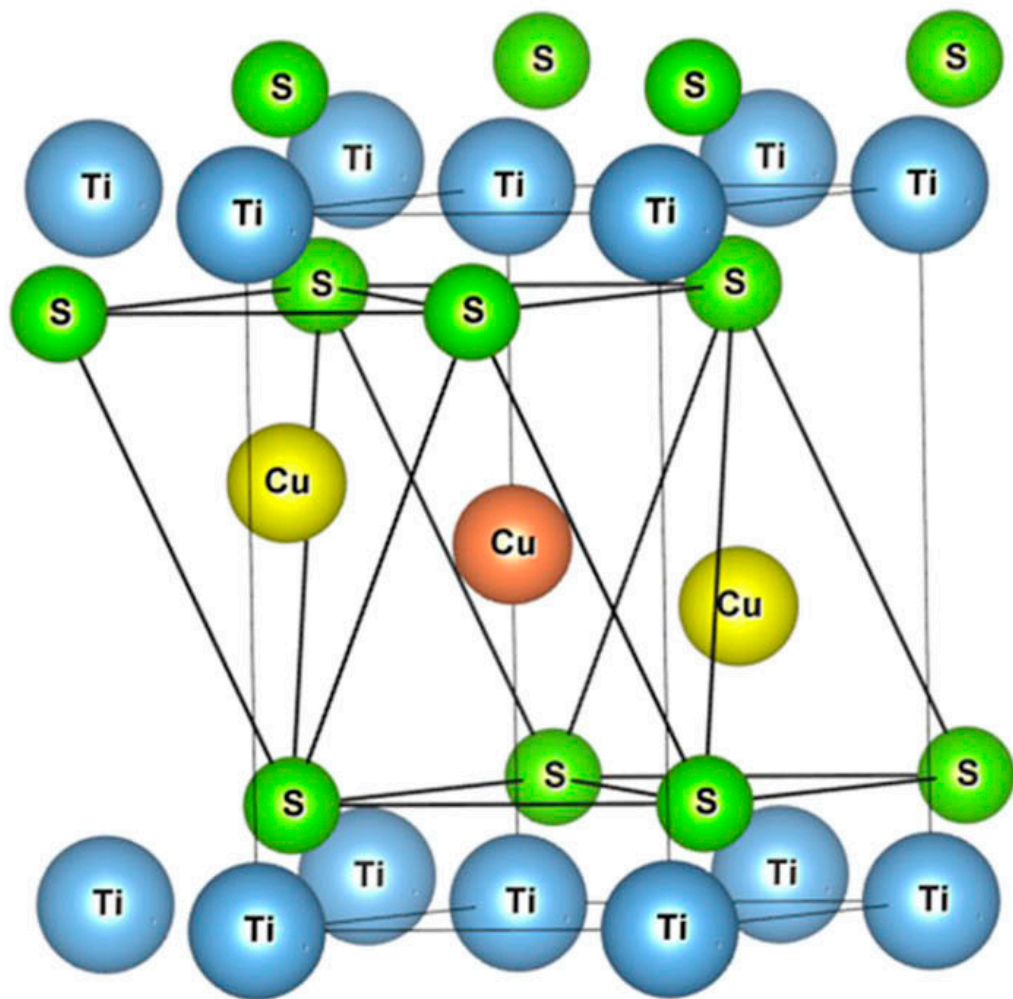
2D-3D transition In Cu–TiS$_2$ system
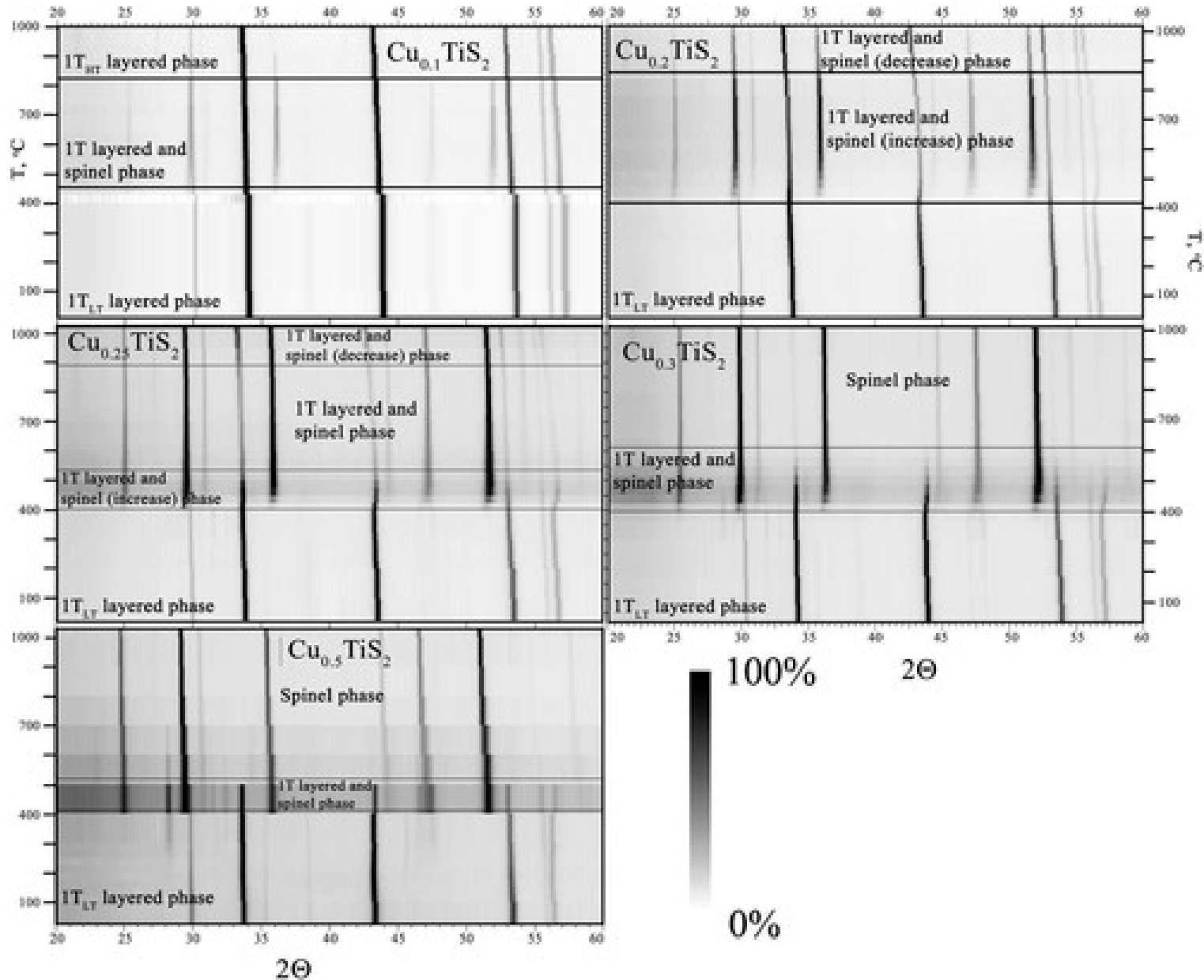
2D-3D transition In Cu–TiS$_2$ system

T (°C)	1T layered phase							Cubic spinel phase			R$_F^2$ (%)	χ²
	a	c	S (⅓ ⅔ z)	Cu (0 0 ½)	Cu (⅓ ⅔ z)		Ti (0 0 ½)	a	Cu (⅛⅛⅛)	S (x x x)		
			z	Occupation	z	Occupation	Occupation		Occupation	x		
Cu$_{0.2}$TiS$_2$												
206	3.4269(1)	5.8106(2)	0.2438(5)	0.198(2)	...	...	...	...	...	...	5.96	1.880
320	3.4331(1)	5.8252(2)	0.2452(5)	0.195(2)	...	...	...	...	...	...	6.44	1.688
451	3.4401(1)	5.8037(2)	0.2593(8)	0.064(2)	...	...	0.005(3)	9.9816(4)	0.763(8)	0.2502(5)	3.90	1.123
483	3.4405(1)	5.7942(3)	0.249(1)	0.059(3)	...	...	...	9.9631(3)	0.611(5)	0.2526(3)	2.89	1.136
514	3.4421(1)	5.7937(3)	0.253(1)	0.045(3)	...	...	0.017(4)	9.9592(2)	0.564(4)	0.2530(2)	3.18	1.064
546	3.4441(1)	5.7982(4)	0.260(1)	0.030(4)	...	...	0.018(5)	9.9604(2)	0.521(3)	0.2529(3)	2.78	1.138
606	3.4482(1)	5.8083(4)	0.243(1)	0.005(3)	...	...	0.074(6)	9.9642(1)	0.512(3)	0.2536(2)	4.55	1.107
637	3.4498(1)	5.8133(4)	0.249(1)	0.038(3)	...	...	0.018(5)	9.9660(1)	0.503(3)	0.2532(1)	1.86	1.105
735	3.4543(1)	5.8365(4)	0.246(1)	0.057(3)	0.45(3)	0.013(2)	0.020(5)	9.9726(1)	0.467(3)	0.2538(2)	2.89	1.565
828	3.4603(1)	5.8677(3)	0.243(1)	0.032(3)	0.454(7)	0.037(2)	0.029(4)	9.9846(1)	0.474(3)	0.2536(2)	2.72	1.296
874	3.4626(1)	5.8881(2)	0.240(1)	0.040(2)	0.431(6)	0.041(2)	0.031(4)	9.9908(1)	0.498(4)	0.2535(2)	2.92	1.770
918	3.4654(1)	5.9051(3)	0.239(1)	0.060(2)	0.445(8)	0.032(2)	0.001(4)	9.9662(4)	0.533(6)	0.2540(3)	4.12	2.410
Cu$_{0.1}$TiS$_2$												
525	3.4422(1)	5.7990(2)	0.2460(6)	0.044(2)	0.35(2)	0.013(2)	0.024(3)	9.9701(8)	0.66(2)	0.2547(8)	8.16	5.921
647	3.4494(1)	5.8129(2)	0.2448(6)	0.038(2)	0.37(2)	0.015(2)	0.023(4)	9.9690(4)	0.50(2)	0.2544(6)	7.05	5.813
918	3.4650(1)	5.8691(2)	0.2428(7)	0.055(2)	0.42(2)	0.020(3)	0.002(4)	...	...	...	9.65	10.47
Cu$_{0.25}$TiS$_2$												
918	3.4664(2)	5.9140(8)	0.236(2)	0.009(6)	0.46(1)	0.052(4)	...	10.0075(1)	0.512(4)	0.2531(2)	6.42	10.81

2D-3D transition
In Cu–TiS$_2$ system
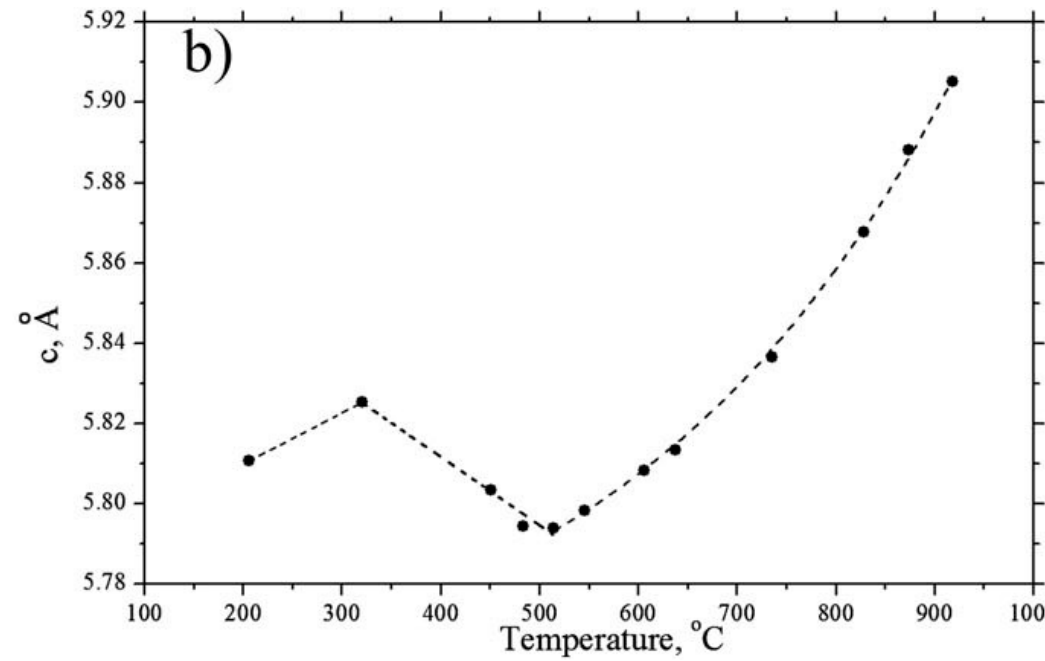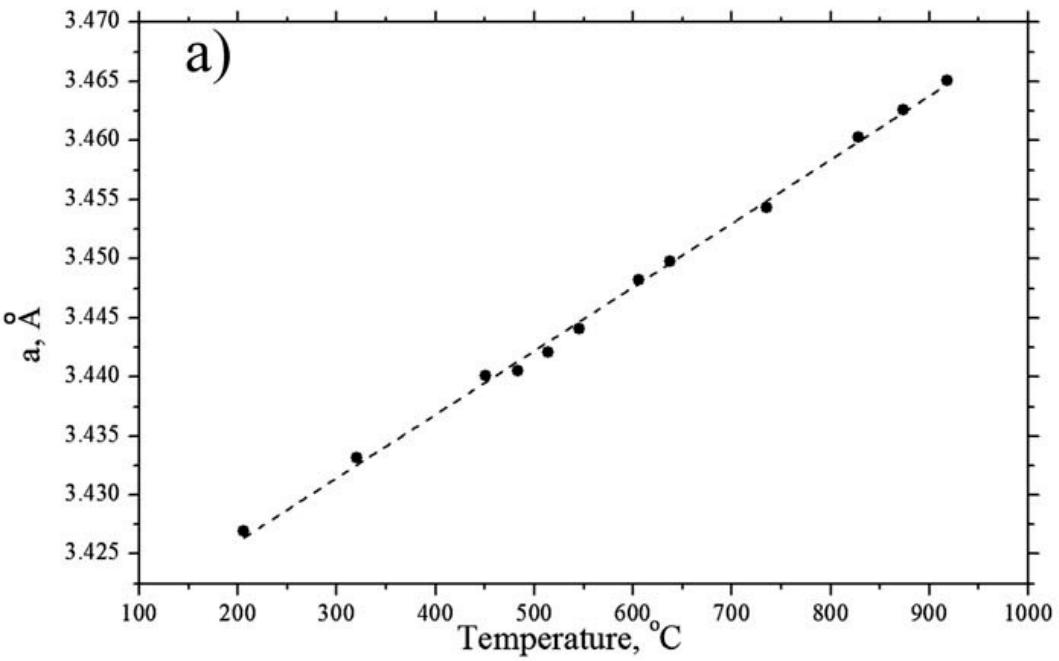
2D-3D transition
In Cu–TiS$_2$ system
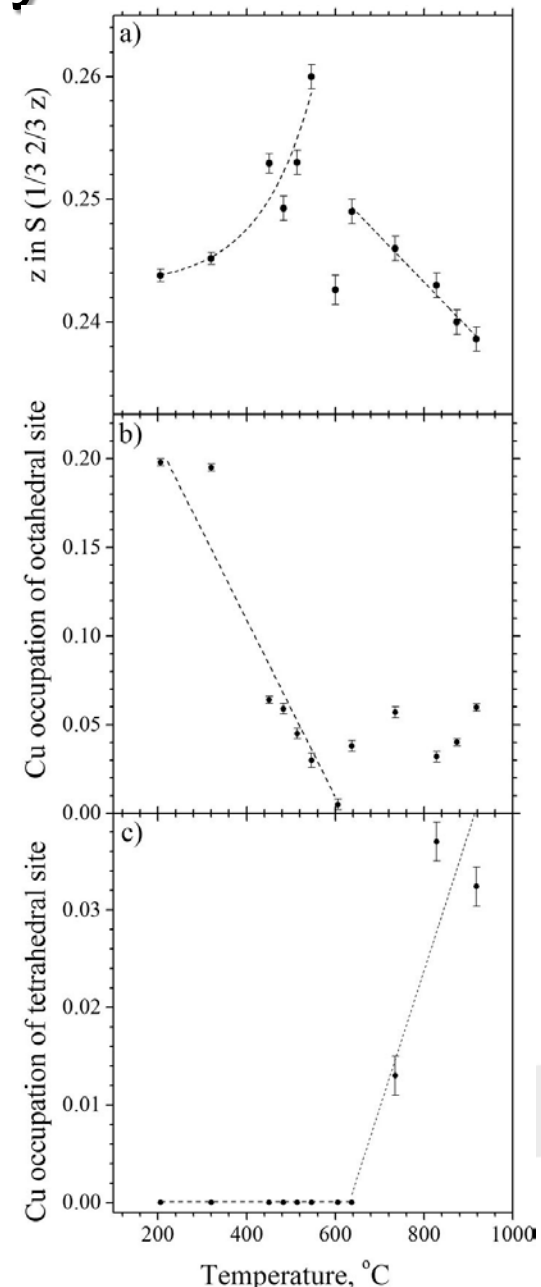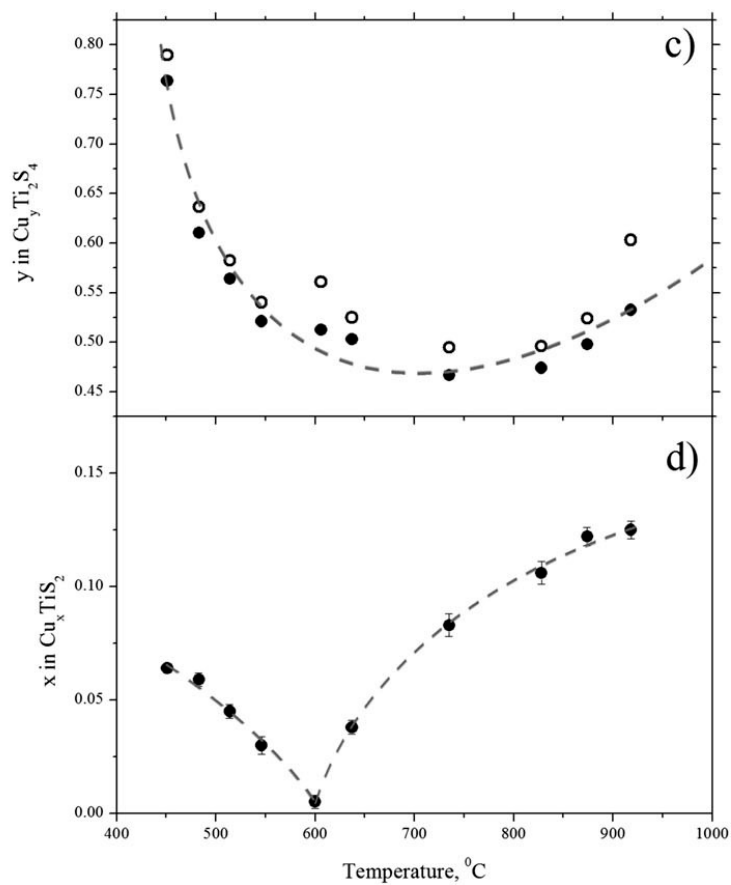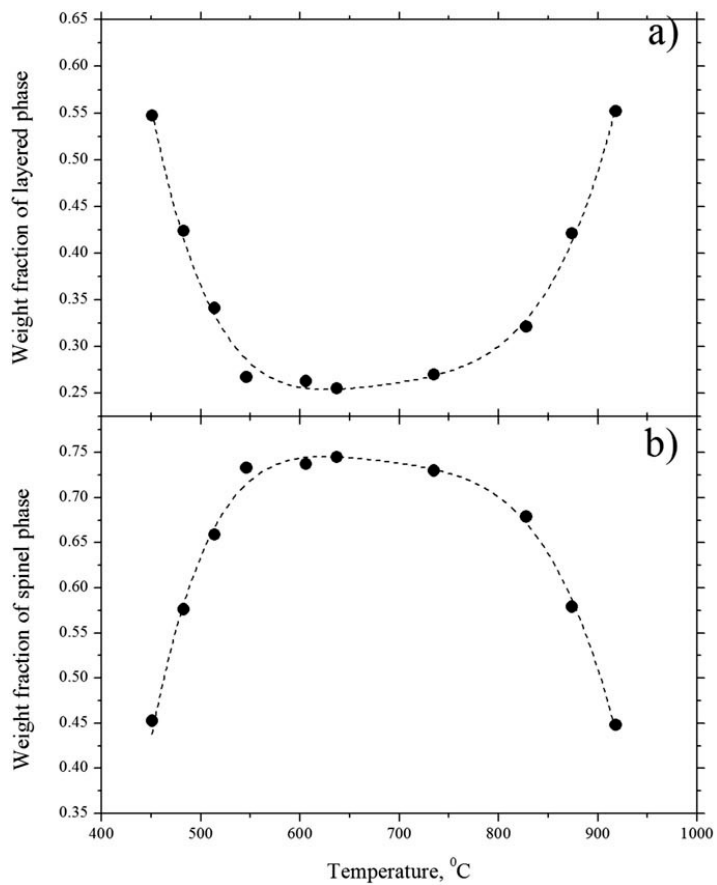
2D-3D transition
In Cu–TiS$_2$ system
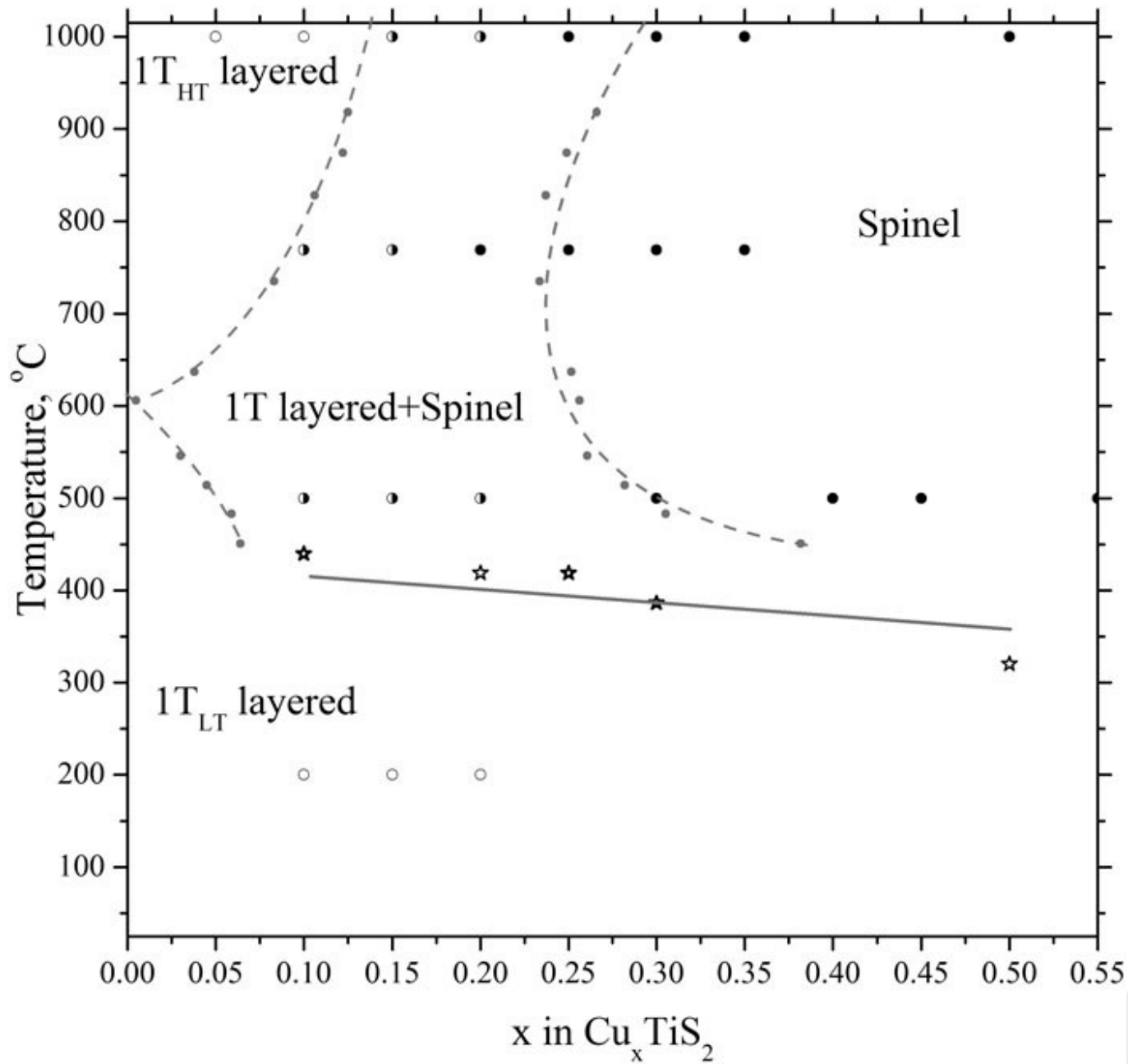
2D-3D transition In Cu–TiS$_2$ system

- It has been found that the stability of the layered phase is determined by the distribution of copper atoms between the octahedral and tetrahedral crystallographic sites.

- The occupation of octahedral sites dominates at low temperatures.

- Upon heating, tetrahedral site occupation is limited and the layered phase becomes unstable and transforms to the spinel.

- Further heating allows the distribution of copper between octahedral and tetrahedral sites; the layered phase becomes stable again.

XRPD in non ambient conditions
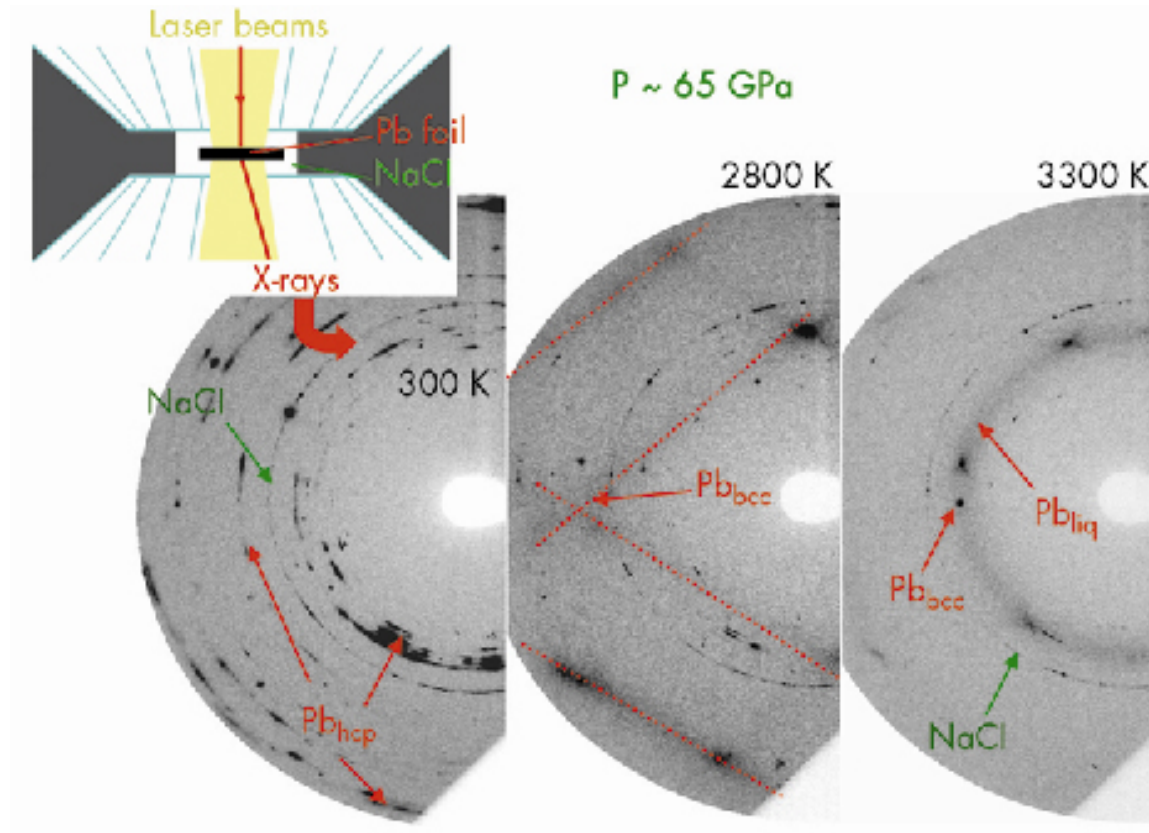
Source: www.esrf.eu

Diffraction for stress analysis

- The stresses in a material are the sum of the contributions from any externally applied load (applied stress) and those arising from the interactions between individual grains or components that are not completely relaxed when no external load is present (residual stresses).

- Stresses lead to deformation, the distances between lattice planes changes in the direction where stress is present.

- Measuring how the peak position (related to the lattice plane distance by braggs law) changes, at different orientations of the sample gives us information on the amount of stress

Diffraction for stress analysis

- Not being aware of residual tensile stresses, that make materials weaker can have disastrous consequences in construction for example:
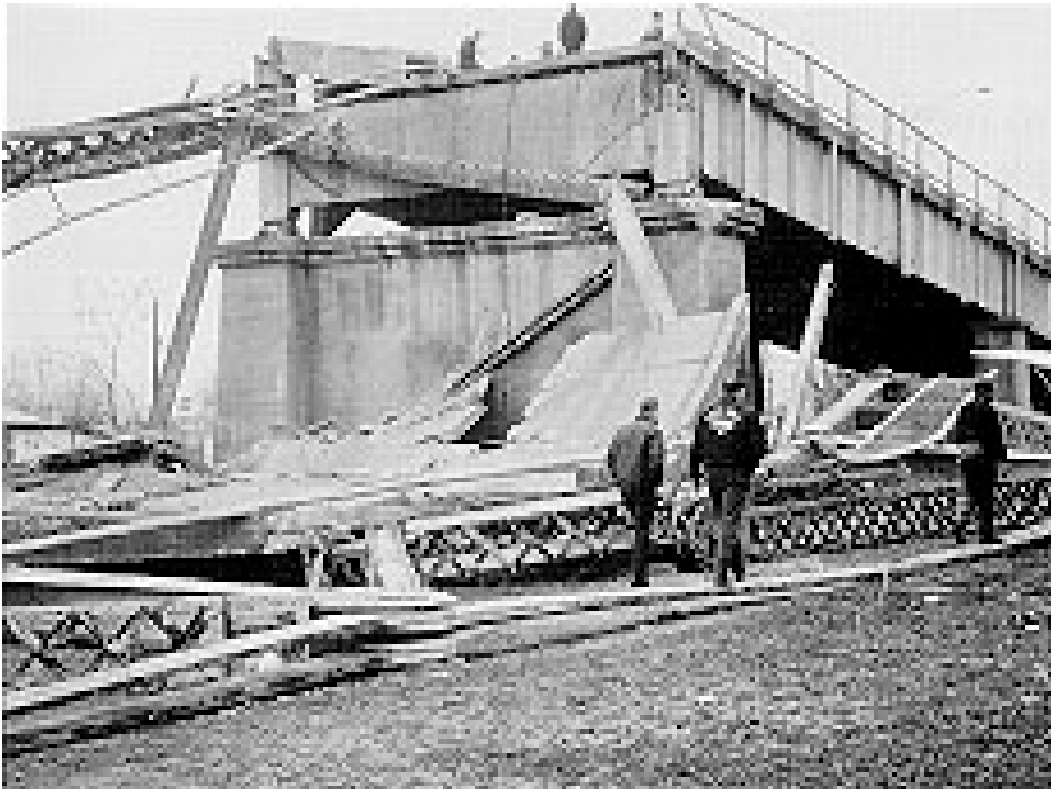
Residual stress is often a cause of premature failure of critical components, and was one factor in the collapse of the suspension bridge at Silver Bridge in West Virginia in December 1967. The eyebar links were castings which showed high levels of residual stress, which in one eyebar, encouraged crack growth. When the crack reached a critical size, it grew catastrophically, and from that moment, the whole structure started to fail in a chain reaction. Because the structure failed in less than a minute, 46 drivers and passengers in cars on the bridge at the time were killed.

- On the other hand residual stresses may be induced in materials on purpose. Compressive residual stress maybe induced in order to strengthen it and increase its fatigue life

crack

$d>d_0$

Tensile stress

$d<d_0$

Compressive stress

d_0
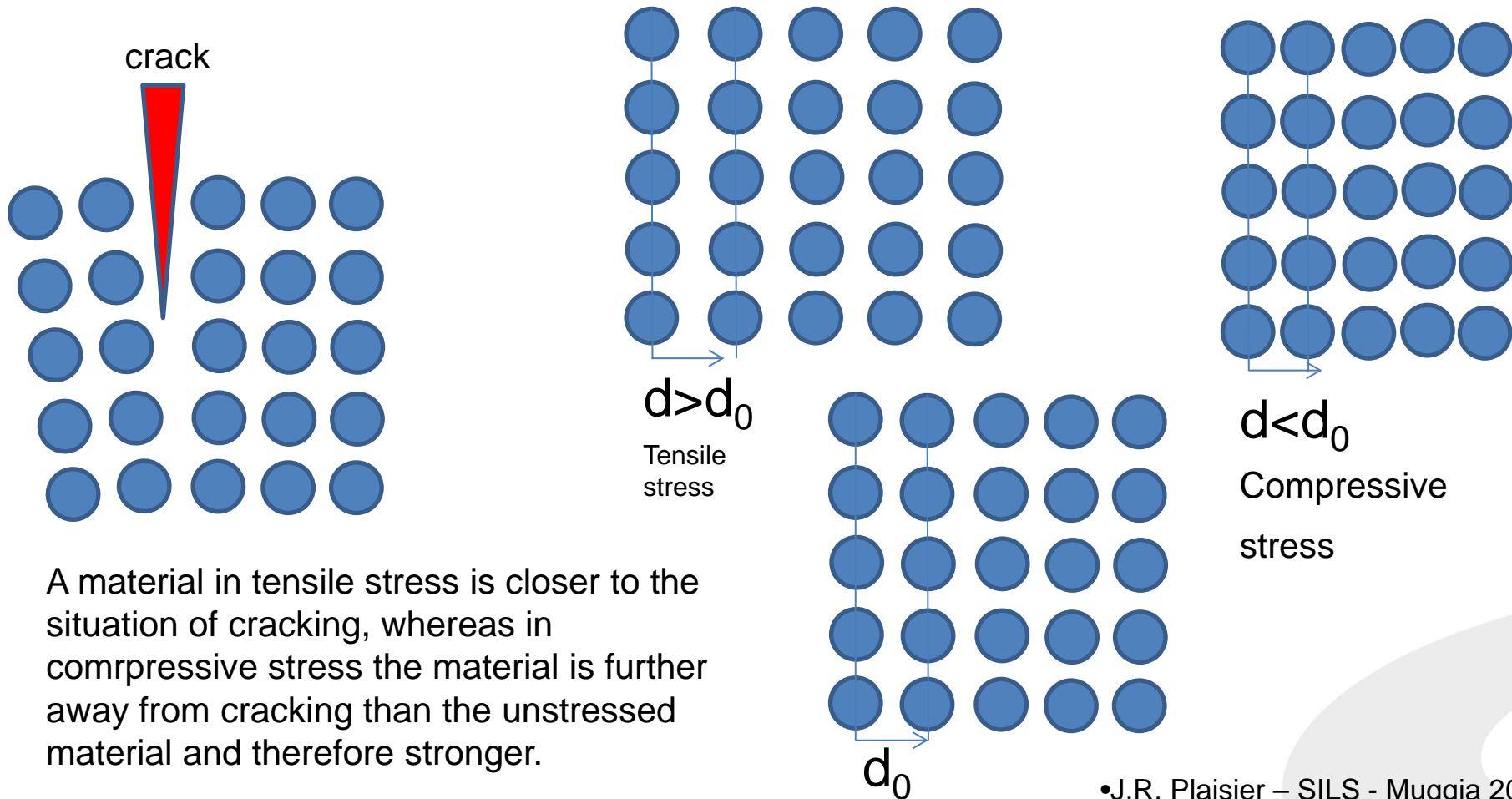
- A material in tensile stress is closer to the situation of cracking, whereas in comrpressive stress the material is further away from cracking than the unstressed material and therefore stronger.

Diffraction for stress analysis

- It is strain that is actually measured: $\Delta d/d_0$

- Residual strain changes interplanar spacings, which shifts the positions of diffraction peaks.

- Strain is resolved differently in different physical directions in the sample.

- Engineering materials are polycrystalline, so some grains are always oriented to diffract enabling stress tensors to be determined.

Diffraction for stress analysis

- When the d-spacing of a reflection is measured, only grains with the planes oriented in a given direction contribute to diffraction. If we change the orientation of the specimen and remeasure the d-spacing we are looking at a different population of grains and we get a different d-spacing due to different stress levels
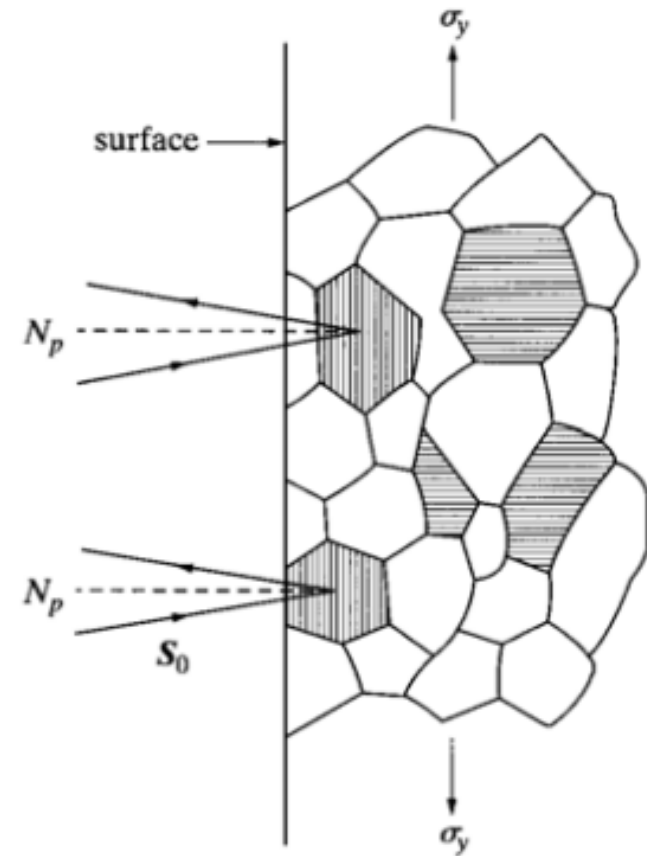
Diffraction for stress analysis
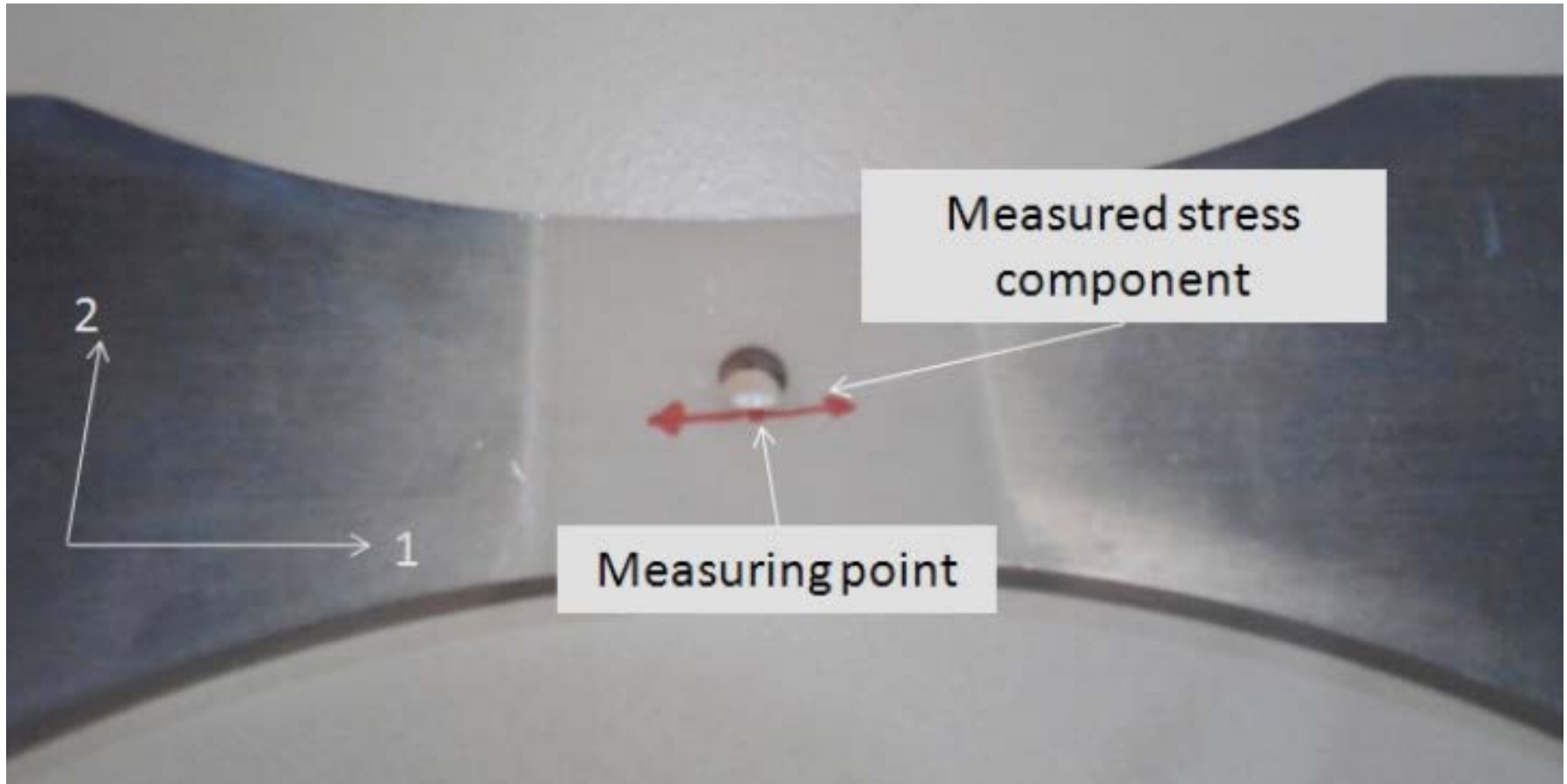
- Alloys of aluminium used in the airplane industry were measured to see the effectiveness of laser peening around a hole.
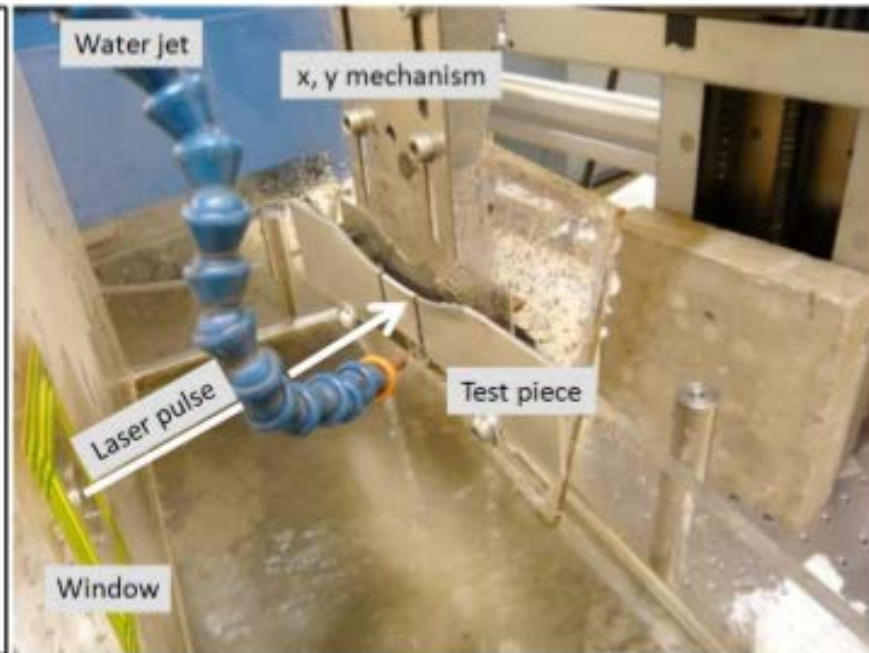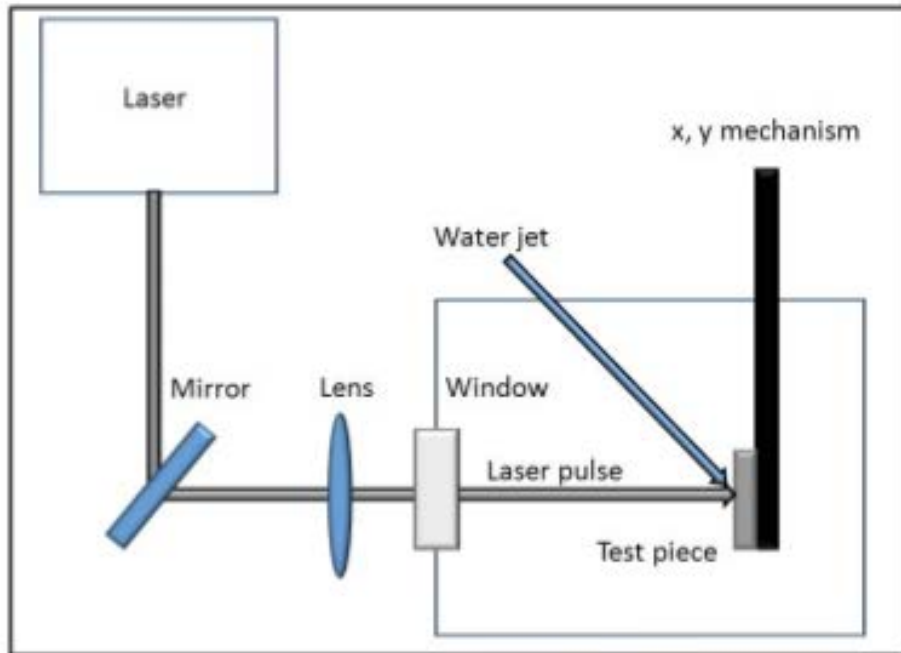
# Diffraction for stress analysis

- The same diffraction peak is measured for different orientatons of the sample
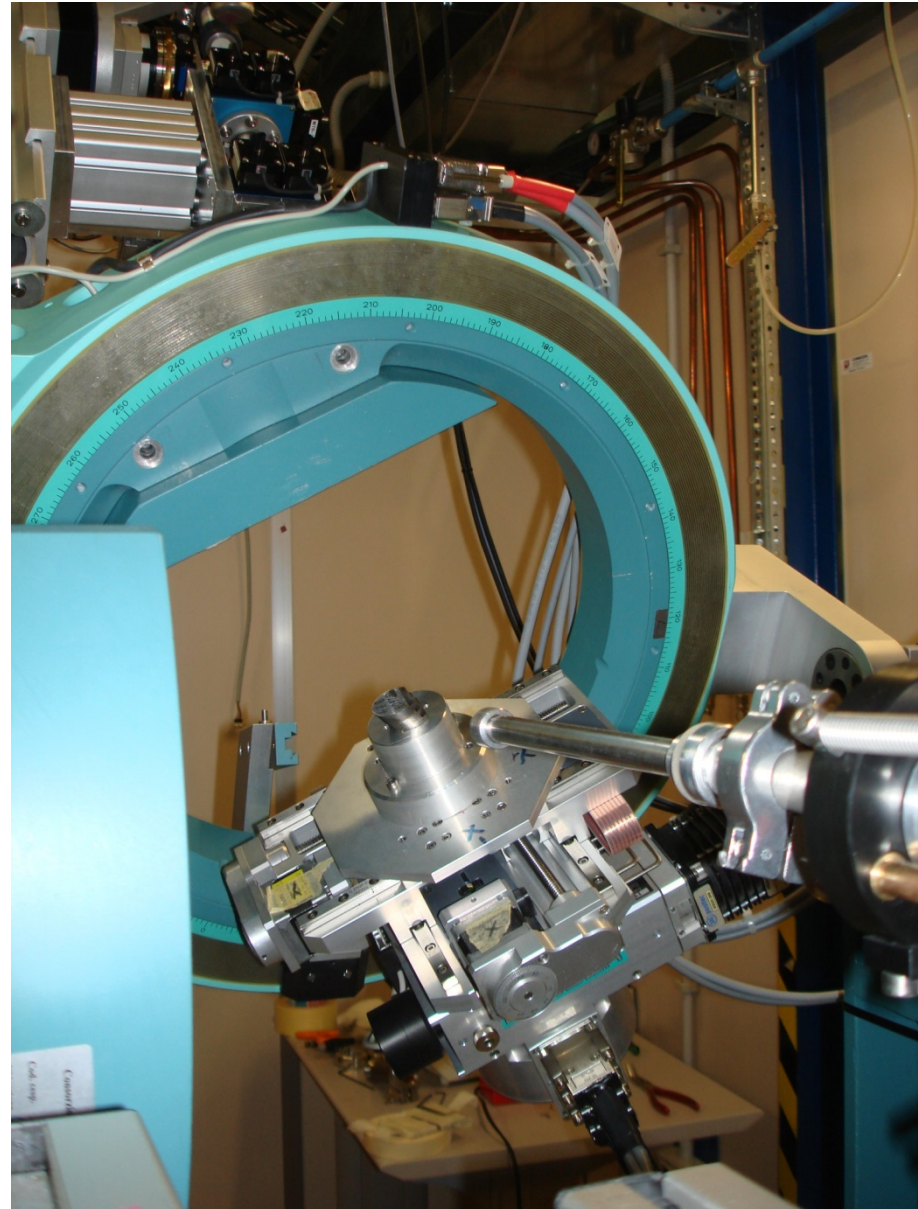
Diffraction for stress analysis

- The posiitionon of the diffraction peak is determiined dor each orientation (d)

Diffraction for stress analysis

D is plotted vs. Sin² ψ and from the slope the stress can be calculated. In this example the stress is compressive
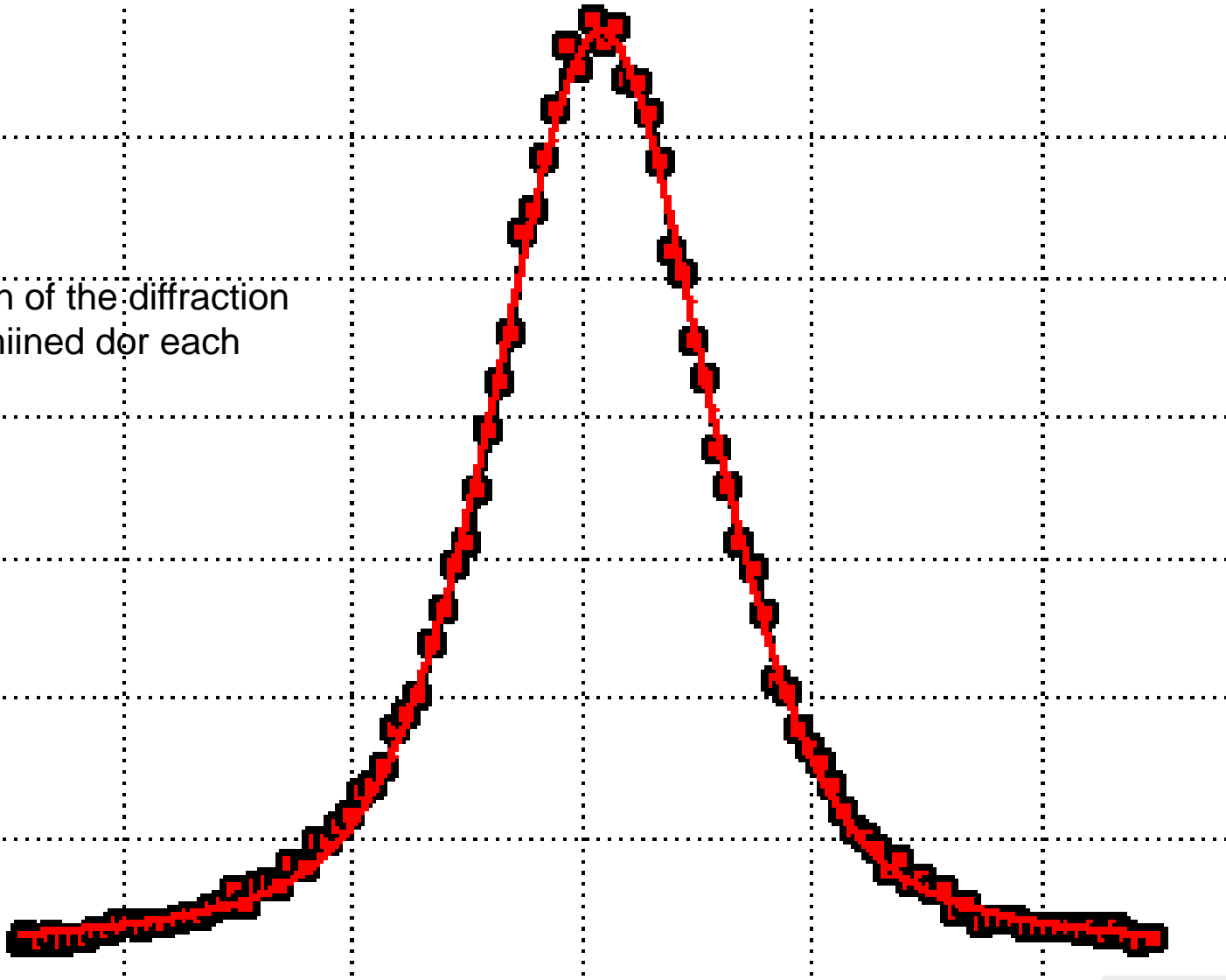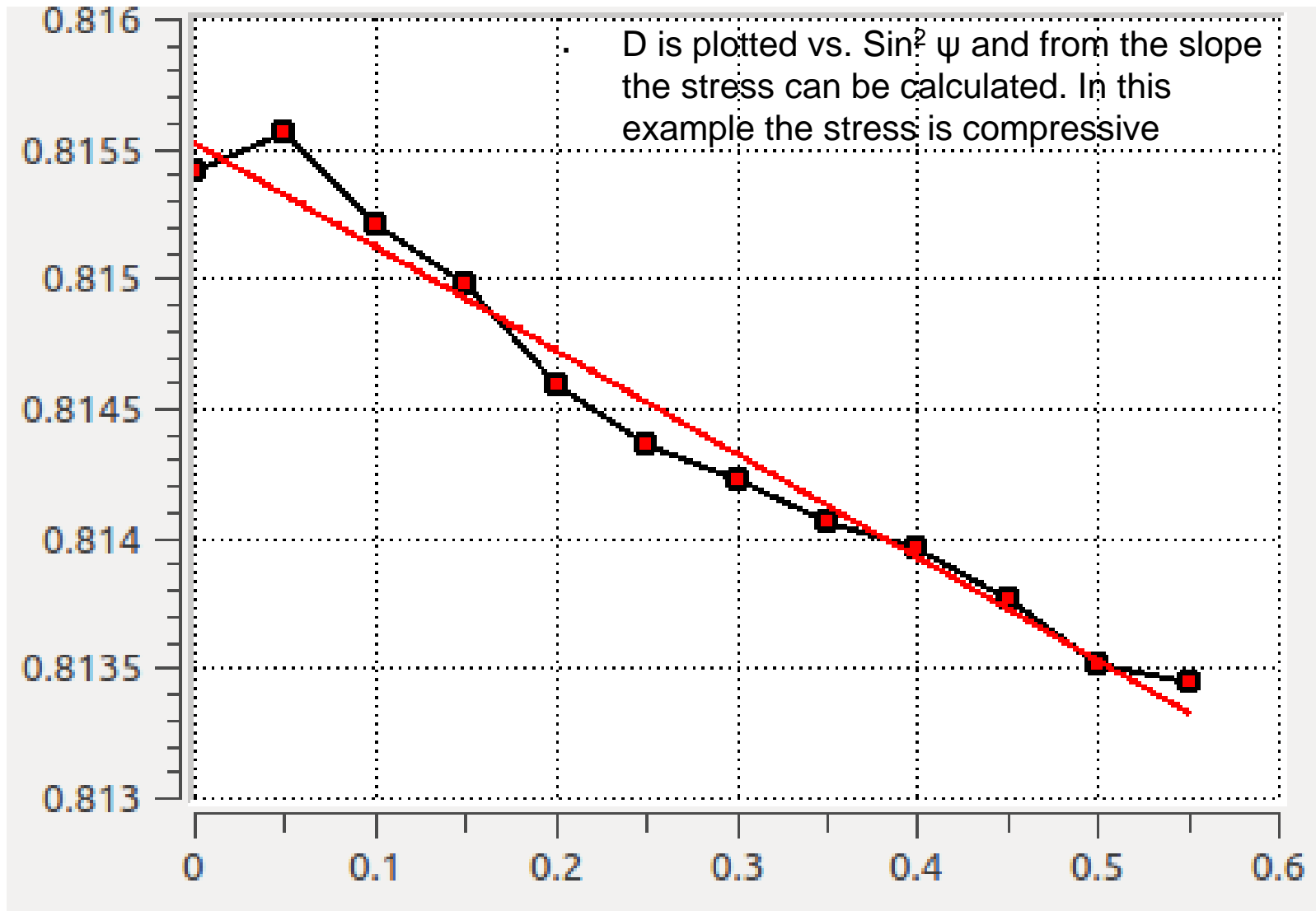
Diffraction for stress analysis
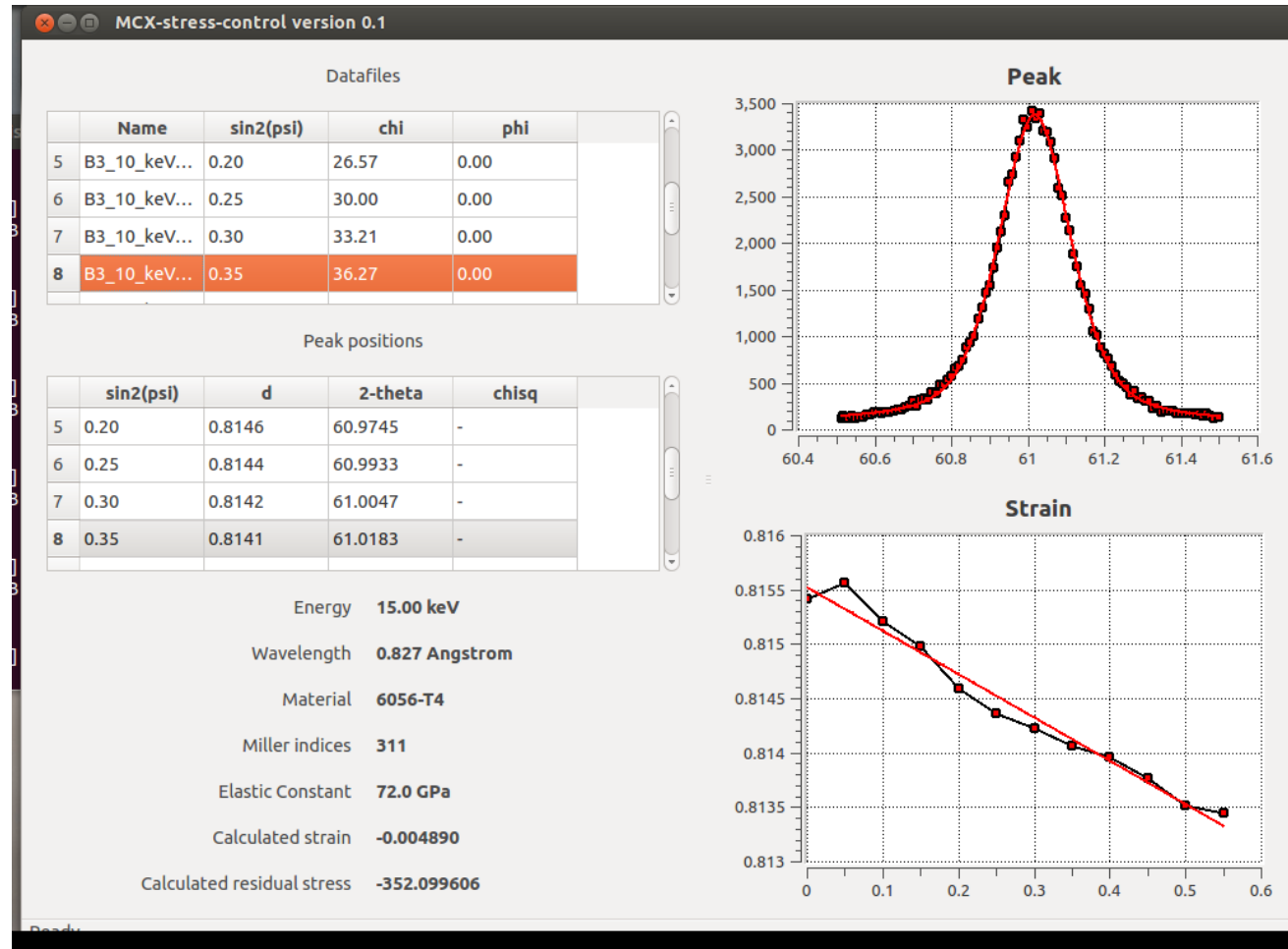
- The result showed that laser peening after drilling the hole acutually weakens tha material, whereas first applying laser peening ad subsequently drilling th hole results in a stringer material
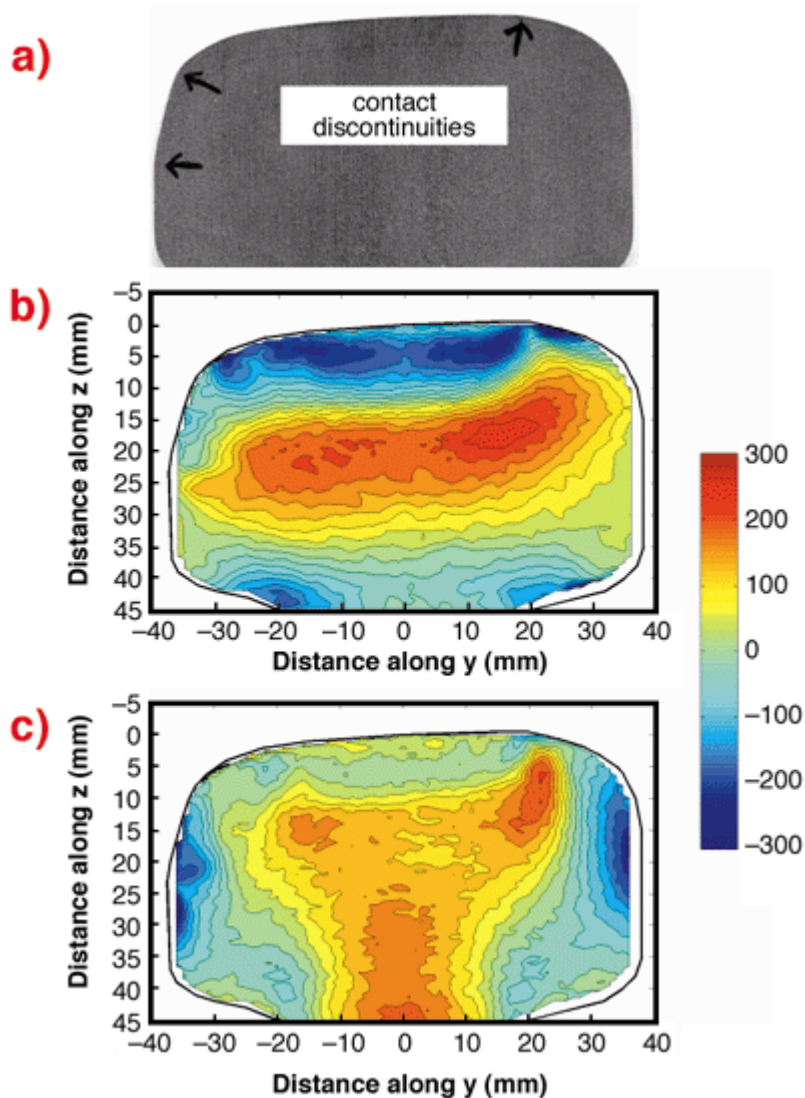
Texture analysis

- Texture analysis is a diffraction technique in which the orientation distribution of the crystallites of a sample is determined.

- Knowledge of texture is important factor in understanding the mechanical, physical or chemical behavior of the material investigated.

- Texture is determined from a set of pole figures. These pole figures are obtained by measuring the intensity distribution of a single (hkl) reflection by tilting and rotating the sample over the orientation sphere.

Texture analysis – an example

- X-ray analysis of texture domains in nonhomogeneous thin films deposited by physical vapour deposition, P. Scardi *et al.*, **Thin Solid Films** 467, 326-333 (2004)

fibre texture

Top layer

Interface layer

CaSZ

SiO_2

Si

720 nm

polycristalline (random oriented grains)
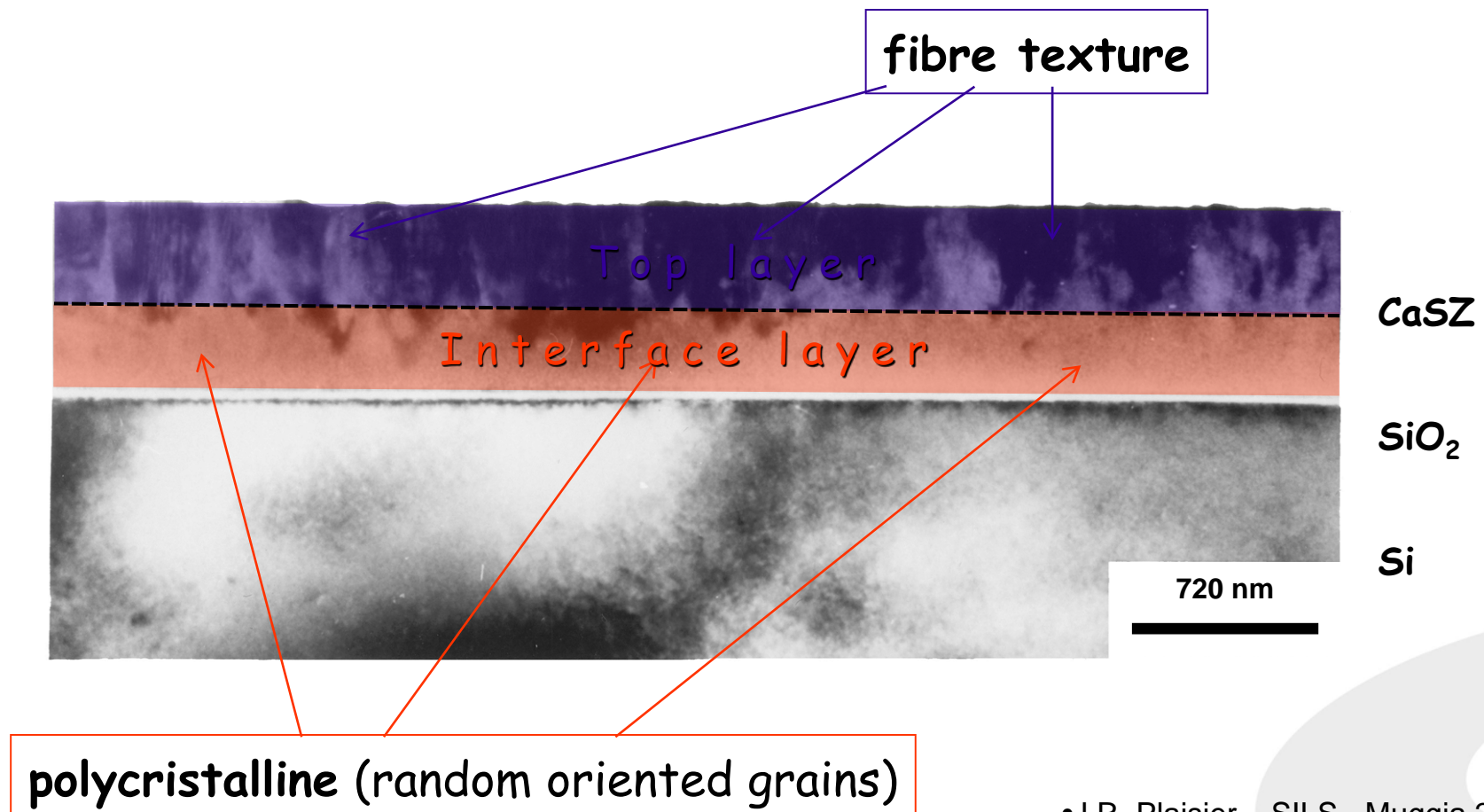
Texture analysis – an example

- Physical vapour deposition (PVD) coatings produced under nonepitaxial conditions may show a complex microstructure, evolving with the thickness of the deposited layer.

- This cannot be studied by means of traditional methods of texture analysis by diffraction, which are implicitly based on the assumption of homogeneous texture throughout the material.

- Synchrotron radiation data (collected with wavelengths just above and just below the absorption edge of Zr) were analysed to understand the evolution of texturein the layer.

(a)

λ = 0.65Å

(b)

λ = 0.75Å
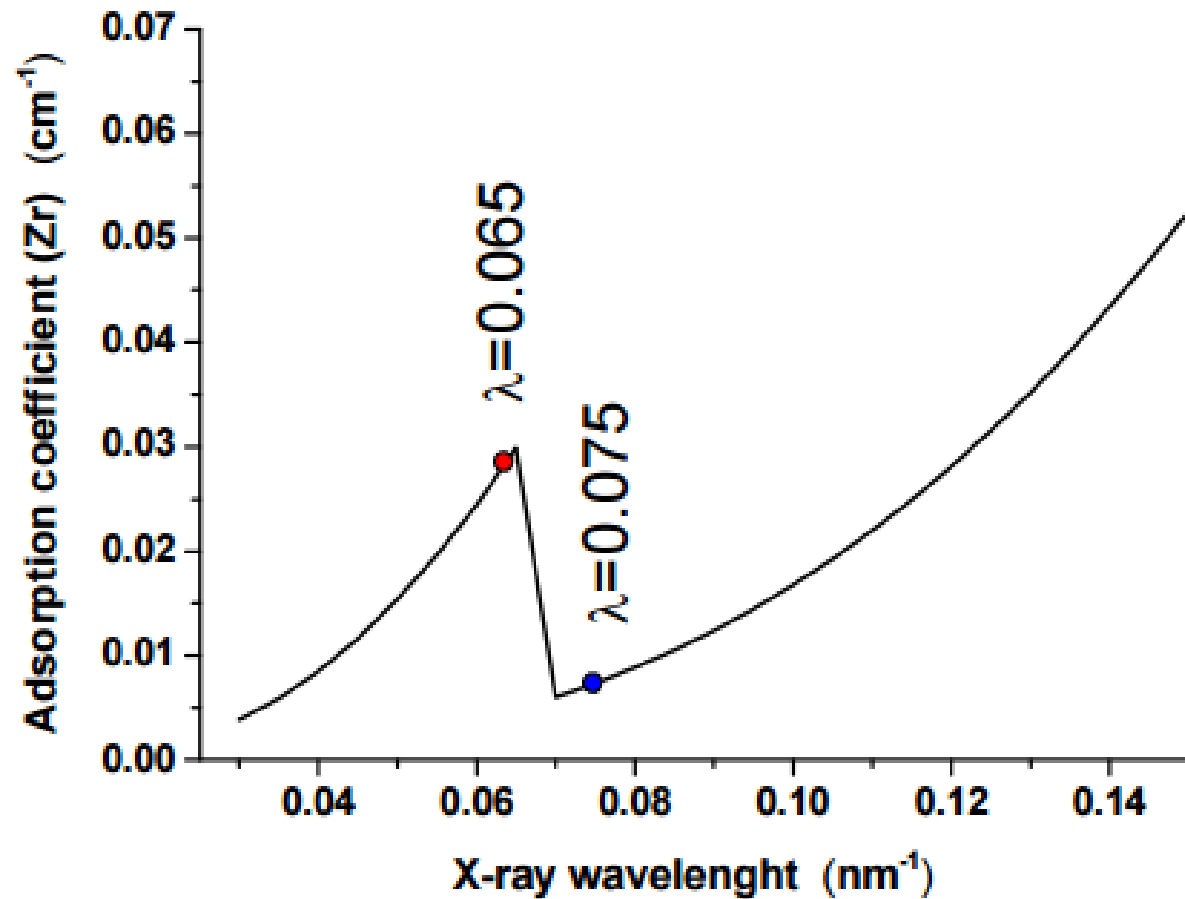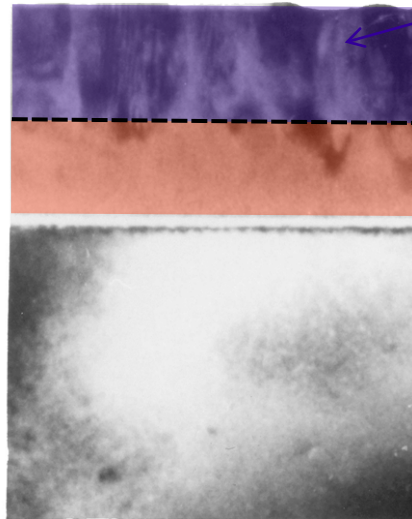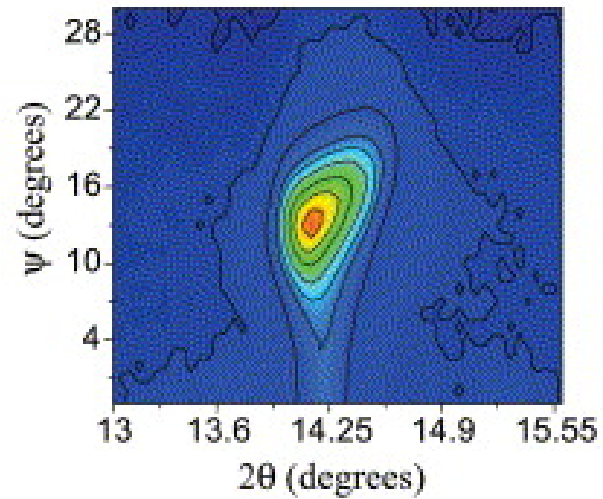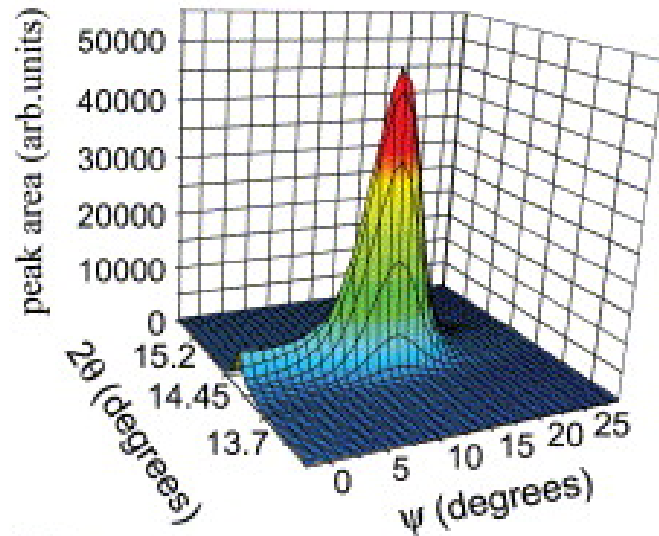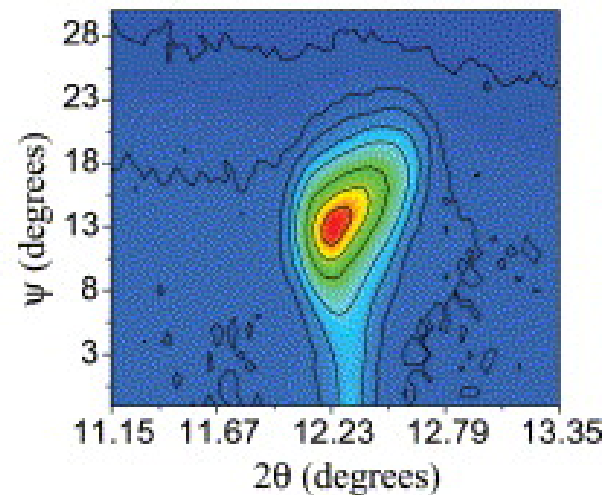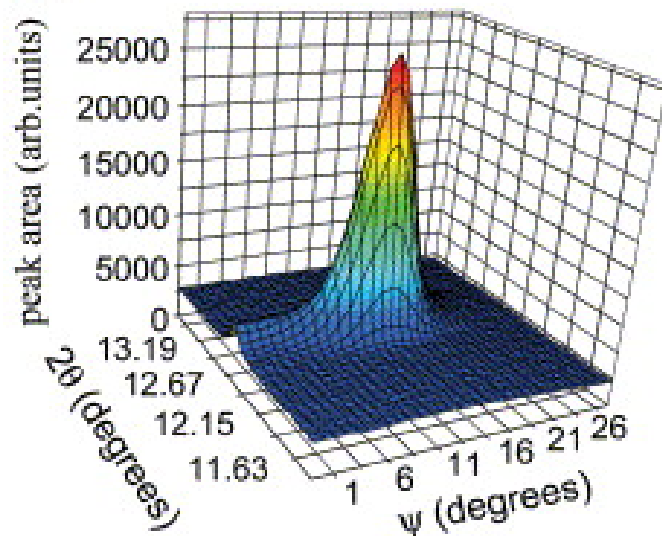
- Correlation between microstructure and bioequivalence in Anti-HIV Drug Efavirenz, C. Fandaruff *et al.*, **European Journal of Pharmaceutics and Biopharmaceutics** 91, 52-58 (2015)

Line profile analsis - example

- Polymorphism and particle size distribution can impact the dissolution behaviour and, as a consequence, bioavailability and bioequivalence of poorly soluble drugs, such as Efavirenz (EFV).

- The aim of this work was to study microstructure, a solid-state property of current interest in the pharmaceutical area, in order to find an explanation for the dissolution and bioequivalence behaviour.

- The microstructure of EFV raw materials was studied by Whole Powder Pattern Modelling (WPPM) of X-ray powder diffraction data.

Line profile analysis - example
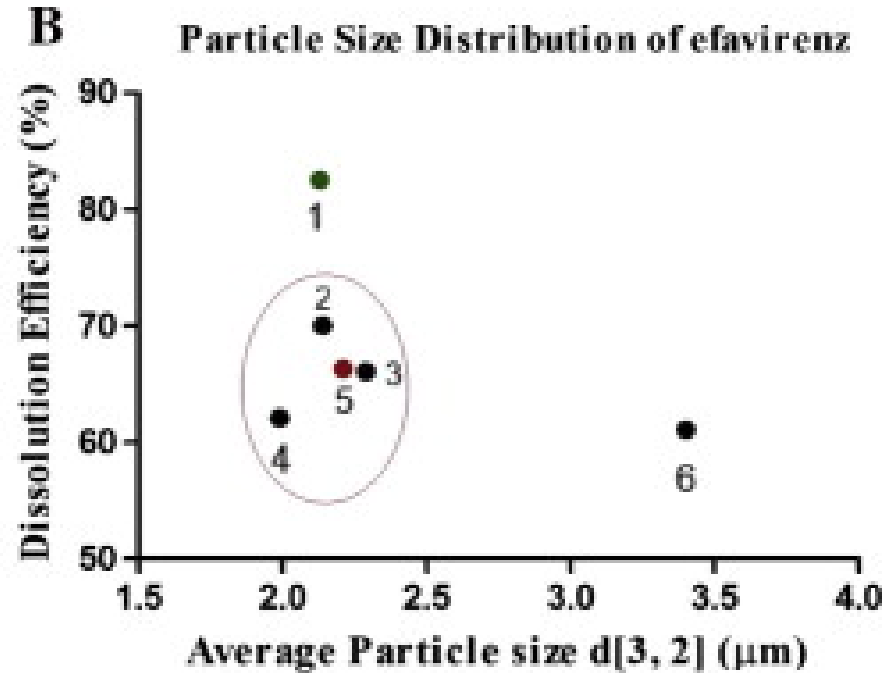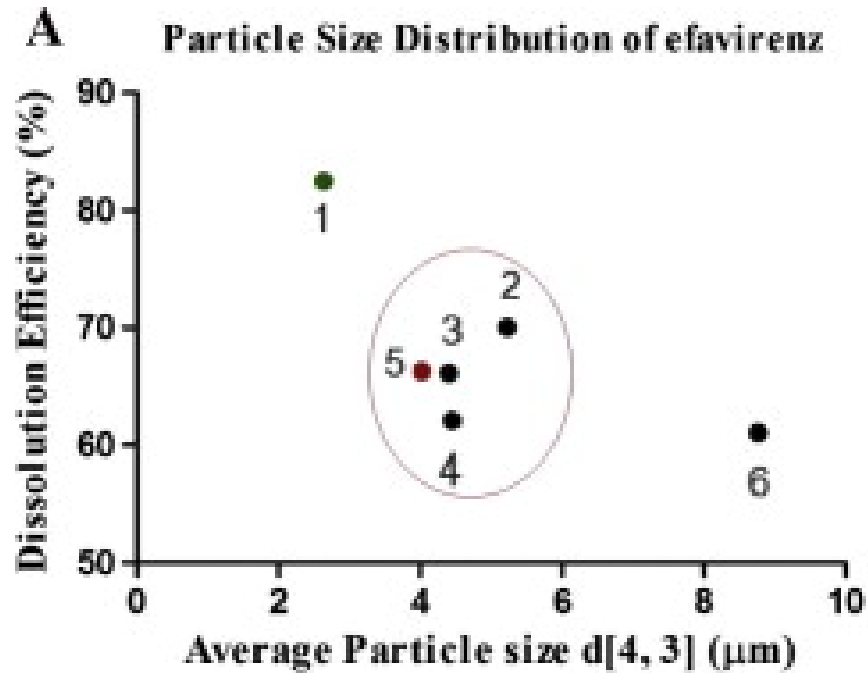
Line profile analysis - example
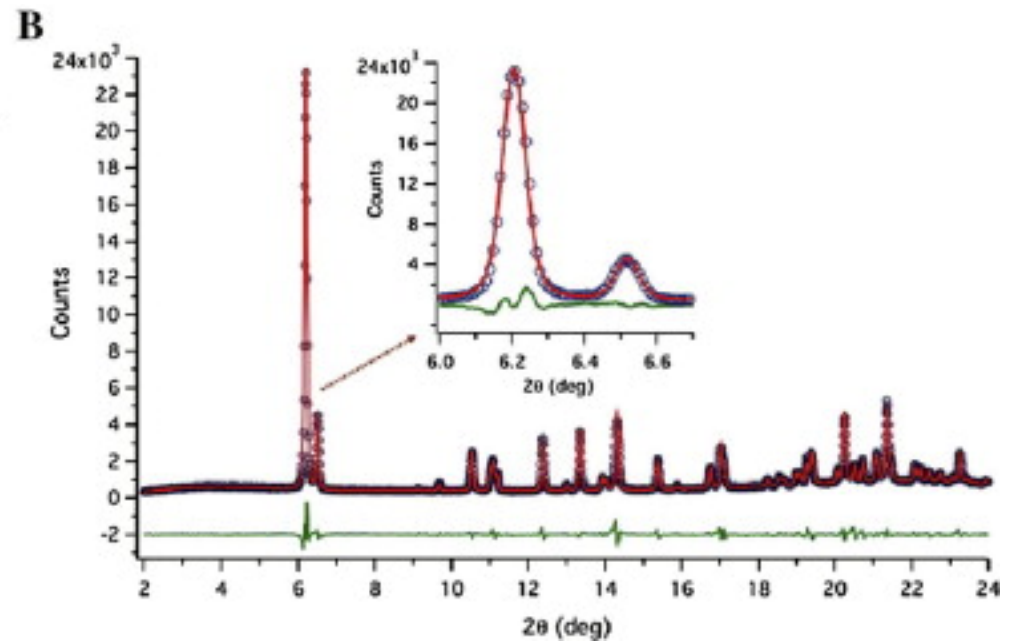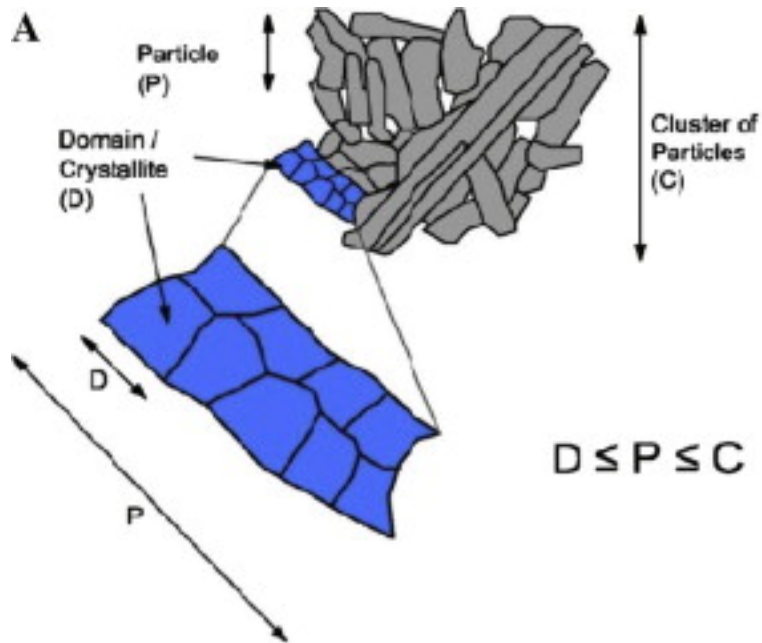
Line profile analysis - example
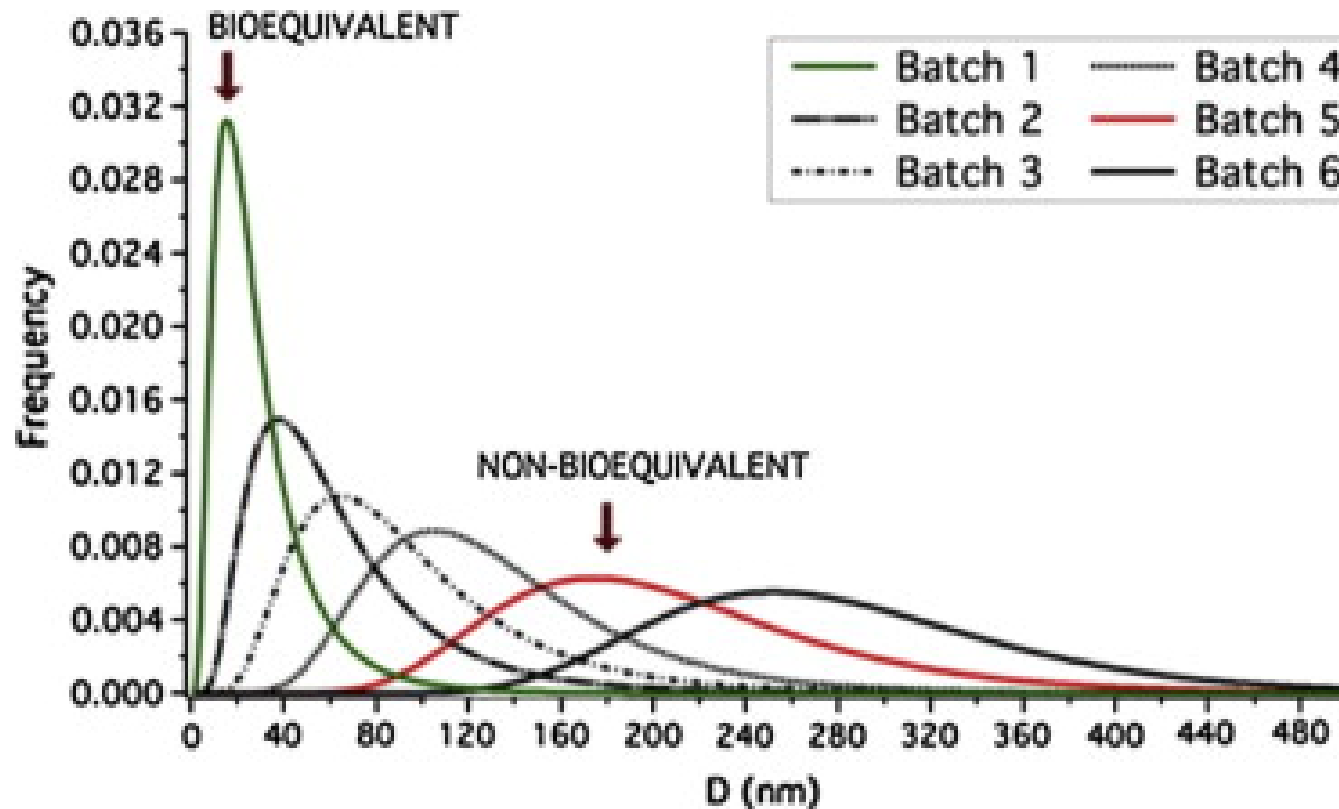
Line profile analysis - example

Crystalline Domain Size Distribution of efavirenz

Thank you!